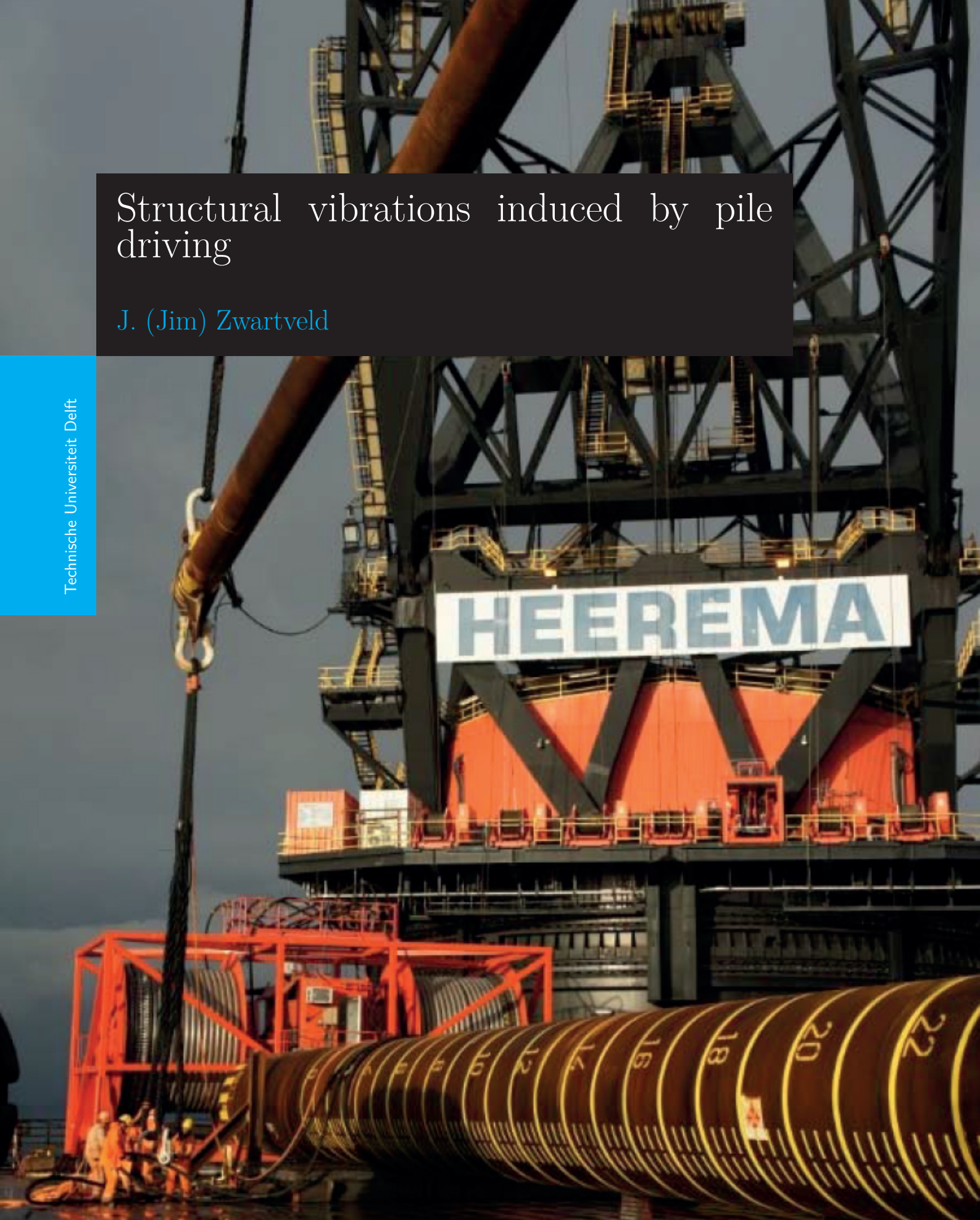


Structural vibrations induced by pile driving

J. (Jim) Zwartveld

Technische Universiteit Delft



HEEREMA

Structural vibrations induced by pile driving

by

J. (Jim) Zwartveld

in partial fulfillment of the requirements for the degree of

Master of Science

in Offshore Engineering

at the Delft University of Technology,

to be defended on Monday January 11, 2016 at 13:00 PM.

Student number:	4131509	
Project duration:	April 13, 2015 – January 11, 2016	
Chairman:	Prof. dr. A.V. Metrikine	TU Delft
Thesis committee:	Dr. ir. A. Tsouvalas	TU Delft
	Ir. R.H.M. Ogink	Heerema Marine Contractors
	Ir. J. Remijn	Heerema Marine Contractors

This thesis is confidential and cannot be made public.

Preface

The thesis that you just picked up summarises eight months of hard work. Work that has been conducted to complete the requirements for the degree of Master of Science in Offshore Engineering at Delft University of Technology. This work has been performed at and in cooperation with Heerema Marine Contractors in Leiden, to help them gain understanding in the topic. It has been written for those who have at least some background knowledge in wave dynamics.

Over the months, I have never lost my interest in the topic which made me work on this thesis with pleasure. It has been a joy working with the people at HMC, the friendly and cooperative atmosphere encouraged me to give my best in this work. Joris (Remijn) and Richard (Ogink) were always available to discuss issues, for which I am very grateful. Each meeting with Apostolos (Tsouvalas) consisted of a blast of information, which initially left me with more questions than I initially had. In the long run these meetings proved very helpful in understanding the problem. Alongside my supervisors, I would like to express my gratitude to prof. Metrikine for his supervision.

The endless support of Jennifer, my family and friends have helped me in taking this last and largest hurdle of my student life. With all of you, the last years have been fantastic.

*J. (Jim) Zwartveld
Leiden, December 2015*

Abstract

For decades, sub-sea pile driving has been performed to safely attach offshore and sub-sea infrastructure such as jackets, templates and manifolds to the supporting soil. In sub-sea pile driving, a hammer is lowered from an installation vessel and similarly descended until the (generally steel tubular) pile reaches his final penetration depth. Multiple types of driving mechanisms are used, where the mechanical impact of a heavy ram is the most common. The ram is lifted within the casing of a hammer and subsequently accelerated until it hits an anvil. This anvil spreads kinetic energy of the ram around the circumference of the pile, where the energy progresses as stress waves. Energy is radiated away from the pile in acoustic pressure and Scholte waves, elastic waves in water and soil, plastic deformation in the soil and heat.

Each blow causes transverse vibrations of the pile, both due to radial expansion of longitudinal stress waves and due to misalignment between hammer and pile. If the pile is in contact with a structure such as a conductor template, it exchanges energy with this structure. Heerema Marine Contractors (HMC) conducted vibration measurements during the installation of the Britannia template, where peak accelerations rapidly increased as the pile reached its final penetration. Values up to 300 m/s^2 were measured. More recently, similar conductor templates needed to be installed. Static design loads were based on these peak accelerations and the mass of the pile sleeve, which most likely causes over-designing of the templates.

The aim of this thesis is to give more insight in the load transfer between pile and conductor template. Pile driving during the installation of the Britannia template is modelled, where it is attempted to validate the model with the measurements. The model describes both the pile and the template with one-dimensional vibration theories. It proved not possible to validate the model for two reasons. Insufficient quality and amount of data made it impossible to validate both sub-models independent of each other. And second; one-dimensional theories do not suffice to describe local accelerations in thick plate girders. In reality, the plate girder act as a waveguide where local variations in the motions along its height might be large. The measurement data show a large increase in the local peak acceleration, which does not necessarily imply a large acceleration of the whole cross section at once and it does not imply a large change in velocity. A better means of assessing peak accelerations is by taking the integral over the peak (i.e. the change in velocity). By this means the value of the peak acceleration is put in perspective with respect to the motions.

A follower is generally placed on top of the pile, to drive the pile up to its final penetration without causing conflict with the construction. It is likely that the presence of this follower increases the radial stiffness of the pile. A range of radial stiffness values was used to model the interaction between pile and template. The analysis showed that an increase in radial stiffness causes a large increase in the transferred force. It is therefore plausible that this is the mechanism that causes a rapid increase in accelerations as the pile reaches its final penetration.

Nomenclature

Symbol	Value	Units	Description
x, y, z			Cartesian coordinates
r, θ, z			Cylindrical coordinates
u, v, w		m	Translational displacements
ψ, ϕ, θ		rad	Rotational displacements
σ, τ		Pa	Stress tensors
q		N/m	Distributed load
N		N	Normal force
Q		N	Shear force
M		Nm	Moment
m		kg	Mass
k		N/m	Spring value
E, W		J	Energy, Work
g	9.81	m/s ²	Gravitational constant
ρ	7,800	kg/m ³	Steel - Density
ν	0.29		Steel - Poisson's ratio
E	$2.1 \cdot 10^{11}$	Pa	Steel - Young's modulus
G	$8.14 \cdot 10^{10}$	Pa	Steel - Shear modulus
D	36	inch	Pile - Diameter
R	18	inch	Pile - Radius
h	1	inch	Pile - Wall thickness
L	55	m	Pile - Length
ρ_s	1,800	kg/m ³	Soil - Density
G_s	5,769	Pa	Soil - Shear modulus
V_s	56.6	m/s	Soil - S-velocity
V_p	91.3	m/s	Soil - P-velocity
ν_s	0.30		Soil - Poisson's ratio
ρ_w	1025	kg/m ³	Water - Density
C_M	2		Water - Inertia coefficient
	938	kg	Anvil - mass
	$9.0 \cdot 10^{10}$	N/m	Anvil - stiffness
	0.028 – 0.173 – 0.049	m ²	Ram - Cross sectional area's
	2.0 – 2.5 – 2.0	m	Ram - Length
v_0	5.7	m/s	Ram - Velocity
E_0	$7.2 \cdot 10^4$	J	Ram - Energy
	7.5 – 2	m	Hammer - Length
	0.55 – 1.03	m	Hammer - Diameter

Contents

1	Introduction	1
1.1	Britannia Field	1
1.2	Dynamics of an impulse	2
1.3	Vibration monitoring results	3
2	Problem Definition	7
3	Model Definition	9
3.1	Structural pile model	11
3.1.1	Axial vibrations.	12
3.1.2	Lateral vibrations.	13
3.2	Hammer model	15
3.2.1	Axial vibrations.	17
3.2.2	Lateral vibrations.	18
3.3	Soil-pile interaction.	20
3.3.1	Horizontal interaction along pile shaft.	20
3.3.2	Vertical interaction along pile shaft	21
3.3.3	Nonlinearity.	21
3.3.4	Vertical interaction at pile tip	22
3.4	Hydraulic influence	24
3.4.1	Hydrostatics.	24
3.4.2	Hydrodynamics	24
3.5	Template model.	25
3.5.1	Governing equations	25
3.6	Pile - template interface	27
3.6.1	Stiffness of the interaction	29
4	Verification and Validation	33
4.1	Verification of the pile model	33
4.2	Verification of the template model.	36
4.3	Validation of the force input	37
4.4	Validation of the combined model	40
4.4.1	Stiffness of the interface	40
4.4.2	Modelled accelerations	42
5	Analysis	45
5.1	Lateral vibrations of the pile.	46
5.2	Interaction force	48
5.3	Stress in the connecting plate girder.	49
5.4	Influence of pile penetration	52
6	Conclusions	53
7	Recommendations	57
7.1	Modelling	57
7.2	Measuring	58

A	Appendix Theories of Continuous Vibration	61
A.1	Introduction	61
A.1.1	Strains and stresses.	61
A.2	Approach	61
A.3	Rayleigh-Love theory for Axial Vibration	62
A.4	Rayleigh theory for lateral vibration.	64
A.5	Timoshenko theory for lateral vibration.	65
A.6	Torsional vibration	66
B	Appendix Finite Difference Formulations	69
B.1	Discretisation of axial equations	69
B.1.1	Discretisation of the governing equations	70
B.1.2	Discretisation of the boundary and interface conditions	70
B.1.3	Embedding the discretised boundary and interface conditions	71
B.1.4	Natural frequencies	74
C	Appendix Finite Element Formulations	75
C.1	Shape functions	75
C.2	Finite element formulation	78
C.3	Elements in arbitrary directions	80
C.4	Element offset at nodes.	81
C.5	Application into Template model	83
C.6	Definition of the pile/template interface.	83

Contents

Chapter 1

Introduction

The problem that lead to this thesis originates from a vibration study that was conducted during the installation of the Britannia well conductor template in 1995. Along this and the next chapters, the problem will be introduced and briefly discussed. A short introduction on the Britannia field and the relevance for HMC is given in Section 1.1. Then in Section 1.2 a short introduction will be given to the class of problems that this problem belongs to. Results from the Britannia template vibration study are shown in Section 1.3

1.1. BRITANNIA FIELD

The Britannia field is located 210 km east of Aberdeen, UK and operated by a joint venture of Conoco and Chevron named Britannia Operator Ltd. The field layout consist of two bridge linked bottom founded platforms and a sub-sea manifold. This 14 slot manifold is tied back to the platform using a 15 km long, heated flow-line. In 1995 the Britannia sub-sea 10 well conductor template and subsequently the 158 m tall jacket were installed. The development of the nearby Callanish and Brodgar fields required the expansion of the platform between 2004 and 2006. A 180 km long pipeline exports gas condensate to the Scottish Area Gas Evacuation (SAGE) terminal in St. Fergus. (Offshore-Technology.com; Heerema, 2006)



Figure 1.1: Right the original Britannia platform (1995) and left the Britannia Sattellite platform (2006) (Paskin, 2013).

Heerema Marine Contractors (HMC) was awarded the contract for the installation of the well conductor template in 1995. This template has two distinct functions. First, it acts as a dock and guide for the drilling process. Secondly, the template is used to guide the jacket onto its desired position via the docking piles (DP). The template was lifted onto the seabed in March of this year. It was first levelled from its mud-mat by three hydraulic jacks. These jacks are visible in Figure 1.2, one is located between Support Pile sleeve 2 (SP2) and SP3 and the other two are located adjacent to SP1. After ensuring that the template is levelled within limits, the piles were stabbed and driven to a final penetration depth of 51.4 m. Both docking piles were stabbed and driven next, whereafter the wells were pre-drilled. Prior to the installation of the jacket, the two docking piles were extended such that the jacket docking cones were aligned with the docking piles. The jacket was installed over the template, whereafter the pre-drilled template wells were tied back to the topside. (Rossross, 2000)

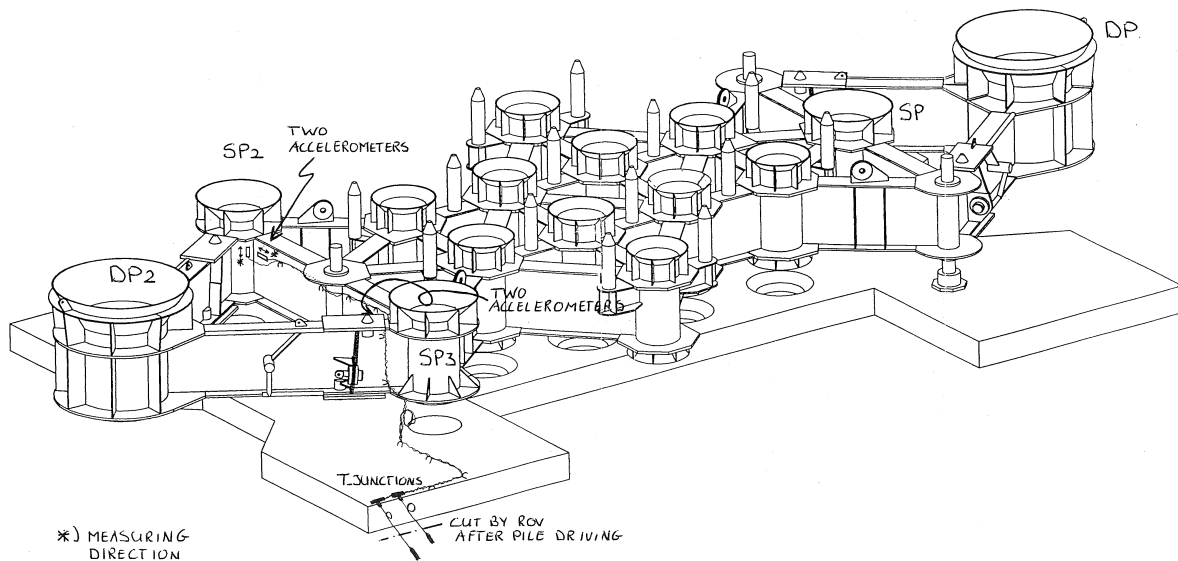


Figure 1.2: Impression of the Britannia template, indicated are the locations of the four accelerometers near the sleeves of SP2 and SP3.

In order to gain more insight in the load transfer that occurs from pile driving, it was decided to install accelerometers on the template and monitor the accelerations during the pile driving process. The results of the vibration monitoring were described in an internal HMC report (van Esch, 1995) and are discussed briefly in Section 1.3.

More recently, HMC was awarded template installation contracts for the Johan Sverdrup and Culzean fields. Both situations required the design of templates, with which it was required to take pile driving loads into account. The Britannia template vibration study raised more questions than results, making the handling of these loads a reasonable issue in the design stage.

1.2. DYNAMICS OF AN IMPULSE

Piles are drilled into the soil through guides. These guides are usually connected to supporting structures such as jackets or sub-sea templates. Hydraulic underwater hammers use the mechanical impact of a ram to press the pile into the ground. The ram is accelerated from a certain height and decelerates as soon as it hits an anvil. During this impact, the momentum and energy of the ram will, to a large extent, be transferred to the rest of the system.

The class of problems that covers pile driving dynamics, is commonly named dynamics of impulses or shocks. An impulse or shock is defined as the abrupt change of a motion, in which the time period considered is short with respect to the fundamental natural frequency of the system (De Silva, 2005). An impulsive load at one end of the pile can not be monitored instantaneously at the other end of the pile.

Kinetic energy that was accumulated in the ram is converted into strain energy and kinetic energy in the pile. The strain energy propagates through the pile as stress waves. Part of the energy is dissipated during the wave propagation, for instance due to the presence of defects in the crystalline structure of the material. At the frequencies related to pile driving, a minor part of the input energy is lost from the pile in the form of acoustic radiation in terms of pressure waves and Scholte waves at the soil-water interface. Part of the energy is transformed into heat. As the stress-wave propagates down, it radiates energy outward into the surrounding fluids and solids. The pile loses a part of its energy into plastic deformations of the soil (Tsouvalas and Metrikine, 2014).

Dynamic properties of the structure and characteristics of the impulse influence the system response. In this case the natural frequencies and modes of vibration of the pile form the dynamic properties of the structure. The characteristics of the impulse can be expressed in terms of shape, amplitude and duration.

The shape of the impulse is influenced by the amount of deformability of the structural elements involved. If for instance the anvil is too stiff, the ram may bounce which may decrease the fatigue lifetime of the hammer. A soft anvil on the other hand may not be efficient in terms of pile drivability. The mass distribution along the length of the ram, also shown schematically in Figure 3.4, causes the impulse to gradually build up and release its energy, without losing contact with the anvil. The blow usually lasts for milliseconds. After this short transient period, the system will continue to vibrate in its natural frequencies. Impulsive loads can be used to determine the natural frequencies of a system, a method named the *impulse excitation technique* (Roebben et al., 1997).

Flexural motions of the pile might interfere with the surrounding pile guide. Upon contact, energy transfers between the template and the pile. A change in energy in this situation causes the template to vibrate. It is these vibrations that were measured during the installation of the three template support piles of the Britannia project.

1.3. VIBRATION MONITORING RESULTS

Obtained data included blow count graphs and recorded hammer energies of the pile stabbing process, as well as time - acceleration plots at four monitored locations for certain blows. Unfortunately raw data was not available, therefore it was not possible to represent the accelerations in the frequency domain.

Figure 1.3 shows the respective horizontal accelerations of pile sleeve SP2 caused by a 72 kJ blow on support pile 2, at a pile penetration of 40 m. Figure 1.4 shows the same graph at a pile penetration of 50.5 m. Comparing these two blows, one can see that the maximum accelerations observed approximately double over the considered penetration range while the energy of the blow remains roughly equal. Besides, the zero drift frequency implies that the maximum bandwidth of the measurement equipment is 200 Hz. Detailed characteristics of the measurement equipment presumably went missing over the years, as the pages weren't included in van Esch (1995).

Increasing of the vertical and horizontal accelerations as a function of pile penetration length is better shown in Figures 1.5 and 1.6 respectively. Several pile penetration lengths show a sudden increase in the maximum accelerations. Average range and maximum measured accelerations that were monitored during support pile driving are shown in Table 1.1. During the whole process of pile driving, the maximum horizontal accelerations measured were 250 m/s^2 .

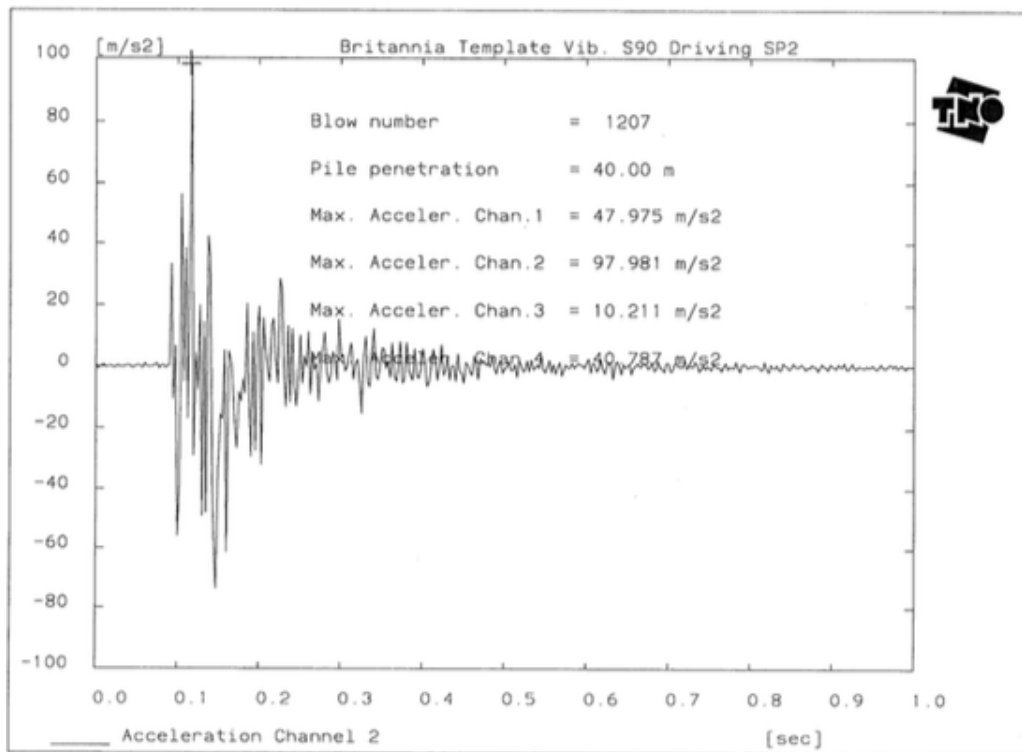


Figure 1.3: Horizontal absolute accelerations of the 'beam' adjacent to the pile sleeve due to blow 1207 during driving of SP2.

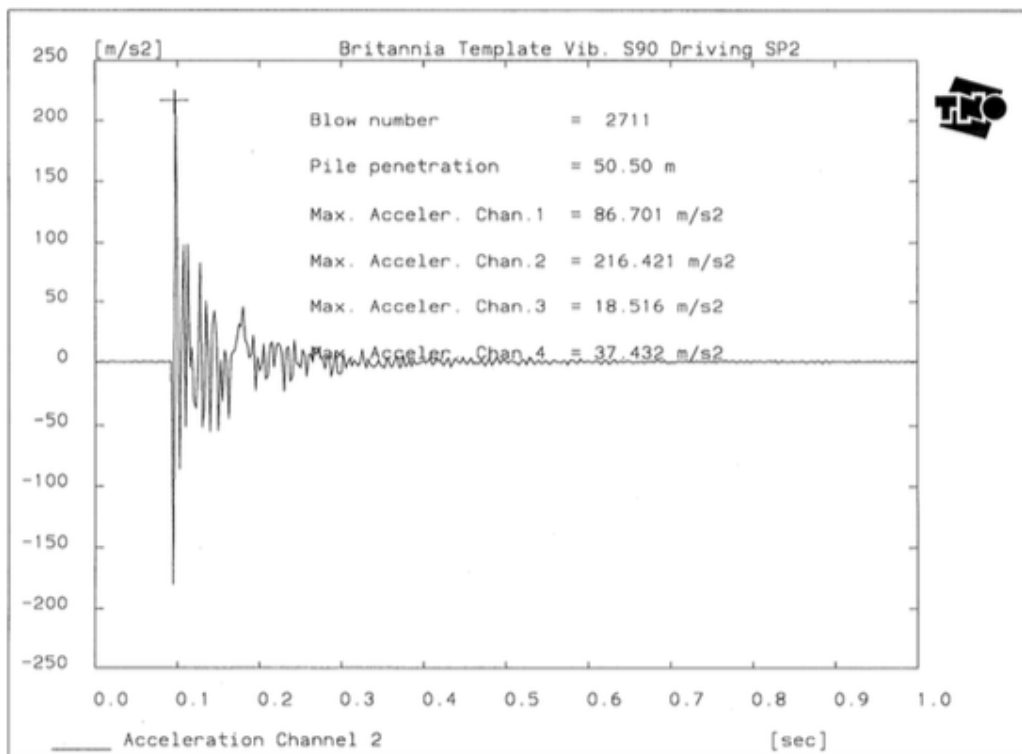


Figure 1.4: Horizontal absolute accelerations of the 'beam' adjacent to the pile sleeve due to blow 2711 during driving of SP2.

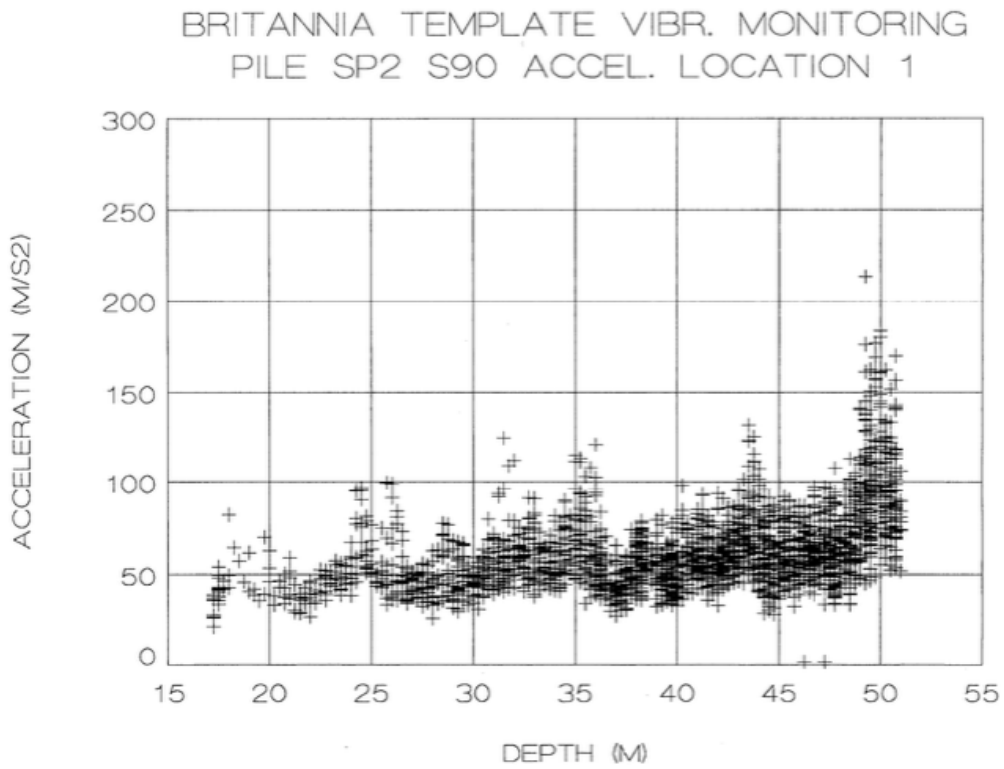


Figure 1.5: Maximum observed vertical accelerations at pile sleeve SP2 due to driving SP2.

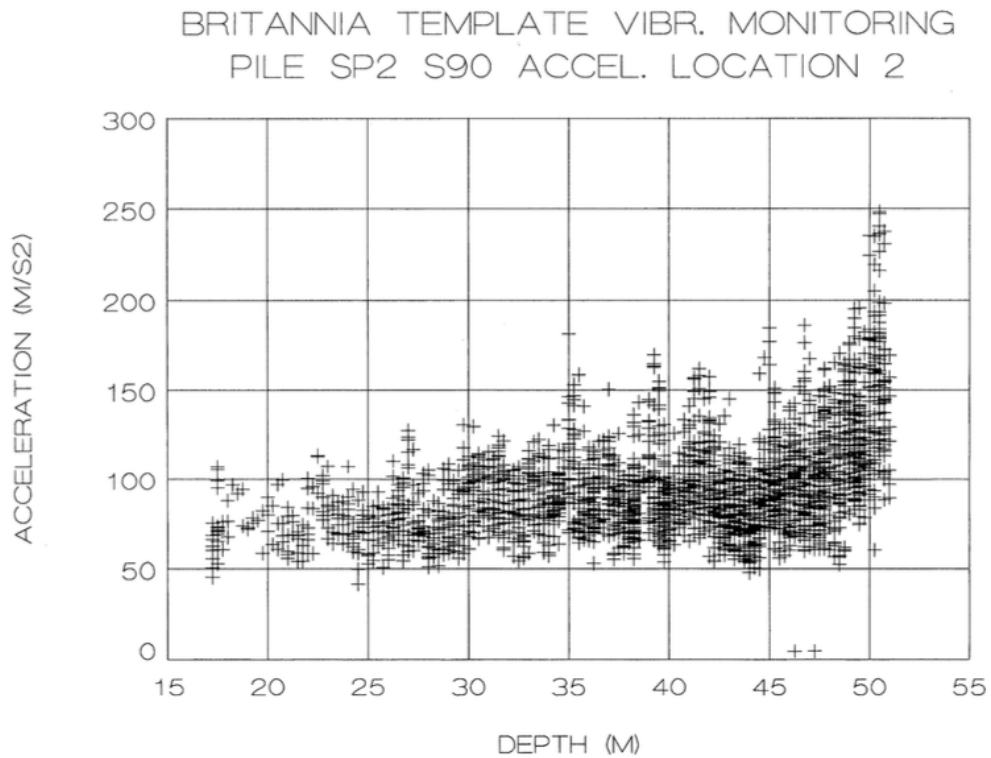


Figure 1.6: Maximum observed horizontal accelerations at pile sleeve SP2 due to driving SP2.

Table 1.1: Average accelerations and maximum accelerations, monitored at sleeves SP2 and SP3 in vertical (v) and horizontal (h) direction while driving piles SP1, SP2 and SP3.

Driving Pile	Acceleration (m/s^2)				Max. Acceleration (m/s^2)			
	Transducer location				Transducer location			
	SP2, v	SP2, h	SP3, v	SP3, h	SP2, v	SP2, h	SP3, v	SP3, h
SP1	5	10	10	15	15	20	20	25
SP2	40-80	55-120	15	20-35	215	250	35	65
SP3	10	20-30	40-70	50-120	25	65	175	250

Chapter 2

Problem Definition

Recent installations of the Culzean and Johan Sverdrup templates reawakened the requirement of understanding the load transfer between pile and pile-sleeve. The design requirement that originated from the Britannia vibration study was that the template should be able to handle accelerations of at least 300 m/s^2 . The results from this study were briefly described in Section 1.3. HMC engineers assumed that Newton's second law of motion is applicable to find the (static) design load due to pile driving. The design cycle orbited in a state of positive feedback, as, according to this design criterium, additional mass causes an increase in the design load. This process leads to the formulation of the problem statement of this thesis.

Problem statement *Pile guiding support structures are likely to be over-designed as not much is known about the effect of the dynamic pile driving loads onto these guiding structures.*

Accelerations seemed to increase rapidly as the distance between the follower tip and the location of the accelerometer decreased, with measured values ranging up to 250 m/s^2 . The cause of this rapid increase was unknown. A straightforward question would be, what causes the accelerations to increase during the final period of driving a pile? Does this increase in accelerations cause the occurrence of a larger load on the template? The vibration report did not give any insight into the mechanism that causes the vibration. The **main objective** of this thesis will therefore be: *to give more insight into the load transfer that occurs from pile driving.*

Above is mentioned that the design load induced by pile driving was based on acceleration data only. In this thesis a model will be formulated that attempts to link measured absolute accelerations to a design load that acts on the template from the pile. The output of this model will then be used to evaluate if the used design criterium is valid. Dynamic analyses in commercial programmes are usually complex and time consuming, which makes it a costly process to perform on a regular basis. What HMC ultimately requires is a simple and straightforward design criterium that includes the effect of pile driving.

The objectives of this thesis can point wise be formulated as;

- Gain more insight into the load transfer that occurs from pile driving.
- Evaluate the design criterium that HMC currently uses.
- If required and possible: formulate a new design criterium and
- give recommendations to HMC on how to handle loads occurring from pile driving.

The model will be formulated in Chapter 3, its data output will be verified and validated in Chapter 4 and analysed in Chapter 5. Conclusions will be drawn based on the data analysis and finally recommendations will be given in Chapter 7.

Chapter 3

Model Definition

In most situations a pile follower is placed on top of the pile. This follower allows the pile to be driven up to its final penetration without causing any conflict between pile and hammer sleeves. The follower is generally a thicker, extended piece of pile. A schematic overview of the situation is shown in Figure 3.1.

The hammer consists of a solid steel ram, the hammer housing and a hammer sleeve that houses a solid steel anvil. The hammer sleeve is placed directly over the top of the follower, this sleeve ensures lateral stability of the hammer with respect to the follower. A blow by the hammer typically consists of the drop of the ram onto the anvil. As the anvil is directly placed on top of the follower, a stress wave will propagate through the follower and further along the pile. After this blow, the ram is lifted again by the hydraulic system in the hammer and the procedure repeats.

The connection between the hammer sleeve and the follower is not tight, therefore the blow is unlikely to be perfectly axial. This may cause a shear force or overturning moment at the top of the pile. Lateral displacement waves may interfere with the pile sleeve in situations where the pile is in direct contact with the sleeve or when the lateral displacements due to the driving process are sufficiently large to cause contact.

The following steps are envisaged to model pile sleeve vibrations;

1. Axial vibration of a pile, caused by the drop of a ram on the top of an anvil.
2. Lateral vibration of a pile, caused by out of verticality and the displacement of the anvil with respect to the top of the follower.
3. Horizontal vibrations of the pile sleeve, caused by lateral vibrations of the pile and influenced by the initial position of the pile with respect to the pile sleeve.
4. Vertical vibrations of the pile sleeve, caused by the variation of loading over the height of the pile sleeve and by friction between the pile and the pile sleeve.

In this chapter, the modelling strategies for the above mentioned steps are elaborated on, as well as the chosen solving strategies. The model that describes axial and lateral vibrations of the pile (in short: the pile model) is elaborated on in Section 3.1. The methods that were used to model the influence of the soil and water are described in Sections 3.3 and 3.4 respectively. In Section 3.5, the model that describes the template (in short: the template model) is presented. Finally, section 3.6 shows the modelling of the interaction between the pile and pile sleeve.

Along this thesis, Cartesian coordinate system is used when no other coordinate system is clearly indicated. The z -axis is generally taken downward. Displacements as a function of location are named u , v and w in x , y and z direction respectively.

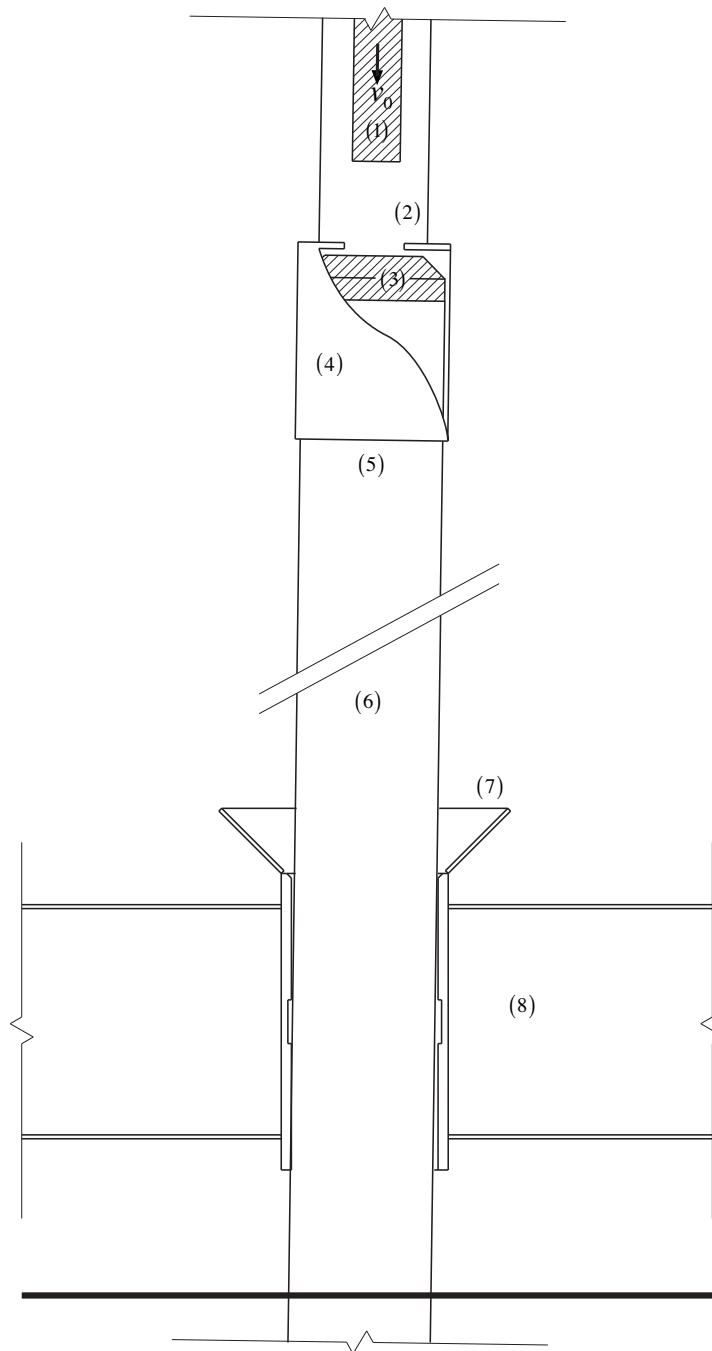


Figure 3.1: Schematic overview of the pile driving situation. In this figure: (1): ram; (2): hammer; (3): anvil; (4): hammer sleeve; (5): follower; (6): pile; (7): pile sleeve; (8): template. The diameter of the drawn pile is 36 inch and the height of the beams that connect the pile guide is 1.50 m, the thick black line at the bottom shows the mudline

3.1. STRUCTURAL PILE MODEL

The structural pile model consists of all steel elements that are not part of the template construction. It consists of a pile that is partly penetrated into soil, with a follower placed on top of the pile. To complete this model, a simplified model of a hammer is placed on top of the follower.

MODELLING STRATEGIES

Piles can generally be seen as a three-dimensional structure in which one dimension (the longitudinal direction) is much larger than the other two dimensions. The structural element can deform in longitudinal direction, in lateral direction and in torsion. Many theories are available to describe vibrations of the pile in before mentioned directions, with differing assumptions forming the basis of each theory. Theories of vibrations for long, slender structural elements can be subdivided into one-dimensional theories and two-dimensional theories.

The definition of a one-dimensional theory is that the motion in longitudinal, lateral or torsional direction is assumed to vary in the longitudinal direction only. If the cross section of the structural element is axisymmetric, the motions in longitudinal, lateral and torsional vibrations are generally assumed uncoupled. Torsional vibrations can be discarded in pile driving analysis, as no torque is applied when the ram hits the top of the pile and piles have an axisymmetric cross section.

The simplest one-dimensional theory that describes longitudinal vibrations in a rod, commonly known as the second order wave equation, was first used in the context of pile driving by Smith (1960). The drawback of this theory is its validity when it is attempted to describe high frequency vibrations. The wave propagation velocity of higher frequency waves is overestimated (Graff, 2012). Other one-dimensional theories that describe axial vibrations include Rayleigh-Love theory, which includes inertia of the lateral motions of the pile, and Bishops theory, which include inertia of the lateral motions as well as shear stiffness (Rao, 2007). These theories are able to describe the dispersion relation, i.e. the relation between wave propagation velocity and wave frequency, of longitudinal waves up to a higher frequency limit.

The most common method to describe lateral vibrations of beams is the (fourth order) Euler-Bernoulli beam theory, which, like the wave equation, is unable to model high frequency vibrations physically correct. The dispersion relation of this theory is linear, which implies that the highest frequency waves propagate at infinite velocity (Graff, 2012). Rayleigh included rotational inertia in his theory and Timoshenko further expanded Rayleigh's theory with the addition of shear correction. Timoshenko's beam theory is commonly used for thick beams, as the contribution of shear stiffness becomes significant as the slenderness of the beam decreases. According to Graff (2012), Timoshenko's beam theory is able to describe the dispersion relation remarkably accurate at higher frequencies.

Another way to describe a pile is by using two-dimensional shell theories. The definition of a thin shell is a three-dimensional body that is bounded by curved surfaces, in which the distance between the curved surfaces is small with respect to the other two dimensions. Different theories have been developed by various academicians, each based on slightly different simplifying assumptions (Leissa, 1973).

A sub-collection of shell theories include theories on thin circular cylindrical shells. A thin circular cylindrical shell can be regarded as a thin shell in which the radius of one curved surface is equal to the pile radius, and the radius of the other curved surface is infinity. The displacement of the shell is assumed constant over the wall thickness, it only varies along the radii, hence two-dimensional. The theory describes the displacement of the shell in three directions: longitudinal, radial and tangential.

In the the one-dimensional theories, the solution can be found by solving a set of sixth order partial differential equations, second order for the longitudinal motion and fourth order for the bending motion. The solution to the two-dimensional theories can be found by solving a set of eighth order partial differential equations; two for the longitudinal displacement, two for the circumferential displacement and four for the radial displacement. Analytical methods to solve differential equations are generally reserved for simple problems. As the differential equation or the boundary becomes more complex, approximate analytical methods can be used to generate a computationally efficient solution.

Numerical methods are easier to implement but require more computational power. Common methods to solve differential equations such as described above include the finite element method (FEM) or finite difference method (FDM). The difference between these methods originates from the formulation approach. The FDM uses a discretisation of the differential equation in space, yielding a second order linear set of equations that describes the problem. It is generally only used as a 'quick and dirty' method, as it is fairly simple to implement. For more complex constructions the FEM is more commonly used. FEM formulations can be found by implementing assumed displacement shapes in the energy variation definition of the chosen theory.

APPLICATION

Due to their relatively simple implementation, the motions of the pile are described by the uncoupled one-dimensional theories of longitudinal and lateral vibration. Interaction between the longitudinal and lateral motions is only achieved at certain boundaries. As the frequency regime of pile driving vibrations is generally high, Rayleigh-Love theory for longitudinal vibration and Rayleigh theory for lateral vibration are used to model the pile. Due to time constraints it has not been possible to implement shear correction. The assumptions that form the basis for these theories and the derivation of the equations of motion are described in Appendix A. Both theories are relatively simple to implement for the chosen solving strategy.

Initially it was attempted to solve the equations by means of a weighted residuals method (Galerkin's method, as described by Rao (2007)). The solution was sought as the sum of a finite amount of harmonic motions that all satisfy the boundary conditions. However, this method failed to describe the initial conditions correctly. In order to correct for the initial conditions, the highest included modes seemed to contain a lot of energy that did not originate from the blow. Including more vibration modes only shifted the problem.

As stated above, the problem can be described using two uncoupled differential equations. The equations of motion and boundary conditions that describe the longitudinal and lateral vibrations are briefly presented in subsections 3.1.1 and 3.1.2 respectively. The analytic methods failed to describe the system correctly, therefore it was decided to discretise the space domain of the model using FDM. The finite difference formulations of the equations of motion that are presented there, are added in Appendix B.

3.1.1. AXIAL VIBRATIONS

Consider a pile that is partly penetrated in the soil, such as shown in Figure 3.2. It can be subdivided into three domains along its length from top to bottom: the first describing the follower; the second describing the top part of the pile and the third describing the penetrated part of the pile. The influence of the soil on penetrated pile domain will be discussed in Section 3.3, here it is included as an added load $q_{v,soil}$.

GOVERNING EQUATIONS

The governing equations for the i -th section are described by (3.1), in this equation: $i = P, F$ for the pile and follower respectively. The function $H(z)$ is the *Heaviside* step function, it indicates that the

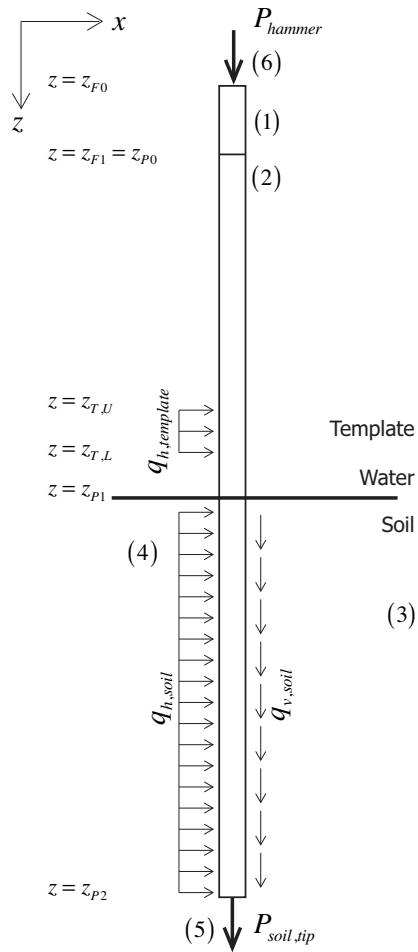


Figure 3.2: Pile model, in which (1) Follower, (2) Pile, (3) Soil frictional resistance, (4) Lateral soil stiffness, (5) Pile tip resistance and (6) Hammer interface.

soil reaction is present for $z \geq z_{P1}$.

$$\rho A_i \frac{\partial^2 w}{\partial t^2} - \rho \nu^2 I_i \frac{\partial^4 w}{\partial t^2 \partial z^2} - E A_i \frac{\partial^2 w}{\partial z^2} = q_{v,soil} \cdot H(z - z_{P1}) + \rho A_i \cdot g \quad (3.1)$$

BOUNDARY AND INTERFACE CONDITIONS

The boundary conditions can be satisfied if the normal force or the displacement at a boundary are defined, as shown in (3.2).

$$w_i(z, t) \quad \text{or} \quad N_i(z, t) = \rho \nu^2 I_i \frac{\partial^3 w_i}{\partial z \partial t^2} + E A_i \frac{\partial w_i}{\partial z} \quad (3.2)$$

The pile/follower combination is loaded at the top by a reaction from the hammer, P_{hammer} .

$$N_F(z_{F0}) = P_{hammer} \quad (3.3)$$

Assuming a rigid connection between the pile and the follower, its interface condition can be described by a force balance between the tip of the follower and the head of the pile and by continuity in the displacement.

$$N_F(z_{F1}) = N_P(z_{P0}) \quad (3.4)$$

$$w_F(z_{F1}) = w_P(z_{P0}) \quad (3.5)$$

The tip of the pile is balanced by the soil reaction to the vertical displacement of the pile, here simplified as a point load.

$$N_P(z_{P2}) = P_{soil,tip} \quad (3.6)$$

INITIAL CONDITIONS

Before the ram hits the anvil, the system is loaded by gravity only. Its initial velocity is therefore zero and its initial displacement is equal to the static displacement.

3.1.2. LATERAL VIBRATIONS

GOVERNING EQUATIONS

The governing equation for the i -th section is (3.7). In this equation, $H(z)$ is the *Heaviside* step function.

$$\rho A_i \frac{\partial^2 u}{\partial t^2} - \rho I_i \frac{\partial^4 u}{\partial z^2 \partial t^2} + E I_i \frac{\partial^4 u}{\partial z^4} = q_{h,soil} \cdot H(z - z_{P1}) + q_{h,template} \cdot \{H(z - z_{T,U}) - H(z - z_{T,L})\} \quad (3.7)$$

BOUNDARY CONDITIONS

In order to satisfy the boundary conditions, two conditions at each boundary need to be defined. The first condition can be defined by either the displacement or the shear force at a boundary (3.8). The second condition is defined by the rotation or moment at the boundary (3.9).

$$u_i(z, t) \quad \text{or} \quad Q_i(z, t) = E I_i \frac{\partial^3 u_i}{\partial z^3} - \rho I_i \frac{\partial^3 u_i}{\partial z \partial t^2} \quad (3.8)$$

$$\frac{\partial u_i(z, t)}{\partial z} \quad \text{or} \quad M_i(z, t) = E I_i \frac{\partial^2 u_i}{\partial z^2} \quad (3.9)$$

The top of the follower is loaded by a shear force, the magnitude of this shear force is the out of verticality α_1 of the hammer reaction P_{hammer} . This out of verticality is caused by the rotational margins of the hammer sleeve.

$$Q_F(z_{F1}, t) = P_{hammer} \cdot \sin \alpha_1 \quad (3.10)$$

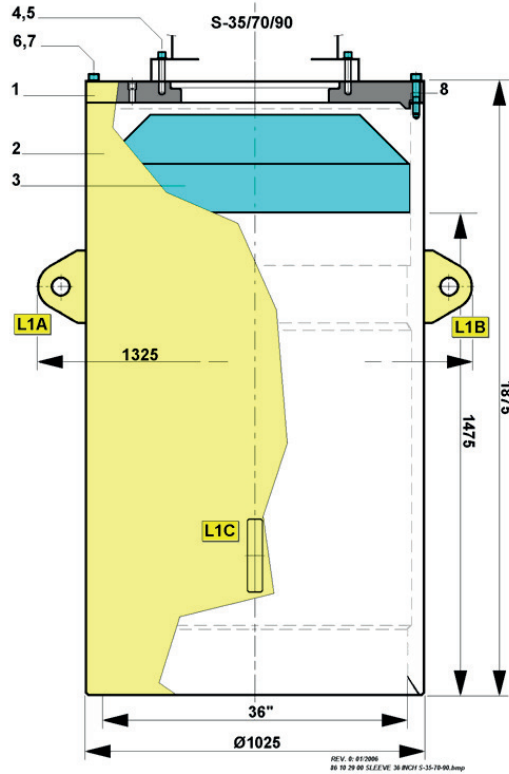


Figure 3.3: Hammer sleeve for 36" piles; 1 shows the connecting ring, 2 shows the pile guiding and 3 the anvil. This sleeve is rigidly connected to the hammer (4 and 5) by screws. (IHC, 2009)

The moment at the top of the follower is assumed zero.

$$M_F(z_{F1}, t) = 0 \quad (3.11)$$

In reality, the follower is placed on top of the pile. A section of 2.5 meter (i.e. 2.5 pile diameters) length extends into the top of the pile. Continuity in the displacement, rotation and moment at the pile / follower interface is assumed. The extra mass that is accompanied by the extended part of the follower is excluded from this analysis.

$$u_F(z_{F1}, t) = u_P(z_{P0}, t) \quad (3.12)$$

$$\frac{\partial u_F(z_{F1}, t)}{\partial z} = \frac{\partial u_P(z_{P0}, t)}{\partial z} \quad (3.13)$$

$$M_F(z_{F1}, t) = M_P(z_{P0}, t) \quad (3.14)$$

$$Q_F(z_{F1}, t) = Q_P(z_{P0}, t) \quad (3.15)$$

Although there might be rotational and shear influences on the pile tip, it is assumed free for simplicity.

$$M_P(z_{P2}, t) = Q_P(z_{P2}, t) = 0 \quad (3.16)$$

INITIAL CONDITIONS

The initial displacement and initial velocity are assumed zero, as it is assumed that the pile is standing vertically.

Another case that is investigated is when the pile has an initial inclination of 1° , which causes it to be subjected to gravity along its length.

R1	Upper ram
R2	Middle ram
R3	Lower ram
H1	Upper hammer
H2	Lower hammer
A	Anvil
F	Follower
P	Pile

Table 3.1: Subscripts used to indicate different sections of the model

3.2. HAMMER MODEL

Several attempts have been made to model the force-time diagram at the top of the follower. Attempts included a kinematic boundary condition to describe the force input, in which the corresponding kinematics have been modelled by assuming rigid body dynamics of a double mass-spring system (Deeks and Randolph, 1993).

Accelerations of the pile and subsequently the template are highly sensitive to the nature of the force input. They are dependent on the mass distribution of the ram and the mass and stiffness characteristics of the anvil, which is not described by a rigid body. This simplified double-mass spring system is also not able to capture reflective waves from the pile system.

The presence of the hammer influences the inertia at the top of the pile, the hammer was initially modelled as a concentrated mass and moment of inertia at the top of the pile. The hammer is a tubular structure with a length of roughly 15% and a mass of roughly 20% of the pile. Long enough for waves propagating up and down the hammer cylinder.

In order to include the kinematics of the hammer and more accurately model the force input in the time domain, it has been decided to create a model of the hammer and directly attach it to the top of the follower.

The hammer consists of two tubular structures that are rigidly connected by bolts (see Figure 3.3). As can be seen in this figure, the hammer and hammer sleeve rest on the anvil which in its turn rests on top of the follower. The ram is encased within the upper tubular of the hammer. Its dimensions are known to the Foundation dept. of HMC, therefore the mass distribution of the ram can be estimated. The model that is shown in Figure 3.4 is proposed.

The theories that were introduced and briefly discussed in Section 3.1 were used to model the longitudinal and lateral vibrations of the hammer structure. The following subsections contain the governing equations that describe the vibrations of the beam and rod elements. In order to keep overview of all equations, the subscripts (A_i) indicated in Figure 3.4 and Table 3.2 will be used to indicate the displacement along and the characteristics of the section.

Modelling the hammer is done with caution as it is unknown what the exact influence of the hydraulics is to the system. Known is the amount of kinetic energy at impact, but as soon as the ram is disconnected from the anvil it is likely that the hydraulics influence the motion of the ram. A second impact of the ram is therefore modelled incorrectly as it is not simply bouncing up and down on the anvil.

As stated before and shown in equation (3.10), the shear force on the top of the follower is assumed a fraction of the normal force. As the second impact of the ram is not likely to occur, it is decided to uncouple shear force from the normal force as the contact between the anvil and follower is lost. By this means the initial force input is modelled accurately and the second impact loads are excluded from the lateral analysis.

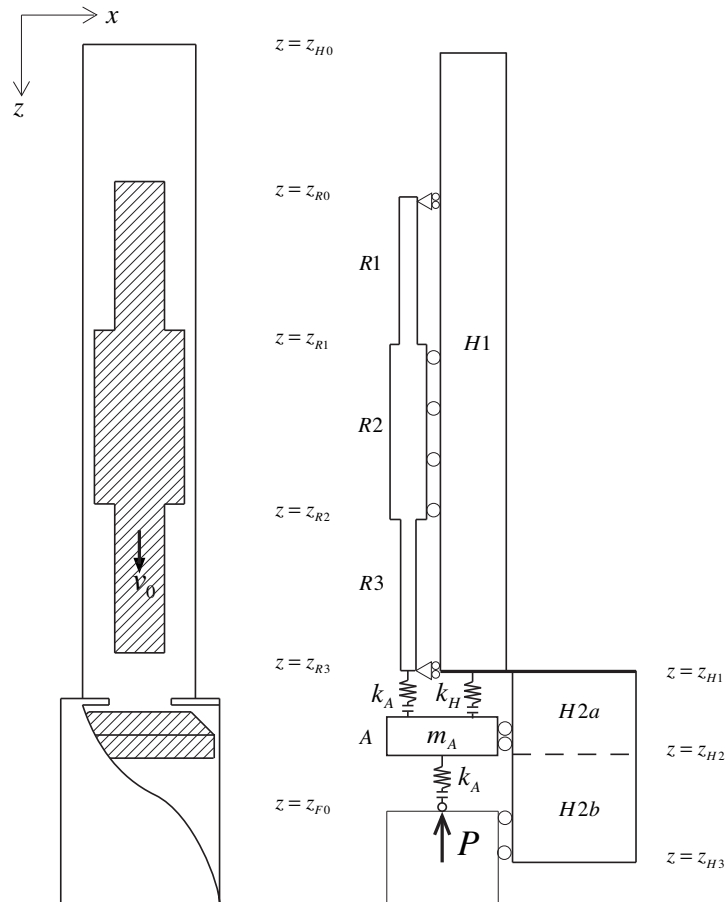


Figure 3.4: Hammer model with: $R1, R2, R3$: different sections of the ram (each their own length and cross sectional area; $H1$: hammer casing; $H2a$: upper section hammer sleeve, without overlap with the follower; $H2b$: lower section hammer sleeve, with overlap with the follower; A : anvil. The force P corresponds to the force input from the pile. k_A and k_H denote the stiffness of the anvil and hammer frame respectively.

3.2.1. AXIAL VIBRATIONS

GOVERNING EQUATIONS

The ram consists of three sections with different cross sectional areas and different lengths. For each section i , the corresponding partial differential equation according to the Rayleigh-Love theory is (3.17). The hammer consists of two sections with different cross sectional areas and different lengths; the hammer is also described with (3.17).

$$\rho A_i \frac{\partial^2 w_i}{\partial t^2} - \rho \nu^2 I_i \frac{\partial^4 w_i}{\partial z^2 \partial t^2} - E A_i \frac{\partial^2 w_i}{\partial z^2} = 0 \quad (3.17)$$

The anvil is connected to the top of the follower, the hammer interface and the bottom of the ram. All interfaces are only able to transmit compressive stresses. These interfaces are modelled by a class of non-linear springs named non-tension springs (NTS). It is described mathematically using the *Heaviside* step function. The governing equation that describes the vertical motion of the anvil is (3.18).

$$\begin{aligned} m_A \ddot{z} + k_A (z_A - w_{R3}(z_{R3})) \cdot H(w_{R3}(z_{R3}) - z_A) \\ + k_A (z_A - w_F(z_{F0})) \cdot H(z_A - w_F(z_{F0})) \\ + k_H (z_A - w_{H1}(z_{H1})) \cdot H(w_{H1}(z_{H1}) - z_A) = 0 \end{aligned} \quad (3.18)$$

BOUNDARY AND INTERFACE CONDITIONS

As stated in Section 3.1, the boundary conditions can be defined by satisfying (3.2).

The upper boundaries of both the ram and the hammer casing are unloaded, this can be expressed as in (3.19) at $z = z_{H0}$ and $z = z_{R0}$.

$$N_{R1}(z_{R0}) = N_{H1}(z_{H0}) = 0 \quad (3.19)$$

The lower boundary of the ram is bound by the stiffness of the anvil. As this connection is not rigid, it can only transmit compressive forces. At $z = z_{R3}$, expression (3.20) is valid.

$$N_{R3}(z_{R3}) = k_A (z_A - w_{R3}(z_{R3})) \cdot H(w_{R3}(z_{R3}) - z) \quad (3.20)$$

The lower boundary of the hammer sleeve, $z = z_{H3}$, is free, as in (3.21).

$$N_{H2}(z_{H3}) = 0 \quad (3.21)$$

Continuity of the normal stress and displacement between adjacent sections of the ram leads to expression (3.22), here $i = 1, 2$ for the upper and lower interface at $z = z_{R1}$ and $z = z_{R2}$.

$$N_{R,i}(z_{R,i}) = N_{R,i+1}(z_{R,i+1}) \quad (3.22)$$

$$w_{R,i}(z_{R,i}) = w_{R,i+1}(z_{R,i+1}) \quad (3.23)$$

The interface between the two adjacent hammer sections consists of a cylindrical plate which rests on the anvil in the static situation. For simplicity it is assumed that the plate is infinitely stiff. A positive displacement of this interface causes a reaction force from the anvil provided that contact between the two elements is made. It can be expressed as (3.24).

$$N_{H1}(z_{H1}, t) - N_{H2}(z_{H1}, t) = k_H (z_A - w_{H1}(z_{H1})) \cdot H(w_{H1}(z_{H1}) - z) \quad (3.24)$$

INITIAL CONDITIONS

As a blow commences, the ram is accelerated with the aid of hydraulics from a certain height with an acceleration of twice the gravitational acceleration. As soon as the impulsive impact has ceased, the ram is lifted again by these hydraulics. Its initial velocity slightly before impact can be derived from the kinetic energy at this time (3.25), assuming that all kinetic energy is transferred into strain energy.

$$E_{blow} = \frac{1}{2} m_R v_0^2 \quad (3.25)$$

At $t = 0$ the ram, along its full length, has an initial velocity v_0 as shown in (3.26). All other sections have no initial velocity and have an initial displacement that is equal to the static displacement.

$$\frac{\partial w_R}{\partial t} = v_0 \quad w_R = 0 \quad (3.26)$$

$$\frac{\partial w_H}{\partial t} = 0 \quad w_H = w_H^{(stat)} \quad (3.27)$$

3.2.2. LATERAL VIBRATIONS

As the ram is entrapped within the hammer casing, its lateral motions are considered coupled to the lateral motions of the hammer. Along section 1b in Figure 3.4, a continuous frictionless connection is assumed between the hammer casing and ram. The upper boundary ($z = z_{R1}$) and the lower boundary ($z = z_{R3}$) of the ram are also considered connected to the hammer casing. The displacements upon and after impact are assumed small, therefore the added inertia from the ram can be

As the displacements of the hammer casing and ram are relatively small with respect to their length, it can be assumed that:

$$z_{H1} \approx z_{R3}$$

The anvil and follower are also considered connected to the hammer casing by means of a frictionless connection.

The mathematical context is explained below.

GOVERNING EQUATIONS

As described in Section 3.1, Rayleigh theory is used to model lateral vibrations.

$$\rho A(z) \frac{\partial^2 u}{\partial t^2} - \rho I(z) \frac{\partial^4 u}{\partial z^2 \partial t^2} + EI(z) \frac{\partial^4 u}{\partial z^4} = 0 \quad (3.28)$$

The cross sectional area ($A(z)$) and area moment of inertia ($I(z)$) in (3.28) are position dependent. For instance between $z = z_{R1}$ and $z = z_{R2}$, $A(z)$ and $I(z)$ are the sum of the cross sectional area and moment of inertia of the hammer and ram section respectively.

Between $z = z_{H0}$ and $z = z_{H1}$:

$$A(z) = A_{H1} + A_{R2} \cdot (H(z - z_{R1}) - H(z - z_{R2})) \quad (3.29)$$

$$I(z) = I_{H1} + I_{R2} \cdot (H(z - z_{R1}) - H(z - z_{R2})) \quad (3.30)$$

Between $z = z_{H1}$ and $z = z_{H3}$:

$$A(z) = A_{H2} + A_F \cdot (H(z - z_{H2}) - H(z - z_{H3})) \quad (3.31)$$

$$I(z) = I_{H2} + I_F \cdot (H(z - z_{H2}) - H(z - z_{H3})) \quad (3.32)$$

In which A_F and I_F indicate the cross sectional area and area moment of inertia of the embedded follower.

BOUNDARY AND INTERFACE CONDITIONS

The top of the hammer (z_{H0}) is considered a free end. At this position no shear force or moment can be present, therefore:

$$M_{H1}(z_{H0}, t) = Q_{H1}(z_{H0}, t) = 0 \quad (3.33)$$

At $z = z_{R0}$ and $z = z_{R1}$ half of the mass of ram section 1a is considered attached, mathematically this is:

$$Q_{H1}(z_{R0+}, t) - Q_{H1}(z_{R0-}, t) = \frac{1}{2}(\rho A_{R1} \cdot L_{1a}) \frac{\partial^2 u_{H1}}{\partial t^2} \quad (3.34)$$

$$Q_{H1}(z_{R1+}, t) - Q_{H1}(z_{R1-}, t) = \frac{1}{2}(\rho A_{R1} \cdot L_{1a}) \frac{\partial^2 u_{H1}}{\partial t^2} \quad (3.35)$$

$$(3.36)$$

At $z = z_R^{(2)}$ half of the mass of ram section 1c is considered attached.

$$Q_{H1}(z_{R2+}, t) - Q_{H1}(z_{R2-}, t) = \frac{1}{2}(\rho A_{R3} \cdot L_{1c}) \frac{\partial^2 u_{H1}}{\partial t^2} \quad (3.37)$$

Continuity in bending moment ($EI(z_{z_R(j)+}) \cdot u(z_{R(j)+}) = EI(z_{R(j)-}) \cdot u(z_{R(j)-})$), rotation ($u'_{z=z_R(j)+} = u'_{z=z_R(j)-}$) and displacement ($u_{z=z_R(j)+} = u_{z=z_R(j)-}$) for $j = 0, 1, 2$ completes four interface conditions at $z = z_{R0}$, $z = z_{R1}$ and $z = z_{R2}$.

At z_{H1} , the following half of the mass of ram section 1c is considered attached and continuity in shear force, bending moment, rotation and displacement makes the boundary conditions:

$$u_{H1}(z_{H1}, t) = u_{H2}(z_{H1}, t) \quad (3.38)$$

$$\frac{\partial u_{H1}(z_{H1}, t)}{\partial z} = \frac{\partial u_{H2}(z_{H1}, t)}{\partial z} \quad (3.39)$$

$$M_{H1}(z_{H1}, t) = M_{H2}(z_{H1}, t) \quad (3.40)$$

and

$$Q_{H1}(z_{H1+}, t) - Q_{H2}(z_{H1-}, t) = \frac{1}{2}(\rho A_{R3} \cdot L_{1c}) \frac{\partial^2 u_{H1}}{\partial t^2}$$

The anvil is considered horizontally attached to the hammer sleeve at z_{H2} .

$$Q_{H2}(z_{H2+}, t) - Q_{H2}(z_{H2-}, t) = m_A \frac{\partial^2 u_{H2}}{\partial t^2}$$

Continuity in moment, rotation and displacement completes the interface conditions here. Finally, at $z = z_{H3}$ the rotation must be equal to the rotation of the follower (3.41) and the shear force must be equal to the shear force present in the follower (3.42).

$$\frac{\partial u_{H2}(z_{H3}, t)}{\partial z} = \frac{\partial u_F(z_{H3}, t)}{\partial z} \quad (3.41)$$

$$Q_{H2}(z_{H3}, t) = Q_F(z_{H3}, t) \quad (3.42)$$

INITIAL CONDITIONS

It is assumed that at $t = 0$, both the ram (3.43) and the hammer (3.44) have no initial horizontal displacement or velocity.

$$\frac{\partial u_R}{\partial t}(z, 0) = 0 \quad w_R(z, 0) = 0 \quad (3.43)$$

$$\frac{\partial u_H}{\partial t}(z, 0) = 0 \quad w_H(z, 0) = 0 \quad (3.44)$$

3.3. SOIL-PILE INTERACTION

Soil generally consists of small particles and pore space that form the soil body. These pore spaces may or may not be filled with water. Deformations of the soil body depends on the characteristics of the soil and of the behaviour of the fluid in the pores. If the permeability of the soil is low, the soil and fluid might deform simultaneously. The piles that were used to secure the Britannia template were driven in clay with low permeability, we limit ourselves to the theory of consolidation for undrained deformations (Verruijt, 2008).

The basic equations of elastodynamics for homogeneous bodies, expressed in cylindrical coordinates are the Navier equations (3.45):

$$\begin{aligned} \frac{\partial \sigma_{rr}}{\partial r} + \frac{1}{r} \frac{\sigma_{r\theta}}{\partial \theta} + \frac{\partial \sigma_{rz}}{\partial z} + \frac{\sigma_{rr} - \sigma_{\theta\theta}}{r} &= \rho \frac{\partial^2 u}{\partial t^2} \\ \frac{\partial \sigma_{r\theta}}{\partial r} + \frac{1}{r} \frac{\sigma_{\theta\theta}}{\partial \theta} + \frac{\partial \sigma_{\theta z}}{\partial z} + \frac{2}{r} \sigma_{r\theta} &= \rho \frac{\partial^2 v}{\partial t^2} \\ \frac{\partial \sigma_{rz}}{\partial r} + \frac{1}{r} \frac{\sigma_{\theta z}}{\partial \theta} + \frac{\partial \sigma_{zz}}{\partial z} + \frac{1}{r} \sigma_{rz} &= \rho \frac{\partial^2 w}{\partial t^2} \end{aligned} \quad (3.45)$$

in which u , v and w are the displacement in radial (r), tangential (θ) and vertical (z) direction respectively.

The following derivations of the influence of soil on pile deformations all consider the soil to consist of thin horizontal layers that extend to infinity. Each thin layer possesses inertia and captures energy in the form of radiation spreading. A drawback of this model is the fact that it is not able to capture the vertical vibration modes of the soil layer, as only horizontal variations are taken into account. Besides, this model assumes that all thin layers displace simultaneously, therefore assuming no shear stress between soil layers. This model therefore underestimates the stiffness and damping characteristics of the real situation.

3.3.1. HORIZONTAL INTERACTION ALONG PILE SHAFT

Consider the case of a cylinder that is placed within a thin horizontal plate in the $r - \theta$ plane, the Navier equations (3.45) can be simplified into (3.46).

$$\begin{aligned} \frac{\partial \sigma_{rr}}{\partial r} + \frac{1}{r} \frac{\sigma_{r\theta}}{\partial \theta} + \frac{\sigma_{rr} - \sigma_{\theta\theta}}{r} &= \rho \frac{\partial^2 u}{\partial t^2} \\ \frac{\partial \sigma_{r\theta}}{\partial r} + \frac{1}{r} \frac{\sigma_{\theta\theta}}{\partial \theta} + \frac{2}{r} \sigma_{r\theta} &= \rho \frac{\partial^2 v}{\partial t^2} \end{aligned} \quad (3.46)$$

A solution to these differential equations, in the case with an imposed displacement of the cylinder wall at $r = r_0$, was derived by Baranov (1967). The displacement of the cylinder wall can be expressed as (3.47) and (3.48).

$$u(r_0, \theta, t) = F(r_0) \cdot \cos \theta \cdot \cos \omega t \quad (3.47)$$

$$v(r_0, \theta, t) = F(r_0) \cdot \sin \theta \cdot \cos \omega t \quad (3.48)$$

The solution to this differential equation can be rewritten in terms of the forces acting on the pile, due to the imposed deformation as in:

$$q_{h,soil} = G(S_{u1} + i \cdot S_{u2}) \cdot u(z, t) \quad (3.49)$$

in which G is the shear modulus of the soil, i is the imaginary unit and S_{u1} and S_{u2} are parameters that describe the influence of (dimensionless) frequency on the pile vibrations. These are the real (S_{u1}) and imaginary (S_{u2}) part of the complex function as derived by Baranov (1967):

$$S_u(a_0, \nu_s) = 2\pi a_0 \times \frac{\frac{1}{\sqrt{q}} H_2^{(2)}(a_0) \cdot H_1^{(2)}(x_0) + H_1^{(2)}(x_0) \cdot H_1^{(2)}(a_0)}{H_0^{(2)}(a_0) \cdot H_2^{(2)}(x_0) + H_0^{(2)}(x_0) \cdot H_2^{(2)}(a_0)} \quad (3.50)$$

in which $a_0 = r_0\omega\sqrt{\rho_s/G}$, r_0 = pile radius, $q = (1 - 2\nu)/2 \cdot (1 - \nu_s)$, ω = radial frequency, ρ_s , ν_s = Poisson's ratio of the soil, $x_0 = a_0\sqrt{2}$ and $H_n^{(2)}$ = *Hankel* functions of the second kind of order n .

The spring and damping coefficients that are used in (3.7) can be determined as:

$$k_L^s = G \cdot \text{Re} [S_u(a_0, \nu_s)] \quad (3.51)$$

$$c_L^s = G \cdot \frac{1}{\omega} \text{Im} [S_u(a_0, \nu_s)] \quad (3.52)$$

The expression of the spring and damper characteristics of the soil is dependent on the dimensionless frequency a_0 Novak (1974). This frequency dependence is most clearly present for dimensionless frequencies below $a_0 = 0.2$, which for the pile considered corresponds to 4.5 Hz. For vibration frequencies above 4.5 Hz, the spring and damping characteristics of the soil are roughly constant. If all natural frequencies of the pile system are above this frequency, the stiffness and damping characteristics can be assumed frequency independent.

3.3.2. VERTICAL INTERACTION ALONG PILE SHAFT

The vertical interaction between the pile and the soil is modelled in a similar way as the horizontal interaction was modelled by considering only shear stresses along the perimeter of the pile (3.53).

$$\frac{\partial \sigma_{rz}}{\partial r} + \frac{1}{r} \sigma_{rz} = \rho \frac{\partial^2 w}{\partial t^2} \quad (3.53)$$

Again, the boundary conditions can be expressed as an imposed vibration at a known frequency at the cylinder boundary and the condition that no waves should propagate towards the pile. (Beredugo and Novak, 1972; Novak, 1974; Verruijt, 2008) The soil reaction to an imposed displacement $w(z, t)$ can be expressed as (3.54).

$$q_{v,soil} = G (S_{w1} + i \cdot S_{w2}) \cdot w(z, t) \quad (3.54)$$

Parameters S_{w1} and S_{w2} can be determined with the following functions:

$$S_{w1} = 2\pi a_0 \times \frac{J_1(a_0) \cdot J_0(a_0) + Y_1(a_0) \cdot Y_0(a_0)}{J_0^2(a_0) + Y_0^2(a_0)} \quad (3.55)$$

$$S_{w2} = \frac{4}{J_0^2(a_0) + Y_0^2(a_0)} \quad (3.56)$$

In which J_n and Y_n are *Bessel* functions of order n of the first kind and second kind, respectively. The spring and damping coefficients that are used in (3.1) can be determined as:

$$k_A^s = G \cdot S_{w1}(a_0, \nu_s) \quad (3.57)$$

$$c_A^s = G \cdot \frac{1}{\omega} S_{w2}(a_0, \nu_s) \quad (3.58)$$

Similar as the soil reaction to lateral deformations, the frequency dependence of the soil reaction for vertical deformations is most apparent below a dimensionless frequency $a_0 = 0.2$.

3.3.3. NONLINEARITY

Up to now it has been assumed that the soil behaves as a linear elastic material along the shaft of the pile. This would mean that the pile will return to its initial position after the response of a particular blow has damped out. In reality, the pile would slip past the soil when the ultimate shear stress is exceeded, and it will stick to the soil again when the wave has passed. This effect is obviously most apparent in the vertical displacement of the pile. It could be important to model the influence of the increasing shear strength of soil, as it influences the magnitude of the reflective waves as they pass the soil layers.

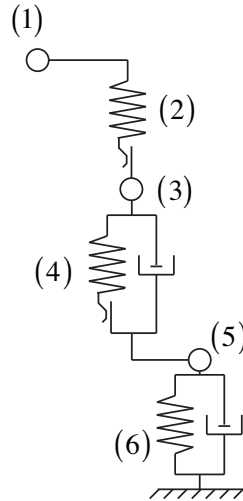


Figure 3.5: The non-linear pile-soil interaction model as described by Naggar and Novak (1994). Here: (1): pile node; (2): stick-slip spring; (3): inner soil element; (4): non-linear soil spring; (5): outer soil element and (6): linear soil spring.

The ultimate shear strength of soil varies with the penetration depth of the pile, while the elasticity moduli for homogeneous soil may be assumed constant. Offshore and onshore, friction along the soil column can be measured using a cone penetration test. The results of this test may be used to determine the final penetration and will generate a rough estimate of the amount of energy required to drive a pile up to its final depth.

Naggar and Novak (1994) used three springs and two elements to model the influence of soil on the dynamic axial response of the pile, see Figure 3.5. First of all a slip spring that connects the pile to the inner element; when the ultimate shear stress is exceeded, the spring is disconnected and this ultimate shear stress is applied to the pile. The inner element is connected to the outer element by a non-linear spring. This non-linear spring describes the region close to the pile at which the ultimate shear stress is exceeded. The outer element is connected to an outer linear spring, that describes the region where low shear stresses occur. They incorporated hysteretic soil behaviour by assuming that the stiffness in the unloading phase is equal to the elastic stiffness.

A simple model to implement the increasing strength of the soil along the height of the column is to use linear springs and increase the stiffness and the damping characteristics of the soil with the penetrated length. Most kinetic energy will be captured by the springs at larger penetrations. Another option is to choose non-linear springs that capture the slipping effect along the pile perimeter. The function that seems to fit the smoothing effect on the stress-strain relation of soil well is the arctangent.

However, it has been decided to exclude the non-linear soil effects on the shaft of the pile in this model. The main interest of this study is in the load transfer between the lateral vibrations of the pile and the pile sleeve. The axial vibrations have mainly been modelled to capture the force input from the hammer correctly. This force input can only be implemented as long as reflective waves that originate from the pile/soil interaction have not reached the hammer.

3.3.4. VERTICAL INTERACTION AT PILE TIP

Many authors modelled the response of soil on the pile tip as the reaction of an elastic half-space that is loaded harmonically by a massless rigid disk. (Lysmer and Richart, 1966; Beredugo and Novak, 1972; Gazetas and Dobry, 1984; Dobry and Gazetas, 1986). It is widely assumed that the effect of soil on embedded foundations, whether it be pile tips or other arbitrary foundations, can be modelled using the assumption that dynamic reactions of the pile tip are equal to dynamic reactions of an elastic half

space. Pile tip damping is modelled as (3.59).

$$\begin{aligned}k_A^t &= \frac{4G \cdot D}{1 - \nu} \\c_A^t &= \rho A \cdot \left[\frac{3.4}{\pi(1 - \nu_s)} \cdot V_s \right]\end{aligned}\tag{3.59}$$

3.4. HYDRAULIC INFLUENCE

3.4.1. HYDROSTATICS

The piles for the project considered were driven at 136 m below sea level. The ambient pressure from the hydrostatic head is roughly 14 times higher than the ambient pressure at sea level, this influences the amount of pressure required to keep the hammer sleeve water-free during driving. Water creates buoyant forces on all steel sections, leading to lower static displacements with respect to the situation in air. As far as the author is aware, the hydrostatic pressure does not have an influence on the dynamics of the structures.

3.4.2. HYDRODYNAMICS

Water may have a significant influence on the out of plane motions of the pile. As the pile accelerates in one direction, it will also accelerate the water that is entrapped within and surrounded by the pile. Hydraulic influences on cylindrical structures are generally applied with Morison's equation (3.60) (Morison et al., 1950).

$$F_{Morison} = \rho_w \frac{\pi}{4} C_M D^2 \cdot \frac{\partial^2 u}{\partial t^2} + \frac{1}{2} \rho_w D \cdot C_D \cdot \frac{\partial u}{\partial t} \left| \frac{\partial u}{\partial t} \right| \quad (3.60)$$

In which ρ_w is the density of water, C_M and C_D are dimensionless force coefficients for inertia and drag respectively.

Morison's equation considers a linear elastic inertia force (commonly referred to as added mass or hydraulic inertia) and a quadratic drag force (commonly referred to as added damping or hydraulic damping). It is generally applicable for slender cylinders where the pile diameter is 10% to 20% of the wave length. Consider the situation where no current or waves is present and all deformations of the pile are induced by the hammer blow. In this case, the amplitude of vibration is small (order of millimeters) with respect to the diameter (approximately one meter) of the structure which implies that Morison's equation can not simply be used for this situation.

Characteristics of water flow around a body are generally expressed using dimensionless numbers such as, but not limited to, the Reynolds number and Keulegan-Carpenter number. The Reynolds number (3.61) gives the ratio between inertia and viscous forces and the Keulegan-Carpenter number (3.62) gives the ratio between drag forces over inertia forces.

$$Re = \frac{\dot{u} \cdot D}{\nu} \quad (3.61)$$

$$KC = \frac{\dot{u} \cdot T}{D} \quad (3.62)$$

In the numbers presented above, \dot{u} is the velocity of the motion, D is the diameter of the element, g the gravitational constant, T the period of the motion and ν the kinematic viscosity of the fluid.

The flow velocity is in the order of decimeters per second, the diameter is approximately 1 meter and the period of vibration is in the order of tens of milliseconds. Given this, the dimensionless numbers can be estimated. It is found that the Reynolds number is in the order of 10^5 and the Keulegan-Carpenter number in the order of 10^{-3} . These numbers tell that the flow around the cylinder due to the hammer blow is inertia dominated, a practical application is that the influence of drag can be neglected (Journée and Massie, 2001).

The effect of hydrodynamics on the deformation of the template is neglected for convenience, as the implementation of this effect into the model is complex and time was a constraint.

HYDRAULIC INERTIA

The added mass term in Morison's equation (3.60) can be implemented by simply adding the inertia term (3.63)

$$\rho_w \frac{\pi}{4} C_M D_i^2 \quad (3.63)$$

to the existing mass term in (3.7).

3.5. TEMPLATE MODEL

The template structure consists of two distinguishable parts. The top part consists of tubular conductors that are interconnected by thick steel elements. Three vertical jacks connect the top part to a large skidded mud-mat, this mud-mat ensures vertical stability of the template structure during installation.

The elements that connect the nodes are very thick H -beam-like structures, in which the height of the structure in some elements is almost equal to its length. The definition of a beam is that two dimensions are small with respect to the third dimension, beam theory can therefore be used as waves are assumed to propagate in one direction only. All three dimensions of some elements of the template structure are in the same order of magnitude, therefore a one-dimensional vibration theory is unlikely to hold. A better means of describing the elements is by considering the two flanges and web as two-dimensional plates. A plate is defined by a solid body that is bounded by two surfaces. The distance between the surfaces, or thickness of the plate, is assumed smaller than the dimensions in the other two directions. For thickness/width ratios smaller than $\frac{1}{20}$, thin plate theory should be used as the effect of shear deformation of the plate is small with respect to the effect of bending deformation. (Rao, 2007)

Despite the fact that the two-dimensional theories are preferred over one-dimensional theories, time constraints limited the implementation of the two-dimensional theories. The deformations of the elements have therefore been modelled using one-dimensional theories only. The lateral deformations of the element are described with Timoshenko's theory and the longitudinal deformations of the element are described with Rayleigh-Love's theory. Torsional deformations include the effect of bending of the flanges that is observed in open cross-sections (Timoshenko, 1945).

All pile and well conductors are formed by shell like structures, each support pile conductor has a shell thickness of 2.5 times the pile wall thickness. The shell-like structures are stiffened with circular plates around the perimeter, these circular plates are directly welded onto the flanges of the connective elements. Each circular plate being 1.5 times thicker than the flange of the connective element. Vertical stiffener plates connect the circular plates along the perimeter of the tube.

The dimensions of the conductors imply a stiff structure, with respect to the stiffness of the pile and with respect to the connective elements. Therefore, it is assumed that the deformations of the conductors are governed by the deformations of the connecting elements. Each conductor is simplified as a mass containing rigid body.

The top frame of the template rests on three jacks, see $J1-J3$ in Figure 3.6 and 3.7. The jack housing consists of a small cylinder that is stiffened by two circular plates. Encased within this cylinder is the jack, which is simply supported on the mud-mat. The jacks can be simplified as three tubular elements, they can be modelled with the same theories as used to model the beam elements.

As the template is modelled as a three-dimensional structure in which rigid bodies are interconnected by beams, solving the complex formulation analytically would be a cumbersome process. As FDM is generally used for simple, one-dimensional formulations such as the pile structure described in Section 3.1, a FEM formulation of the problem would be more appropriate in this situation.

3.5.1. GOVERNING EQUATIONS

Each beam element may deform in longitudinal direction, in lateral direction and it may twist. In this section, the differential equations that accompany the one-dimensional theories considered are presented. The derivation of these theories is included in Appendix A. The finite element formulations and the derivation of the finite element formulations are included in Appendix C.

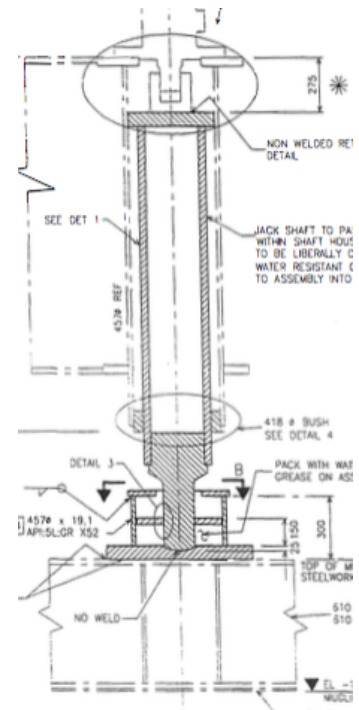


Figure 3.6: An impression of the jacks within the jack housing, left and right are the connecting elements.

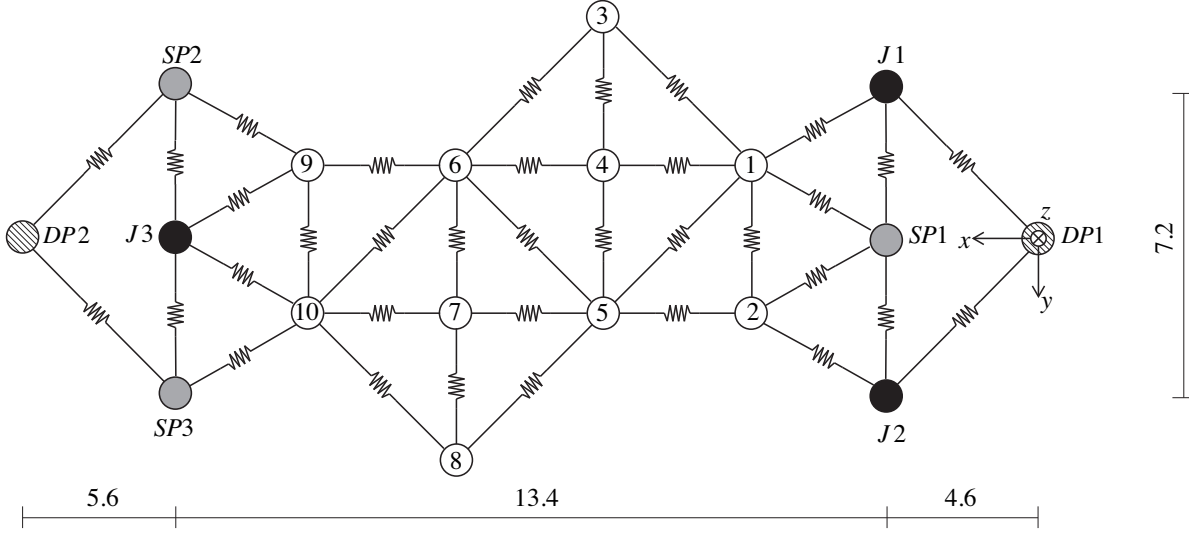


Figure 3.7: Top view of the proposed model for the Britannia template. The well conductors are numbered 1 to 10; the positions of the three jacks are indicated in black and numbered J1 to J3; the position of the supporting pile sleeves are indicated in grey and numbered SP1 to SP3; the position of the docking pile sleeves are indicated with hatches and numbered DP1 to DP2. Measures are in meters.

AXIS DEFINITION

Consider an element with its longitudinal axis in the global x -direction. Its displacement in longitudinal direction will be named u , its displacement in the horizontal transverse direction is v and its displacement in the vertical transverse direction is w . Positive rotations can be found by using the right-hand rule and will be named θ , ϕ and ψ for rotation around the x , y and z respectively.

LONGITUDINAL VIBRATIONS

As presented in Sections 3.1 and 3.2 in this chapter, the longitudinal deformation of the beam is modelled using Rayleigh-Love theory for axial vibration. The differential equation that formulates the problem for element i is shown in equation (3.64).

$$\rho A_i \frac{\partial^2 u_i}{\partial t^2} - \rho \nu^2 I_{P,i} \frac{\partial^4 u_i}{\partial x^2 \partial t^2} - E A_i \frac{\partial^2 u_i}{\partial x^2} = 0 \quad (3.64)$$

LATERAL VIBRATIONS

Unlike the formulation of the lateral vibrations of the pile, shear deformation is included in the formulation of the lateral vibrations of the elements that connect conductors. The problem for displacement in the z direction and rotation around the y -axis for element i can be described by the two second order differential equations as (3.65) and (3.66).

$$\rho A_i \frac{\partial^2 w_i}{\partial t^2} - \kappa_{z,i} A_i G \left(\frac{\partial^2 w_i}{\partial x^2} - \frac{\partial \phi_i}{\partial x} \right) = 0 \quad (3.65)$$

$$\rho I_{y,i} \frac{\partial^2 \phi_i}{\partial t^2} - \kappa_{z,i} A_i G \left(\frac{\partial w_i}{\partial x} - \phi_i \right) - E I_{y,i} \frac{\partial^2 \phi_i}{\partial x^2} = 0 \quad (3.66)$$

The definition of the differential equations for lateral vibrations in the y direction are (3.67) and (3.68).

$$\rho A_i \frac{\partial^2 v_i}{\partial t^2} - \kappa_{y,i} A_i G \left(\frac{\partial^2 v_i}{\partial x^2} - \frac{\partial \psi_i}{\partial x} \right) = 0 \quad (3.67)$$

$$\rho I_{z,i} \frac{\partial^2 \psi_i}{\partial t^2} - \kappa_{y,i} A_i G \left(\frac{\partial v_i}{\partial x} - \psi_i \right) - E I_{z,i} \frac{\partial^2 \psi_i}{\partial x^2} = 0 \quad (3.68)$$

In these equations, I_y and I_z are the area moments of inertia around the y and z axis respectively, κ_y and κ_z are the shear coefficients in y and z directions respectively. The shear coefficient is dependent on the geometry of the cross section and can be derived by dividing the total shear stress on a cross section by the product of the shear coefficient and the cross sectional area.

TORSIONAL VIBRATIONS

Torsional vibrations of an open element, such as element i considered here, can be described by (3.69). This is a fourth order equation of which the fourth order derivative describes the warping effect.

$$\rho I_{x,i} \frac{\partial^2 \theta_i}{\partial x^2} - GI_P \frac{\partial^2 \theta_i}{\partial x^2} + EI_{fl,z,i} \frac{h_i^2}{2} \frac{\partial^4 \theta_i}{\partial x^4} = 0 \quad (3.69)$$

In this equation, I_x is the area moment of inertia of element i around the x -axis, $I_{fl,z,i}$ is the moment of inertia of the flanges of element i around the z -axis and h_i is the distance between the centres of gravity of the two flanges. The last term describes the effect of flange bending while the second term describes the the torsional shear stiffness.

BOUNDARY CONDITIONS

Each element is bounded to a cylindrical conductor, these conductors are assumed infinitely stiff which means that force and moment equilibrium in and around all three directions must exist. The beams are connected to the conductor at a certain distance from the centre of the conductor, the influence of this so-called offset needs to be taken into account at all element boundaries. The method used to implement it is described in Appendix C.

As briefly described above, the jacks are assumed simply supported at the mud-mat. This means that they are restricted to translate and free to rotate in all directions, given that the displacements are small with respect to the dimensions of the members.

3.6. PILE - TEMPLATE INTERFACE

The pile sleeve is modelled as a rigid body that is able to deform in and around the three directions. Each pile sleeve is connected to two or more elements that influence all motions of the pile. The interaction between pile and template can, as far as the author is aware, be modelled using two different mechanisms.

The first mechanism is shown in the mechanics scheme (right) of Figure 3.8 by means of a continuous set of springs. It is based on the assumption that the pile and sleeve can vibrate in different frequencies. The spring stiffness is influenced, among other things, by the ability of both the sleeve and the pile to deform in radial and tangential directions. A major advantage of this method is the fact that it is relatively easy to mathematically describe the connection and disconnection of the pile with the pile sleeve; by implementing slight alterations of the governing equations. However, the deformation of the pile and sleeve in radial and tangential directions is unknown, an attempt to derive the stiffness is done in Section 3.6.1.

Second, the pile and sleeve can be joined along the length of the pile sleeve, leaving out the need to define the unknown magnitude of the continuous springs ((4) in Figure 3.8). With this method it becomes more complex to model the disconnection of the pile from the pile sleeve as the pile and template are joined in one system.

It is unlikely that the pile and pile sleeve remain in contact for the full duration of the vibrations, therefore the first mechanism is preferred for its relative simplicity in modelling this disconnection. The load exerted on the pile, shown by $q_{h,template}$ in Figure 3.2, can mathematically be described with (3.70). In this equation, $H(u)$ denotes the Heaviside step function, x and ϕ are the horizontal displacement and the rotation of the pile sleeve and $u(z, t)$ is the horizontal displacement of the pile. K denotes the stiffness of the interaction between pile and sleeve.

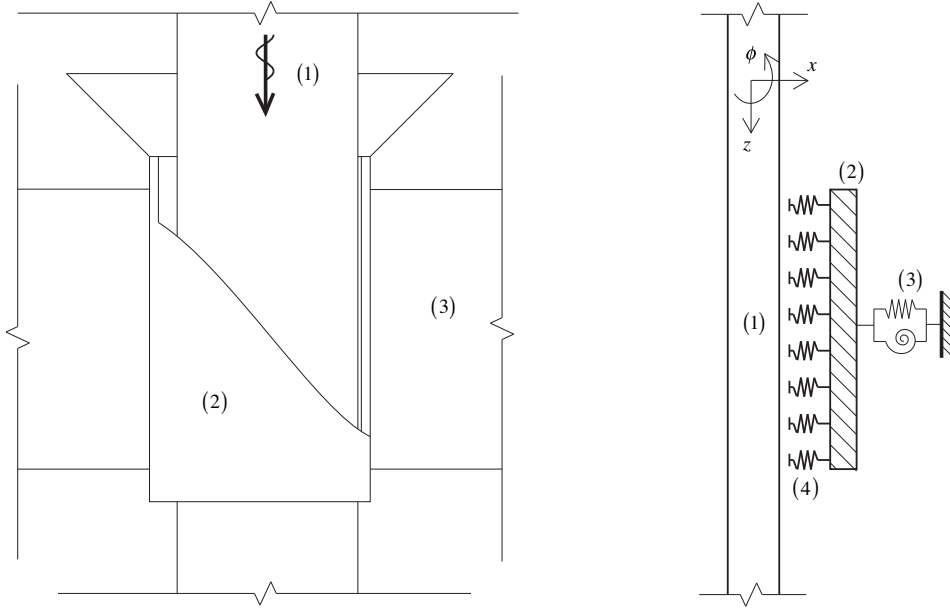


Figure 3.8: Left: overview drawing of the pile (1), pile sleeve (2) and connecting elements (3) and right: mechanics scheme of the situation in which (4) shows the continuous springs that describe the interaction between pile and sleeve upon contact.

$$q_{h,template}(z, t) = -K \cdot \{u(z, t) - (x - z \cdot \phi)\} \cdot H(u(z, t) - (x - z \cdot \phi)) \quad (3.70)$$

The force (F_x) and moment (M_y) that load the pile sleeve can be expressed in terms of the horizontal load on the pile as (3.71). In this equation, z_0 and z_1 are the top and bottom of the contact area of the pile sleeve.

$$F_x(t) = - \int_{z_0}^{z_1} q_{h,template}(z, t) dz \quad M_y(t) = - \int_{z_0}^{z_1} z \cdot q_{h,template}(z, t) dz \quad (3.71)$$

The implementation of the pile - template interface into the numerical models is included in Appendix C.

3.6.1. STIFFNESS OF THE INTERACTION

The interaction between pile and pile-sleeve can be modelled using the interaction stiffness K in (3.70). The value for this interaction is difficult to find, as it is dependent on several variables. These variables include the frequency of loading, the contact area size, the contact area variation along the vertical and circumferential directions and especially the position of the load with respect to the boundaries.

In the case considered, the sleeve is stiffened in radial and vertical directions. The cylindrical section of the sleeve is 2.5 times thicker than the pile (2.5 inch versus 1 inch). In order to make a simplified assumption for the stiffness, it is assumed that the deformation of the interaction is dominated by the deformation stiffness of the pile (or: the radial shell stiffness).

The radial shell stiffness is approximated by considering a thin cylindrical shell of length L , radius R and wall thickness h as in Figure 3.10. The shell is loaded by an harmonic unit load $F(\theta, z, t)$ over a length of 1 m. Radial displacement caused by this load gives an approximation of the stiffness at this location¹. The real situation of a pile sticking out of the soil more closely resembles a clamped-fixed cylindrical shell. This situation is however more difficult to approximate analytically as the axial mode shapes are not simply harmonic functions but a combination of harmonic and hyperbolic functions. The interest here is how the shell deforms in radial direction (u_r), it is assumed that the situation sketched in Figure 3.10 gives a reasonable approximation.

The magnitude of the load is likely to differ over the circumference, as is shown in Figure 3.9. In the case considered, the pile is loaded over an angle of 2α and over a length of 1 m. The shape of the load in circumferential direction is approximated with a squared cosine, as shown in (3.72). The integral of this equation over the circumference and over the length of the pile gives unity.

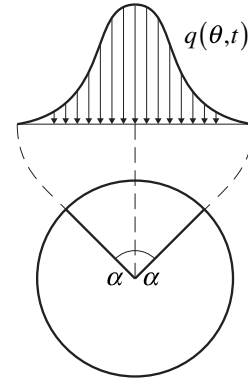


Figure 3.9: Cross-section that shows the variation in loading along the circumference.

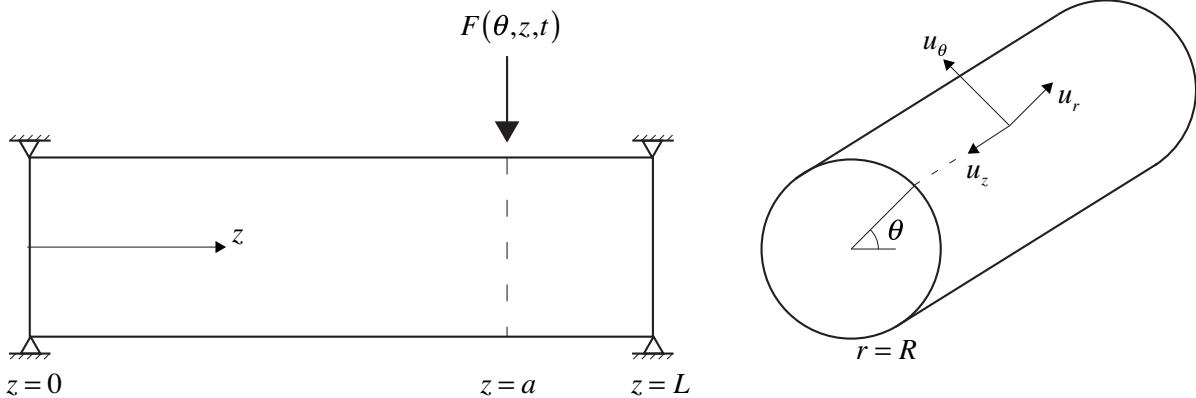


Figure 3.10: Thin cylindrical shell used to derive local radial shell stiffness.

$$F(z, \theta, t) = \begin{cases} \frac{1}{\alpha} \cos^2\left(\frac{\pi}{2\alpha}\theta\right) \cos \omega t & -\alpha < \theta < \alpha \quad a - \frac{1}{2} < z < a + \frac{1}{2} \\ 0 & \text{else} \end{cases} \quad (3.72)$$

Suppose the pile is described by Reissner's theory for thin cylindrical shells, of which the equations of motion are defined by (3.73). The derivation of this theory can be found in Leissa (1973) or other

¹In order to determine the shell deformation, the circumferential rigid body mode, $n = 1$ in (3.84)-(3.86), should be excluded.

works.

$$\begin{bmatrix} L_{11} & L_{12} & L_{13} \\ L_{21} & L_{22} & L_{23} \\ L_{31} & L_{32} & L_{33} \end{bmatrix} \times \begin{bmatrix} u_z(z, \theta, t) \\ u_\theta(z, \theta, t) \\ u_r(z, \theta, t) \end{bmatrix} = \begin{bmatrix} 0 \\ 0 \\ F(z, \theta, t) \end{bmatrix} \quad (3.73)$$

in which the stiffness and inertia operators as a function of the vibration frequency ω are

$$L_{11} = \frac{Eh}{1-\nu^2} \left(\frac{\partial^2}{\partial z^2} + \frac{1-\nu}{2R^2} \frac{\partial^2}{\partial \theta^2} \right) + \omega^2 \rho h \quad (3.74)$$

$$L_{12} = L_{21} = \frac{Eh}{2R(1-\nu)} \frac{\partial^2}{\partial z \partial \theta} \quad (3.75)$$

$$L_{13} = L_{31} = \frac{Eh\nu}{R(1-\nu^2)} \frac{\partial}{\partial z} \quad (3.76)$$

$$L_{22} = \frac{Eh}{R^2(1-\nu^2)} \left(1 + \frac{h^2}{12R^2} \right) \frac{\partial^2}{\partial \theta^2} + \frac{2Eh}{R^2(1+\nu)} \left(1 + \frac{h^2}{12R^2} \right) \frac{\partial^2}{\partial z^2} + \omega^2 \rho h \quad (3.77)$$

$$L_{23} = L_{32} = \frac{Eh}{R^2(1-\nu^2)} \left(\frac{\partial}{\partial \theta} - \frac{h^2}{12} \frac{\partial^3}{\partial z^2 \partial \theta} - \frac{h^2}{12R^2} \frac{\partial^3}{\partial \theta^3} \right) \quad (3.78)$$

$$L_{33} = \frac{Eh}{1-\nu^2} \left(1 + \frac{h^2}{12} \frac{\partial^4}{\partial z^4} + \frac{h^2}{6R^2} \frac{\partial^4}{\partial z^2 \partial \theta^2} + \frac{h^2}{12R^4} \frac{\partial^4}{\partial \theta^4} \right) - \omega^2 \rho h \quad (3.79)$$

The displacement field must satisfy the boundary conditions (3.80)-(3.83) at both ends of the pile.

$$u_\theta(0, \theta, t) = u_\theta(L, \theta, t) = 0 \quad (3.80)$$

$$u_r(0, \theta, t) = u_r(L, \theta, t) = 0 \quad (3.81)$$

$$N_{zz}(0, \theta, t) = N_{zz}(L, \theta, t) = \frac{\partial u_z}{\partial z} + \frac{\nu}{R} \left(\frac{\partial u_\theta}{\partial \theta} + u_r \right) = 0 \quad (3.82)$$

$$M_{zz}(0, \theta, t) = M_{zz}(L, \theta, t) = -\frac{\partial^2 u_r}{\partial z^2} + \frac{\nu}{R^2} \left(\frac{\partial u_\theta}{\partial \theta} - \frac{\partial^2 u_r}{\partial \theta^2} \right) = 0 \quad (3.83)$$

The functions (3.84)-(3.86) are assumed to satisfy these boundary conditions.

$$u_z(z, \theta, t) = \sum_m \sum_n U_{zmn} \cos \frac{m\pi z}{L} \cos n\theta \cos \omega t \quad (3.84)$$

$$u_\theta(z, \theta, t) = \sum_m \sum_n U_{\theta mn} \sin \frac{m\pi z}{L} \sin n\theta \cos \omega t \quad (3.85)$$

$$u_r(z, \theta, t) = \sum_m \sum_n U_{rmn} \sin \frac{m\pi z}{L} \cos n\theta \cos \omega t \quad (3.86)$$

in which m and n denote the longitudinal and circumferential vibration modes respectively. Now, the next step would be to describe the force $F(z, \theta, t)$ as Fourier series, in terms of the radial vibration modes (3.87).

$$F(z, \theta, t) = \sum_{n=1}^{\infty} \sum_{m=1}^{\infty} f_{rmn} \cdot \sin \frac{m\pi z}{L} \cdot \cos n\theta \cdot \cos \omega t \quad (3.87)$$

in which the amplitude of the radial force is found as

$$f_{rmn} = \int_0^L \int_{-\pi}^{\pi} F(z, \theta) \cdot \left\{ \frac{2}{L} \sin \frac{m\pi z}{L} \right\} \cdot \left\{ \frac{1}{\pi} \cos n\theta \right\} d\theta dz \quad (3.88)$$

It is possible to describe the force amplitude f_{rmn} in terms of the real amplitudes U_{zmn} , $U_{\theta mn}$ and U_{rmn} for a certain vibration mode m, n and frequency ω using matrix \hat{L} .

$$\begin{bmatrix} \hat{L}_{11} & \hat{L}_{12} & \hat{L}_{13} \\ \hat{L}_{21} & \hat{L}_{22} & \hat{L}_{23} \\ \hat{L}_{31} & \hat{L}_{32} & \hat{L}_{33} \end{bmatrix}_{mn\omega} \times \begin{bmatrix} U_{zmn} \\ U_{\theta mn} \\ U_{rmn} \end{bmatrix} = \begin{bmatrix} 0 \\ 0 \\ f_{rmn} \end{bmatrix} \quad (3.89)$$

The stiffness and inertia operators in terms of the vibration modes and frequency are

$$\hat{L}_{11} = \frac{Eh}{1-\nu^2} \left(\left(\frac{m\pi}{L} \right)^2 + \frac{1-\nu}{2R^2} n^2 \right) + \omega^2 \rho h \quad (3.90)$$

$$\hat{L}_{12} = \hat{L}_{21} = \frac{Eh}{2R(1-\nu)} \left(\frac{nm\pi}{L} \right) \quad (3.91)$$

$$\hat{L}_{13} = \hat{L}_{31} = \frac{Eh\nu}{R(1-\nu^2)} n \quad (3.92)$$

$$\hat{L}_{22} = \frac{Eh}{R^2(1-\nu^2)} \left(1 + \frac{h^2}{12R^2} \right) n^2 + \frac{2Eh}{R^2(1+\nu)} \left(1 + \frac{h^2}{12R^2} \right) \left(\frac{m\pi}{L} \right)^2 + \omega^2 \rho h \quad (3.93)$$

$$\hat{L}_{23} = \hat{L}_{32} = \frac{Eh}{R^2(1-\nu^2)} \left(n - \frac{h^2}{12} \left(\frac{m\pi}{L} \right)^2 n - \frac{h^2}{12R^2} n^2 \right) \quad (3.94)$$

$$\hat{L}_{33} = \frac{Eh}{1-\nu^2} \left(1 + \frac{h^2}{12} \left(\frac{m\pi}{L} \right)^4 + \frac{h^2}{6R^2} \left(\frac{nm\pi}{L} \right)^2 + \frac{h^2}{12R^4} n^4 \right) - \omega^2 \rho h \quad (3.95)$$

Eventually we're interested in the radial displacement due to the unit load. The inverse of this displacement gives an indication of the stiffness. Cramer's rule can be used to find an efficient solution, in which the radial displacement amplitude U_{rmn} can be expressed in terms of the modes and frequency. The displacement amplitude at $\theta = 0$ and $x = a$ is

$$u_r(a, 0) = \sum_{n=2}^N \sum_{m=1}^M U_{rnm} \sin \left(\frac{m\pi}{2} \right) \quad (3.96)$$

in which

$$U_{rnm} = \frac{\det \hat{L}_3}{\det \hat{L}} \quad \text{and} \quad \hat{L}_3 = \begin{bmatrix} \hat{L}_{11} & \hat{L}_{12} & 0 \\ \hat{L}_{21} & \hat{L}_{22} & 0 \\ \hat{L}_{31} & \hat{L}_{32} & f_{rmn} \end{bmatrix} \quad (3.97)$$

The stiffness due to the unit load will therefore be

$$K(\omega) = \frac{1}{u_r(a, 0, \omega)} \quad (3.98)$$

Chapter 4

Verification and Validation

This chapter contains the steps and results associated with the verification and validation of the individual parts of the model. Validation of the model is essential, as an unvalidated model can not be used to draw conclusions with full confidence. The main function of a model is to help the users of the model in decision making, these decisions can not be made based on a model that does not resemble reality.

Verification of a model can be defined as "ensuring that the computer program of the computerised model and its implementations are correct" (Sargent, 2005). The purpose of verification of a model is finding and fixing modelling errors. Verification of the pile model has been done by verifying the natural frequencies of the model with analytically derived natural frequencies. The template model has been verified by comparing static displacements with static displacements of the same model, but modelled with commercial software. In order to yield the same displacements, the mass and stiffness distribution in the model needs to comply.

Validation of the model has been attempted by quantitatively comparing the force input from the hammer with measured data. The shape of the force input function is important as steeper and narrower peaks in the force-time diagram may yield larger accelerations. This is important as acceleration data on the template was available to validate the template motions.

4.1. VERIFICATION OF THE PILE MODEL

Verification of the model that describes longitudinal and lateral vibration in the pile, is performed by evaluating the natural frequencies and resonance frequencies of both pile systems. The methods to derive these natural frequencies are described in Appendices B. The conditions for a verified model are:

- First of all, all undamped natural frequencies should be harmonic. The resulting set of eigenvalues should contain imaginary values only.
- Secondly, all damped natural frequencies should contain a negative real part. Positive real eigenvalues indicate a gain in energy for that certain mode of vibration. This represents an unphysical situation as the amount of energy input to the system is controlled by the hammer.

When above items passed, the method can further be verified by comparing the natural frequencies of a simplified model with analytically found natural frequencies of a similar system. Here, the system shown in Figure 3.2 is taken as a reference. In order to simplify this step; the influence of the template, the soil influence at the pile-tip and the damping characteristics of the soil have been discarded. The aim of this step is to verify if the numerical method describe the same situation as the analytically obtained situation.

	40 m		50 m	
	Analytic	FDM	Analytic	FDM
1		146.2112		183.4468
2	330.4296	327.2763	345.2393	344.8251
3	617.3508	612.7209	619.8495	618.7551
4	906.0626	902.5022	907.8754	906.7734
5	1196.9482	1194.0323	1199.8438	1198.5206
6	1490.7604	1487.6670	1493.3564	1491.5268

Table 4.1: Comparison of the first six natural frequencies of the longitudinal motions, as determined analytically and numerically for pile penetrations of 40 m and 50 m. All values are in rad/s .

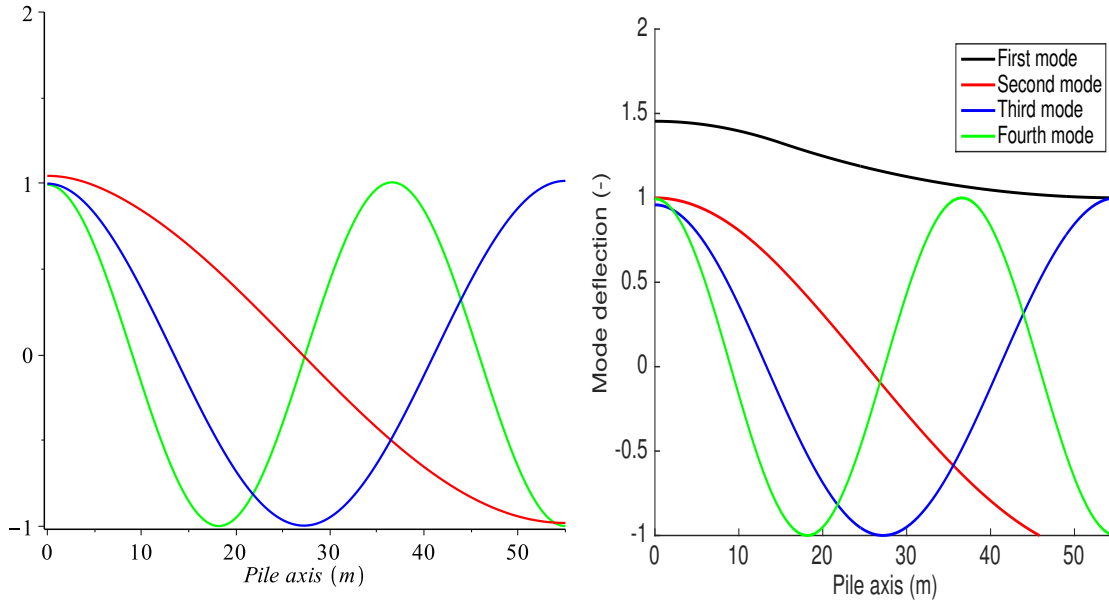


Figure 4.1: Plot of the first four axial modes of vibration, as derived with Galerkin's method (left) and FDM (right). Natural frequencies of these modes correspond to the values presented in Table 4.3 for a pile penetration of 40 m.

COMPARISON OF LONGITUDINAL NATURAL FREQUENCIES

The undamped natural frequencies have been determined using a numerical and an analytical method¹ for pile penetrations of 40 m and 50 m. The frequency dependent soil stiffness, introduced in Section 3.3, has been linearised around a radial frequency of 50 Hz. This value corresponds to the first natural frequency of the undamped and non-penetrated pile.

The first six natural frequencies of the longitudinal motion and the first four corresponding modes of vibration are presented in Table 4.3 and Figure 4.1. The differences between the analytically and numerically derived natural frequencies originate from the different handling of the frequency dependence of the soil stiffness and the method used to derive the natural frequencies. It seemed not possible to describe the first vibration mode with Galerkin's method. This mode corresponds to a rigid body motion for the non-penetrated pile. Despite this, the natural frequencies and the modes of vibration derived using both methods correspond to each other. The influence of the frequency dependence of the soil is negligible for the frequencies considered in this analysis, as all natural frequencies of the longitudinal vibration are relatively high. The magnitude of the soil stiffness can therefore rightfully be linearised around its maximal value.

¹Finite differences and Galerkin's method respectively.

	40 m			
	Analytic (1)	FDM (1)	Analytic (2)	FDM (2)
1	15.2689	15.6324	16.3158	16.7143
2	89.2535	88.4453	95.4370	97.3360
3	160.7795	156.2981	211.4512	207.4932
4		161.0423		212.3650
5	166.7718	165.6974	215.8364	215.6690

Table 4.2: Comparison of the first five natural frequencies of the lateral motions, as determined analytically and numerically for pile penetrations of 40 m. All values are in *rad/s*.

COMPARISON OF LATERAL NATURAL FREQUENCIES

The first five natural frequencies of the lateral vibration of the pile have been derived and are presented in Table 4.3. The pile model considered was a free-free beam that has been connected to lateral springs along the penetrated part of the pile, of which the governing equation is the undamped version of (3.7). The general solution of the problem is assumed in the form

$$u_i(z, t) = \sum_{n=1}^4 C_n \exp \gamma_i z \cos \omega t \quad (4.1)$$

For convenience, the origin of the pile is chosen at the interface between un-penetrated and penetrated sections. After applying the boundary conditions at $z = -L_1$ and at $z = L_2$ and the interface conditions at $z = 0$, the frequency equation is found. The frequency equation is the determinant of (4.2).

$$M = \begin{bmatrix} C_1^1 & C_1^2 & -S_1^2 & -S_1^1 \\ -S_1^2 & -S_1^1 & -C_1^2 & -C_1^1 \\ C_2^1 \cdot \gamma_1^2 / \gamma_2^2 & C_2^2 & S_2^2 \cdot \gamma_1 / \gamma_2 & S_2^1 \cdot \gamma_1^3 / \gamma_2^3 \\ S_2^1 \cdot \gamma_1^2 / \gamma_2^2 & S_2^2 & -C_2^2 \cdot \gamma_1 / \gamma_2 & -C_2^1 \cdot \gamma_1^3 / \gamma_2^3 \end{bmatrix} \quad (4.2)$$

in which

$$\begin{aligned} C_i^1 &= \cos(\gamma_i L_i) + \cosh(\gamma_i L_i) & C_i^2 &= \cos(\gamma_i L_i) - \cosh(\gamma_i L_i) \\ S_i^1 &= \sin(\gamma_i L_i) + \sinh(\gamma_i L_i) & S_i^2 &= \sin(\gamma_i L_i) - \sinh(\gamma_i L_i) \end{aligned}$$

The value L_i for $i = 1, 2$ is the un-penetrated and penetrated length respectively and γ_1 and γ_2 are the wavenumbers for the un-penetrated and penetrated sections of the beam. These wave-numbers relate to the frequency by the dispersion relations (4.3). In the dispersion relation, ω is the radial frequency, c_0 is the wave velocity in the material, k is the radius of gyration and κ is the ratio between soil stiffness and the mass per unit length of the pile. In the case considered, the soil stiffness / bending stiffness ratio was 0.92% and 1.64% for the stiffness around the first natural frequency and $\omega \rightarrow \infty$ respectively.

$$\gamma_1 = \sqrt{\frac{\omega^2}{c_0^2} + \frac{\omega}{c_0} \sqrt{\frac{1}{4} \frac{\omega^2}{c_0^2} + \frac{1}{k^2}}} \quad \gamma_2 = \sqrt{\frac{\omega^2}{c_0^2} + \sqrt{\frac{1}{4} \frac{\omega^4}{c_0^4} + \frac{(\omega^2 - \kappa)}{c_0^2} \frac{1}{k^2}}} \quad (4.3)$$

The natural frequencies in Table 4.3 have been determined for soil stiffness around the first natural frequency (1) and for the high frequency soil stiffness ($\omega \rightarrow \infty$) (2). Vibration mode number four² was not found analytically, possibly due to the high density of natural frequencies in this region. Despite this, the two methods yielded reasonably similar values for the natural frequencies.

²The mode shapes were compared.

4.2. VERIFICATION OF THE TEMPLATE MODEL

The template model is a complex structure that extends mainly in two dimensions, it has been discussed in detail in Section 3.5. The elements that connect the shell-like conductors are modelled using a finite element beam formulation. Suppose the template consists of N conductors, then the finite element formulation yields a $6N \times 6N$ mass and stiffness matrices to describe all 6 degrees of freedom. The discretised dynamic model can be described by the Eigenvalue problem in (4.4), should only contain negative Eigenvalues.

$$(K - \lambda M) \vec{x} = 0 \quad (4.4)$$

Verifying the found natural frequencies, the same way as has been done for the pile model, is not realistic as the structure is too complex. Other means to verify whether the mass and stiffness matrices describe the model correctly, is by reflecting the static displacements of this model with static displacements of a commercial FEM programme³. Table 4.2 shows the vertical and rotational displacements of the template model. The values are derived using the FEM formulations described in Appendix C and using *SACS*.

The found static displacements approximate the values derived with *SACS* with reasonable accuracy. Both models incorporate the effect of shear deformation and offsets at the nodes. Although it is attempted to keep the variables in both models consistent, a slightly different definition of the boundary conditions may explain the differences observed in Table 4.2. It has been found that *SACS* does not incorporate the effect of flange bending, which is observed in open beam cross-sections. The method that was used to define Table 4.2 also excluded this effect.

Table 4.3: Vertical displacements and rotations around the horizontal axes of the model, defined in Section 3.5. Results are derived with the methods described in Appendix C and derived with Bentley's *SACS*. Displacements are in *mm* and rotations in 10^{-3} *rad*.

Node	Vert. displ.		Rot. around x		Rot. around y	
	Model	<i>SACS</i>	Model	<i>SACS</i>	Model	<i>SACS</i>
DP1	1.5363	1.5427	-0.0013	-0.0003	-0.3629	-0.3624
DP2	1.4632	1.5019	0.1157	0.1150	0.2254	0.2288
SP1	0.4279	0.4323	0.0023	0.0022	0.1298	0.1296
SP2	0.0096	0.0322	0.1194	0.1189	0.0251	0.0281
SP3	0.8430	0.8599	0.1121	0.1110	0.0251	0.0282
J1	0.0312	0.0403	0.2139	0.2110	-0.0182	-0.0172
J2	0.0312	0.0403	-0.2164	-0.2138	-0.0094	-0.0135
J3	0.0703	0.0908	0.1151	0.1144	-0.2290	-0.2246
W1	0.7679	0.7729	0.0413	0.0405	0.1431	0.1431
W2	0.8025	0.8054	-0.0308	-0.0309	0.1710	0.1704
W3	1.0334	1.0413	-0.0172	-0.0178	0.0432	0.0438
W4	1.0546	1.0605	0.0341	0.0333	0.0405	0.0412
W5	1.2236	1.2268	0.0869	0.0859	0.0717	0.0723
W6	0.9928	1.0014	0.0643	0.0635	-0.0789	-0.0775
W7	1.2492	1.2552	0.1214	0.1204	-0.0554	-0.0539
W8	1.6736	1.6764	0.1770	0.1757	-0.0594	-0.0579
W9	0.5885	0.6017	0.0876	0.0869	-0.1640	-0.1616
W10	0.9124	0.9233	0.1349	0.1340	-0.1553	-0.1530

³In this case Bentley's *SACS*, a FEM package that is used to analyse beam formulations of jackets in particular.

4.3. VALIDATION OF THE FORCE INPUT

The only measurements that were conducted during installation of the Britannia template were accelerations on the pile sleeve, in vertical and horizontal direction. Measurements of the force input by the hammer are confidential and are not allowed to be published here. The absolute value of the maximum force, the time required to built up to the plateau value and the total duration of the pulse were quantitatively compared.

The modelled force input at the top of the follower is derived from the relative displacement of the top of the follower and the anvil, see Figure 3.4. Figure 4.3 shows the force input at the top of the follower and the normal force within the pile, in the time domain (a) and in the frequency domain (b).

This normal force has been derived by calculating the local strain and strain-velocity at this section of the pile⁴. The time needed to build up the force until its maximum value seemed rather short, with respect to what was measured. In terms of shape and magnitude, the normal force diagram at the top of the pile (Figure 4.3, dash-dotted line) resembled the measured diagram. An improvement in the modelled force can be gained only when the mass distribution of the ram is exactly known.

From $t = 0$ the ram starts passing energy to the anvil which in its turn passes energy to the follower. As the anvil moves down, the hammer starts to accelerate due to its gain in potential energy. At $t = 5$ ms the hammer casing makes contact with the anvil (see Figure 4.3 (a) and 4.3 (c)). The chosen ram and anvil parameters cause the ram to detach from the anvil after $t \approx 3$ ms, the ram moves down at a slower velocity than the ram. The ram and anvil make contact again at $t \approx 12$ ms, causing a second blow. This second blow does not contain much energy as can be seen in Figure 4.3 (a), however the ram seems to gain a little in energy due to the second contact.

The spectrum in Figure 4.3 (b) shows the frequencies of the first blow between 700 Hz and 3000 Hz. The peak between 60 Hz and 105 Hz correspond to the recurring effect of the ram impact (i.e. first and second blow). The second blow seems to be influenced by the first reflecting waves from the pile-soil interaction, as shown in Figure 4.4. This plot shows an accumulation of strain energy at $z = 20$

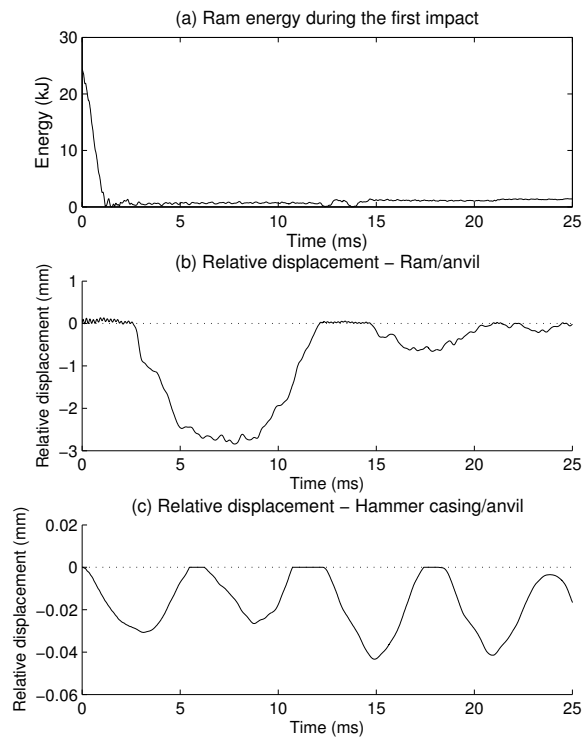


Figure 4.2: (a): Amount of energy in the ram during blow. (b): relative displacement between ram and anvil and (c): relative displacement between hammer casing and anvil.

⁴The reference length between nodes was 0.5 m.

<i>Hammer</i>	IHC S-90
E_{ham}	24 kJ
m_{anv}	938 kg
k_{anv}	57.8 GN/m
D_{pile}	36 inch

Table 4.4: Input details used to derive Figure 4.3.

m and $t \approx 5.5$ ms, presumably caused by modelled soil-pile interaction. A Winkler foundation with a constant stiffness along the penetrated section of the pile was used to model the influence of soil. An accumulation of strains is expected due to the sudden increase in stiffness as the wave propagates downward. This accumulation is not seen at lower penetrations as the majority of the energy is radiated into the soil.

In reality the pile slips past the soil layers as the ultimate shear strain or cohesion of the soil is exceeded. This local accumulation of strains that is shown in Figure 4.4 is therefore not expected to occur in reality.

Ram/anvil contact after the first blow has finished, does not contribute to the drivability of the pile. It may give unwanted effects to the fatigue lifetime of the hammer. It is therefore assumed that, given that the ram detaches from the anvil, the hydraulic system in the hammer damps any second impact.

It is expected that the lateral vibrations of the pile have the largest contribution to the force transfer. These lateral vibrations are predominantly caused by the out of verticality of the initial blow. To exclude the effect of the second impact on the lateral vibration, this coupling between the axial force input, and the lateral force input is removed after the first blow has finished.

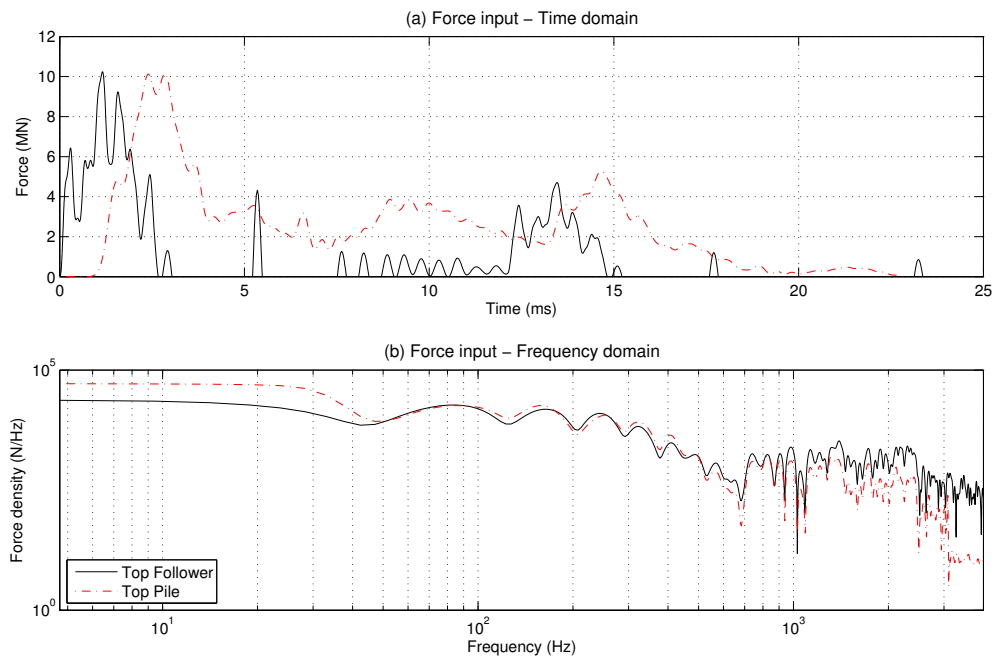


Figure 4.3: Force input in (a) time domain and (b) frequency domain.

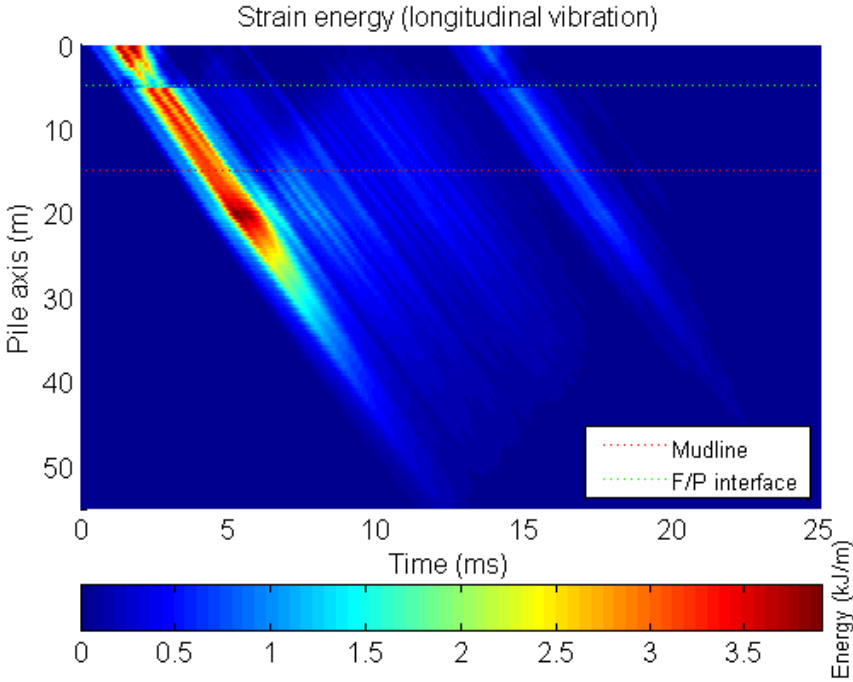


Figure 4.4: Longitudinal strain energy per unit length, in space and time along the vertical axis of the pile.

4.4. VALIDATION OF THE COMBINED MODEL

Unfortunately raw data of the accelerations is unavailable as the measurements were conducted in 1995. Therefore it is only possible to fit modelled accelerations to plotted time-acceleration profiles, of which two examples are shown in Figures 1.3 and 1.4. These figures show a maximum horizontal acceleration of 97.981 m/s^2 for a penetration of 40 m and a maximum horizontal acceleration of 216.421 m/s^2 for a penetration of 50.5 m. The range of maximum measured accelerations at 40 m pile penetration is 50 to 150 m/s^2 , for a pile penetration of 50 m this is 75 m/s^2 to 250 m/s^2 (see Figure 1.6).

The zero drift frequency that can be derived from Figures 1.3 and 1.4 implies that the bandwidth of the measurement equipment was 0 to 200 Hz. In Figure 4.3 (b) can be seen that amplitudes of the force input are observed up to frequencies of at least 3 kHz. It is therefore possible that the *actual* accelerations during pile driving are significantly higher than the measured values shown in Figure 1.3.

With the model described in Chapter 3 it is attempted to approximate the measured accelerations. The actual situation still contains many uncertainties. A slight difference in diameter between pile and sleeve gives the pile some rotational freedom, it is therefore possible that the pile is driven at a slight angle with the vertical. This initial slope may cause the pile system to 'hang' into the pile sleeve under the gravitational load.

The initial location of the pile within the pile sleeve and subsequently the direction of loading may yield different measurements. It is assumed that the pile is loaded in the same direction as the accelerometer was installed. This load case is shown in Figure 4.5 and should provide the largest displacements in the measured direction.

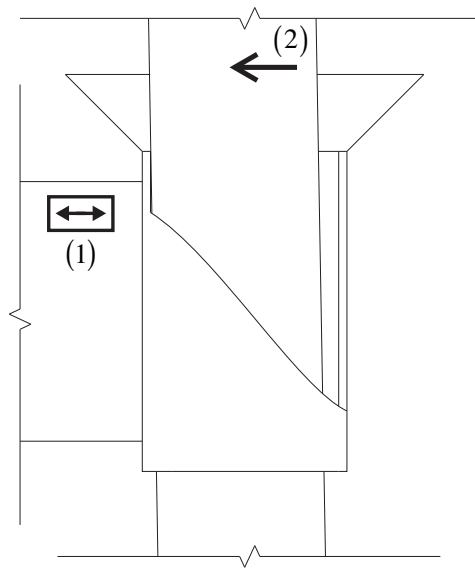


Figure 4.5: The considered load case, in which (1) accelerometer including measuring direction and (2) the direction of loading.

4.4.1. STIFFNESS OF THE INTERFACE

The case of a simply supported thin cylindrical shell has been modelled to give an idea about the radial deformability of the pile and therefore the stiffness of the interaction. In this analysis, the zero'th and first circumferential modes ($n = 0, 1$) have been excluded in order to investigate the deformation of the shell itself. The pile sticking out of the soil is better modelled as a clamped - free tube, however time constraints limited the analysis of this case. The modelled situation gives some insight in the behaviour of the interaction between an harmonically applied unit load and a cylindrical shell over the expected frequency domain.

Sufficient circumferential and axial modes have been included ($M = 500$ and $N = 85$ in (3.96)) such that the force function is reasonably approximated with Fourier series. Figure 4.6 shows the stiffness

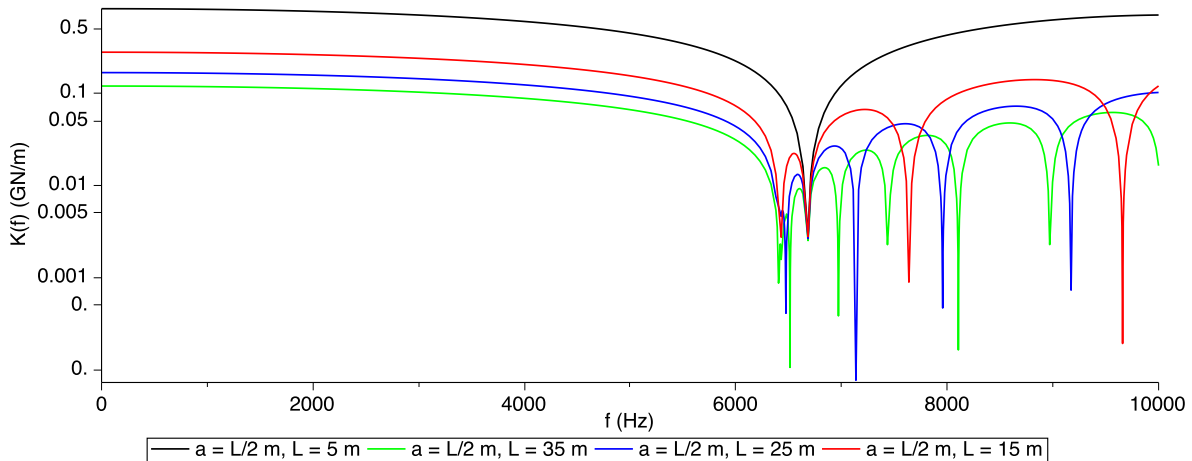


Figure 4.6: Interaction stiffness spectrum for five different pile lengths. Dimensions of the cylinder were $h = 1''$ and $R = 18''$.

for $\alpha = 3^\circ$ and four different lengths $L = 5, 10, 20, 30$ m. In this particular situation, the quasi-static stiffness of the shell increases as the length of the cylinder shrinks. The sharp peaks between 7.5 kHz and 10 kHz correspond to the circumferential vibration modes ($n = 2$) of the shell.

Excitation in one of the natural frequencies of the pile causes a larger radial displacement of the pile. Assuming that the stiffness of the interaction is proportional to the reciprocal of the radial displacement, the stiffness should be low around the sharp peaks in the stiffness spectrum of Figure 4.6.

Interesting to see is the increase in (quasi-static) radial stiffness for shorter cylinder lengths. The distance of the point of loading to the boundaries of the system seems to have a large influence on the stiffness of the interaction. A shorter tube causes the first natural frequency of circumferential mode $n = 2$ to increase.

Now, how does the situation of the simply supported tube compare to the situation of the pile? Can this situation be used to qualitatively determine the level of deformation in the pile? Most likely not, because the distance between the point of loading and the soil is small and the influence of boundary conditions seems to be large. Figure 4.7 shows the radial displacement due to a unit load at $z = 0$, for pile lengths of 5 and 20 m. The displacement field for the longer pile shows that any disturbance within 5 m from the center of the applied load has an influence. It can be seen that the boundaries of the shorter pile influence the displacement field to a large extend.

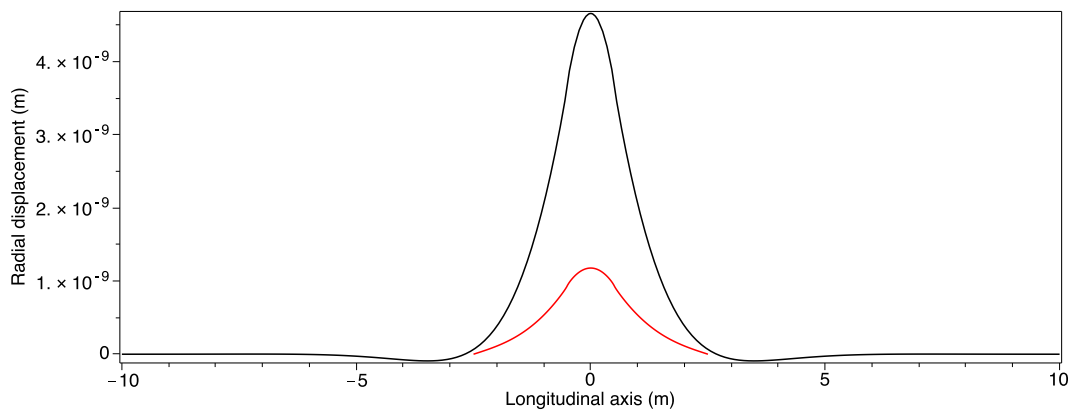


Figure 4.7: Static radial displacement due to a unit load along the longitudinal axis of the cylinder, for $\theta = 0^\circ$. In red, $L = 5$ m and in black, $L = 20$ m.

The modelled situation restricts bending of the shell in circumferential direction at the upper boundary. In reality a follower is placed on top of the pile, the follower may restrict "bending" of the pile to a certain degree. When the distance between the follower and the point of loading reaches this threshold of 5 m, the stiffness of the interaction will be larger. The distance between the top of the pile sleeve and the soil is 3 m, which means that the presence of the soil is likely to influence the stiffness of the interaction. The stiffness of the interaction will therefore probably be found somewhere between 1 and 10 GN/m for this geometry ($D = 36''$, $h = 1''$). Further analysis is however required to give a better approximation.

4.4.2. MODELLED ACCELERATIONS

Modelled acceleration plots for four different (linear) interaction stiffness values are shown in Figure 4.8. In each of these situations, the pile has been given an initial inclination of 1° . This causes the pile to hang onto the template and create an initial (static) interaction.

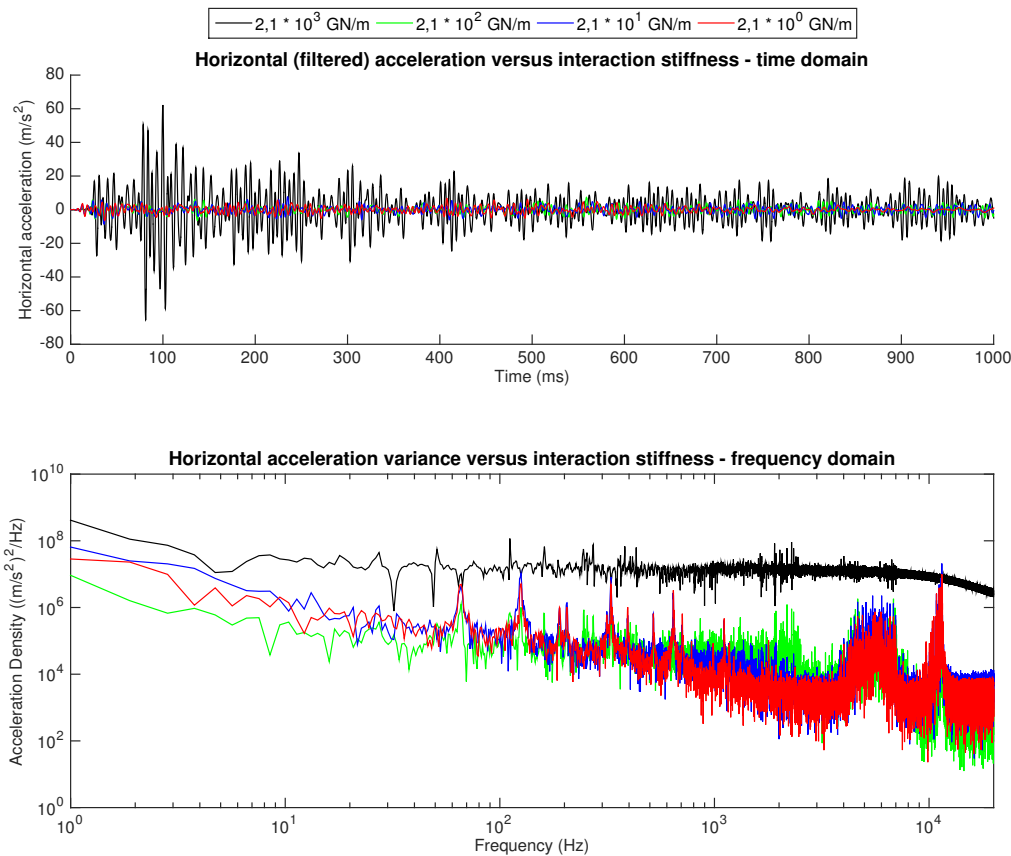


Figure 4.8: Modelled, filtered lateral accelerations (time domain) and unfiltered lateral accelerations (frequency domain) of pile sleeve SP2 for different levels of interaction stiffness between pile and sleeve.

Each dataset has been treated with a low-pass filter⁵ in order to make a comparison with the measured accelerations. The figure contains the unfiltered acceleration variance density spectra, where (longitudinal) natural frequencies of the element are clearly visible for stiffness values of $2.1 \cdot 10^0$, $2.1 \cdot 10^1$ and $2.1 \cdot 10^2$ GN/m around 70 Hz, 120 Hz, 300 Hz and 600 Hz. Excitations around 2 kHz correspond to excitations in the frequencies of the force input. These spectra show high activity around 5 and 10 kHz, caused by the modelled initial contact between pile and pile sleeve⁶.

Although the accelerations for the stiffness of $2.1 \cdot 10^3$ GN/m seem to approach the measured values, this stiffness is much larger than the expected stiffness range that was discussed in Section 4.4.1. The accelerations for the other stiffness values does not seem to exceed 10 m/s^2 for the bandwidth considered, where approximately 100 m/s^2 was measured.

From these data can only be concluded that measured accelerations can not be reproduced with this model. Given that these acceleration - time plots are the only means available to validate the motions of the template, it is not possible to validate the model. Therefore it is not possible to make conclusions with full confidence.

It is important to note the difference between "near-field" and "far-field" vibrations in the structural elements. In the near-field, the stress distribution along the height of the elements is non-linear. When the sleeve is loaded locally at a certain position, the stress wave from this load will propagate in longitudinal and transverse directions. After a certain distance (i.e. the far-field), the vertical distribution in the stresses will become linear. It is not unlikely that these far-field vibrations will not occur, given the dimensions of the structural elements.⁷

In the chosen modelling strategy, horizontal motions of the element are assumed to consist of the longitudinal and rotational motions of beam cross-sections. In other words, the only vertical variation in horizontal motions that this model describes is linear. Therefore this model fails to accurately describe the near-field accelerations that are measured slightly after the impact.

⁵An elliptic (Cauer) filter with a passband frequency of 200 Hz, a stopband frequency of 300 Hz, a passband ripple of 0.5 dB and a stopband attenuation of 75 dB has been used.

⁶The initial displacement of the template is caused by the static deflection. This static deflection caused the pile sleeve to push the pile sideways. Four non-tension springs were used to model the interaction. The model needed to search for the optimal initial position, which of the four springs were activated and which were not. This apparently created a loop in which the model searched for the optimal activation of springs. As soon as the first lateral waves rolled in, this effect is diminished and modelling continued as was defined.

⁷The structural elements were plate girders with a height of 1.5 m and a length of approximately 2.5 m.

Chapter 5

Analysis

Despite the fact that this model is not validated and cannot be used to qualitatively describe the vibrations in the template, the interaction can still be analysed quantitatively to gain more insight in the load transfer itself. It is not possible to investigate the high frequency impact waves that propagate through the member. It is these high frequency impact waves that yield the largest local strains, and it is therefore these high frequency waves that should be designed for. This model can still be used to analyse the energy flux and the forces that may act on the template. The free vibration bending motions of the template, that remain after the initial high frequency impact waves have damped out, can also be analysed¹.

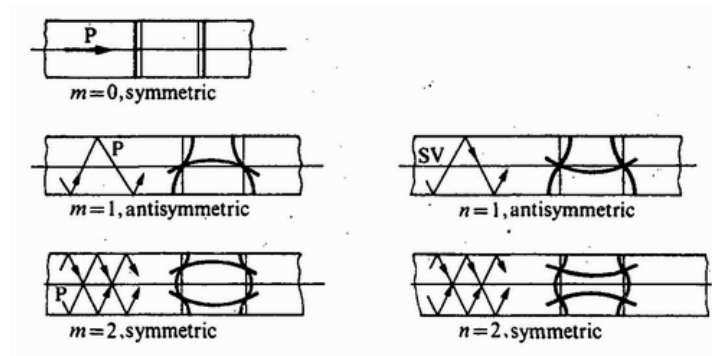


Figure 5.1: The first few P- and SV-modes in a mixed boundary plate (from (Graff, 2012)).

In Section 4.4.1 expectations for the range of stiffness values has been given. As was briefly discussed here, its value is highly dependent on the distance between the point of loading (at the pile) and boundaries of the pile. The presence of the follower, which is placed on top of the pile, might increase the interaction stiffness between pile and sleeve.

Energy enters the lateral motions of the pile through the interaction between ram, anvil and the top of the follower. Upon contact with the pile sleeve, energy might be transferred between the template and the pile. In Section 5.1, the energy balance in the lateral pile is analysed. The forces that are expected

¹The vibrations of the structural element are more accurately described by plate theories, as these theories consider the motions to vary in two dimensions. Like a beam, a plate has infinitely many vibration modes that all satisfy the boundary conditions of the plate in two dimensions. Bardell et al. (1996) and Graff (2012) show that the first symmetric P (push-pull) mode of a plate corresponds to the first longitudinal mode in a beam. The first antisymmetric P-mode corresponds to the first flexural mode of a beam. These two modes roughly have the same stress distribution as the distribution assumed in the beam theories, which can be seen in Figure 5.1. Graff (2012) described in his Chapter on *wave propagation in plates and rods* that the modes $n > 0$ show dispersivity. Higher frequency propagating waves in plates move at higher velocities. From which may be concluded that at a certain moment in time, the motions of the structural element are described by the low frequency modes only. This is under the assumption that the high frequency waves are not reflected by (far-field) boundaries.

to occur during impact is presented in Section 5.2. Finally, an attempt is made to analyse the stresses acting on a plate girder in Section 5.3.

5.1. LATERAL VIBRATIONS OF THE PILE

The lateral pile - template model is modelled as a system in which energy is initially stored as potential energy in static deflections. Energy may leave the system as radiation energy in the soil. Along this thesis it has been assumed that a fraction of the axial pile driving load acts as a shear force at the top of the follower. Energy enters the lateral vibration modes, of which the amount can be computed with (5.1). This influx of energy causes the pile to vibrate in its natural frequencies. It is found that for a pile that has an initial inclination of 1° , the work performed by the force is around 15 J. A pile that has no initial inclination and therefore no static bending strains gains around 50 J. The difference originates from the fact that a non-inclined pile has no initial bending strains and has no (modelled) gravity influence. Therefore the non-inclined pile has less resistance to deformation and it has a higher velocity term in (5.1). Despite the fact that the undeformed pile gains more energy and possibly leads to higher loads, contact between pile and pile sleeve is crucial for modelling energy fluxes. The results presented in this Chapter are based on a pile that has an initial inclination of 1° .

$$W = \int_{t_0}^{t_1} F(t) \cdot \frac{du}{dt} dt \quad (5.1)$$

Figure 5.2 shows the energy that is present in the lateral motions of the pile in the time domain (a) and frequency domain (b). A lower interaction stiffness causes less resistance to the initial inclination of the pile, which causes a larger initial pile inclination and therefore a larger initial strain energy value. It shows that the amount of energy added to the system ranges from 20% to 25% of the static energy.

The frequency domain plot shows that the energy in this motion is concentrated in the first bending modes of the template beams around 25 Hz and in the first lateral mode of the pile around 1.25 Hz. Longer modelling time would be favourable, as the frequency of the first mode of vibration is below the Nyquist frequency. Despite this, figures c) and d) clearly show that the period of the first lateral pile mode is around 800 ms. The excitations around 2 kHz again correspond to excitations of the force input, or interaction between ram, anvil and follower. As explained in Footnote 6 on page 43, the excitations around 5 kHz correspond to the initial contact between pile and pile sleeve.

The pile is initially inclined in one direction and in contact with the template. It is given a 'push' in the direction of inclination, after which it starts move in the same direction. As the pile slows down, the pile reaches its maximum inclination and maximum bending strains around 100 ms. While the pile is vibrating the magnitude of the contact with the template increases and declines, this transfer of energy between pile and template is shown until 500 ms. Around 500 ms the kinetic energy of the pile is largest and the strain energy is minimal. At this point, the pile is standing straight and moving away from the point of contact with the pile sleeve. Removing the contact between pile and sleeve causes the pile to continue vibrating in its own natural frequencies; the excitation around 25 Hz is damped after 500 ms. After the final contact, the waves that originate from the interaction with the template propagate upward (towards the hammer) and downward (towards the pile tip). The upward propagating waves will reflect and return downward, the downward propagating waves will be damped by the soil. Dispersion causes the waves around 25 Hz to propagate faster and therefore damp out faster than the waves at the first natural frequency of the pile.

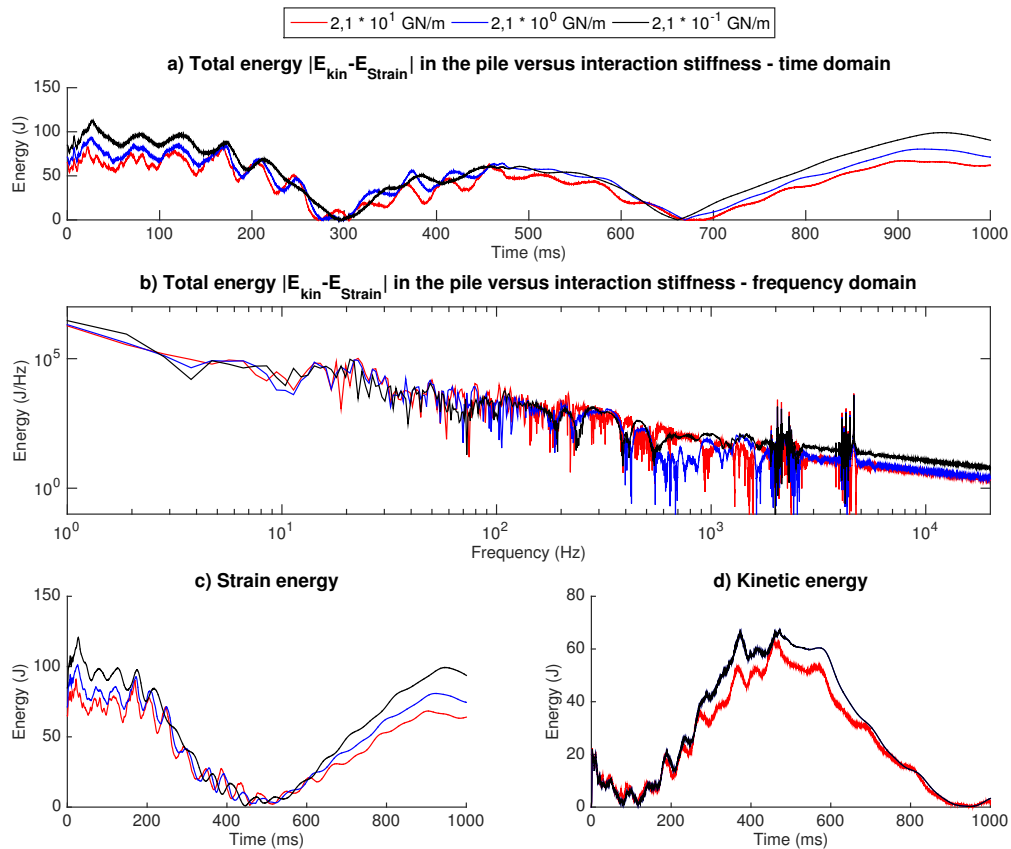


Figure 5.2: Total energy captured in the lateral vibrations of the pile, for different levels of interaction stiffness between pile and sleeve in a) time domain and b) frequency domain. Plots c) and d) show the evolution of strain and kinetic energy over time.

5.2. INTERACTION FORCE

Force is only transferred if the pile and sleeve make contact. Its modelled value has been derived by considering the relative displacement and the modelled interaction stiffness. In Section 5.1 was shown that, for the modelled interaction stiffness values, contact occurs during the first 500 ms. Figure 5.3 confirms that force transfer occurs during the first 500 ms. These figures show an increase in the magnitude of the load amplitudes as the stiffness increases. The magnitude of the total impulse, i.e. the integral of the load over time, seems to scale linear with the increase in stiffness, as is shown in Table 5.1. To put things in perspective: the longitudinal spring value, i.e. EA/L of the connecting plate girder is approximately 4 GN/m.

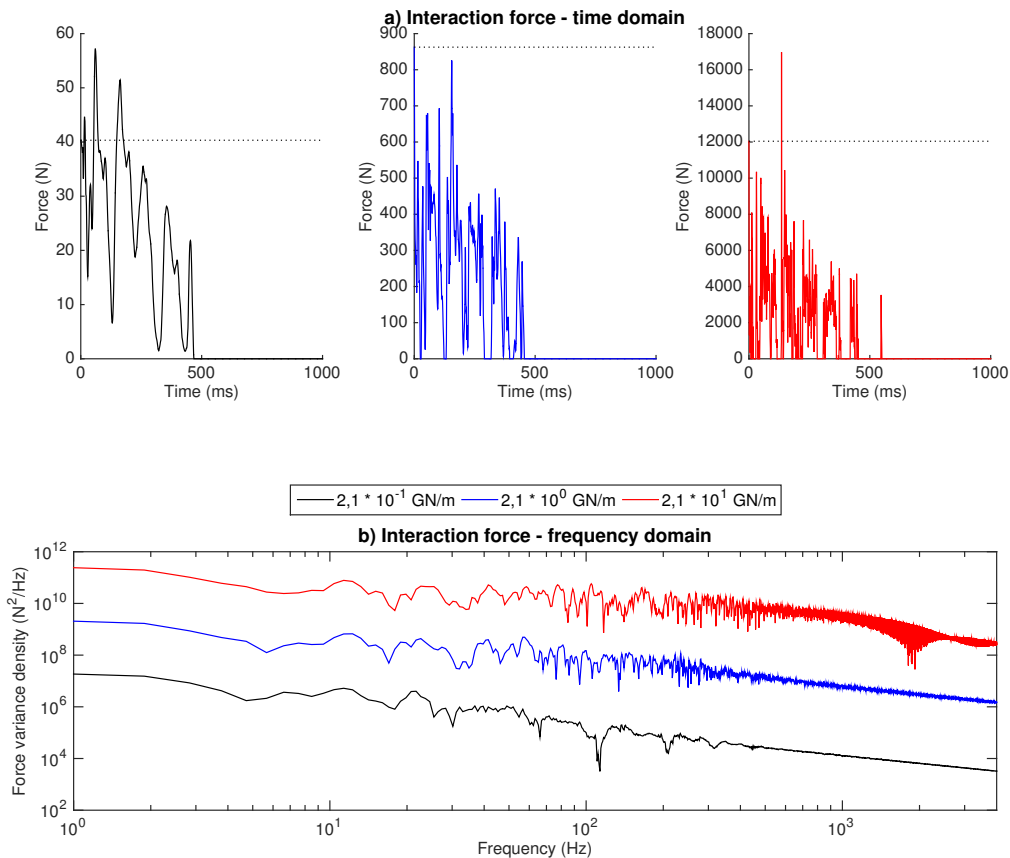


Figure 5.3: The interaction force, i.e. relative displacement between pile and pile sleeve times interaction stiffness, for interaction stiffness values of 2.1 GN/m and 21 GN/m in the time domain (a) and its variance in the frequency domain (b). The dotted lines in a) indicate the computed static load, caused by the inclined pile hanging into the pile sleeve.

A quantitative comparison between the variance density spectra can be done if these spectra are 'placed over each other'. Figure 5.4 shows the variance density spectra that have been normalised around the low frequency values of the lowest stiffness value. These spectra show a cut-off frequency that is dependent on the stiffness of the interaction. The three spectra fit quite well up to approximately 20 Hz. The two spectra that correspond to the two stiffer interactions seem to fit reasonably well up to 60 Hz. Finally, the stiffest spectrum seems to contain frequencies up to approximately 200 Hz. Vibrations at the force excitation frequency (around 2 kHz) are not visible in the interaction force spectra.

This effect can be explained by considering the transfer function of a one dimensional mass-spring system. Each transfer-function can be subdivided into three regions in the frequency domain. In the

quasi-static region, the response to an arbitrary force is roughly equal to the static response to a static force of the same magnitude. The response at high frequencies goes to zero and third, the response at intermediate frequencies is amplified.

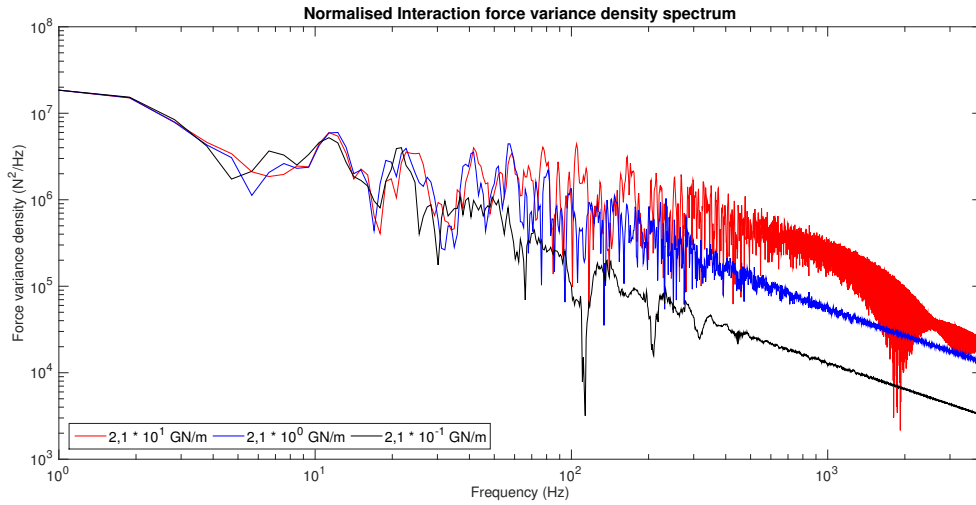


Figure 5.4: Normalised variance density spectra for the considered range of interaction stiffness values.

The amount of energy transferred to the template has been computed in a similar way as the gain in energy for the lateral pile vibration has been derived with (5.1). Here, du/dt is the velocity of the pile sleeve in the direction of loading. The amount of energy transferred over the period considered ranges up to 10% of the energy input from the hammer.

Table 5.1: Energy and impulse transferred to the pile sleeve during the first natural period of the pile.

Stiffness (GN/m)	Work (J)	Impulse (Ns)
$2.1 \cdot 10^{-1}$	$1.43 \cdot 10^{-3}$	$11.6 \cdot 10^0$ Ns
$2.1 \cdot 10^0$	$6.99 \cdot 10^{-2}$	$11.1 \cdot 10^1$ Ns
$2.1 \cdot 10^1$	$1.37 \cdot 10^0$	$10.6 \cdot 10^2$ Ns

5.3. STRESS IN THE CONNECTING PLATE GIRDER

The pile sleeve where the pile driving load is introduced, is connected to three plate girders (see Figure 1.2 or 3.7). This load, which is of impulsive nature, causes waves propagating and decaying in the connecting plate girders. The initial, high-frequency waves that describe the stress distribution right after impact are not captured in this model. What rests after the high frequency waves have damped out, are is the first anti-symmetric P-mode of the plate girder (otherwise known as the first bending mode).

This model considers the connecting plate girders as beams. The most dominant motions, i.e. the motions which contain most energy, are the transverse and longitudinal motions of the beam. Figure 5.5 shows the energy density spectra for these motions. Again may be noted that the excitations in the transverse vibrations at 5 kHz and 10 kHz originate from the initial contact problem, see the footnote on page 43. These spectra show that transverse vibrations above 30 Hz are damped, which is an indication that the theory is not valid or the mesh-size is too large². The system attempts to excite the beam at 300 Hz and 400 Hz for instance. When the mesh-size is chosen inappropriately, it may be possible that the excitation frequency is higher than the highest natural frequency of the discretised beam. In this situation it is likely that the natural frequencies that respond to excitations at 300 Hz and 400 Hz

²In this situation, the plate girder of length 2.8 m is subdivided into 10 sections of 0.28 m.

have a non-linear stress distribution over the height of the plate girder. Therefore further reducing the mesh-size is probably useless.

Interesting to see in these spectra is their correspondence over a wide range of frequencies. This suggests that the response is similar regardless of magnitude of the force or energy transferred to the template. The normal stress at the top of the plate girder in Figure 5.6 and the vertical displacement of the sleeve in Figure 5.7 agree responses over the considered values of the interface stiffness are similar. An increase in vertical motions and an increase in bending stresses is expected, regarding the interaction force that has been modelled in Figure 5.3. A slight increase in normal-stresses of the longitudinal modes for increasing stiffness can be seen in Figure 5.6. The bending strains however, do not show this increase while larger loads have been observed. In Section 4.2 has been shown that the template model accurately describes the static displacements in vertical direction. This implies that the model fails to accurately describe the bending moment *interaction* at the pile sleeve, an effect most likely caused by a bug of which the origins are unknown. The vertical displacement of the pile sleeve, shown in Figure 5.7 and caused by the variation in horizontal loading over the height of the pile sleeve, also shows no variation for increasing stiffness.

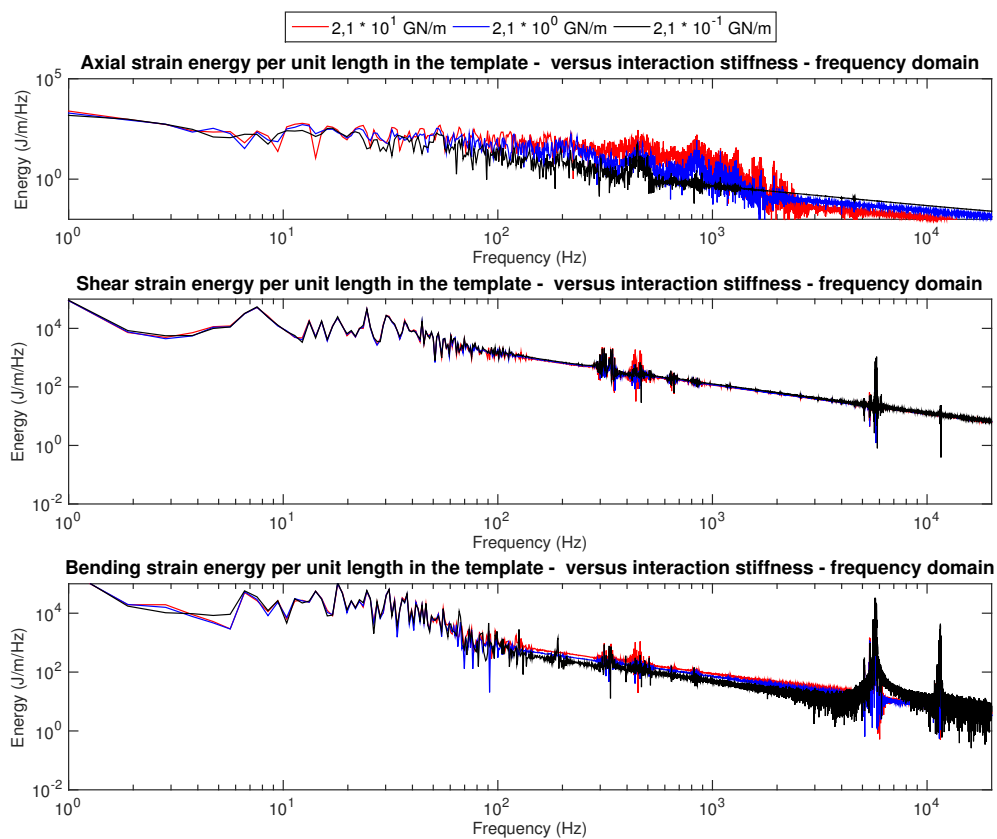


Figure 5.5: Strain energy density spectra for the longitudinal motion, bending motion and shearing motion of a thin section of a connecting plate girder.

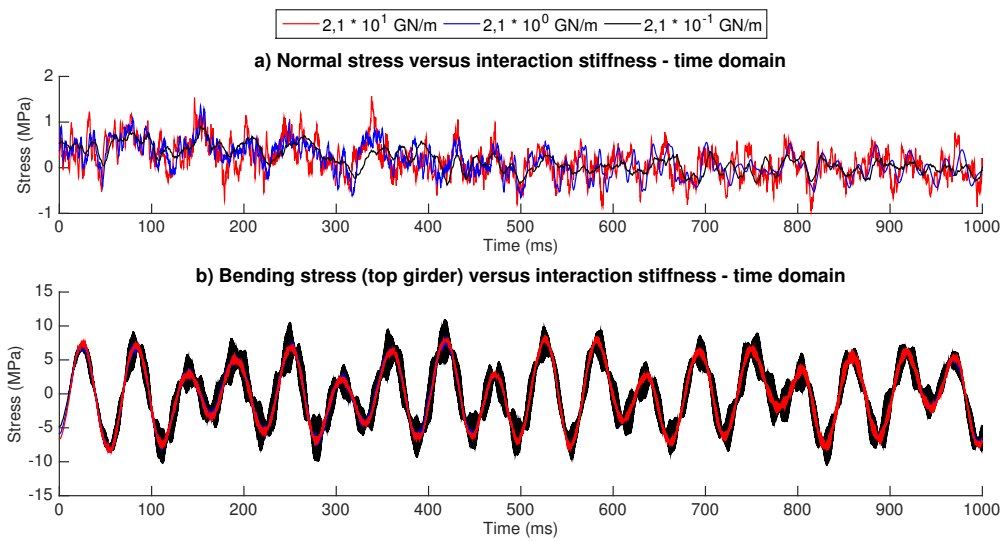


Figure 5.6: Modelled normal stress due to longitudinal motions in a) and bending motions in b), over time in the monitored plate girder.

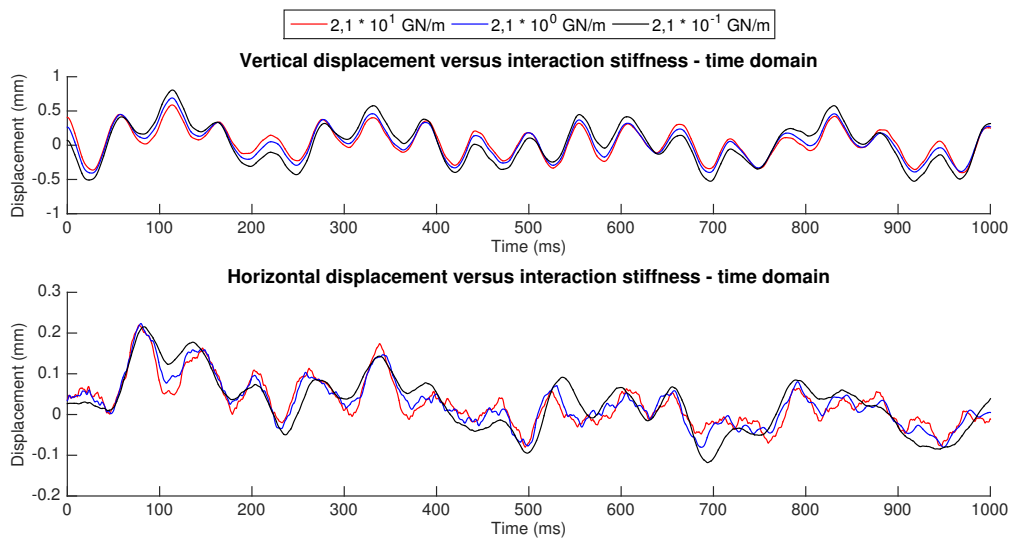


Figure 5.7: Global displacement of the horizontal (i.e. in the direction where the accelerometer measures and the sleeve is loaded) and vertical motions of the pile sleeve.

5.4. INFLUENCE OF PILE PENETRATION

The results of the vibration monitoring report showed that the response increased as the pile was penetrated deeper. It would be interesting to see if this same reaction is seen when the stiffness of the interaction is kept constant. Figure 5.8 shows that larger penetrations lead to lower responses for the initial contact; the largest response is seen for shallower piles.

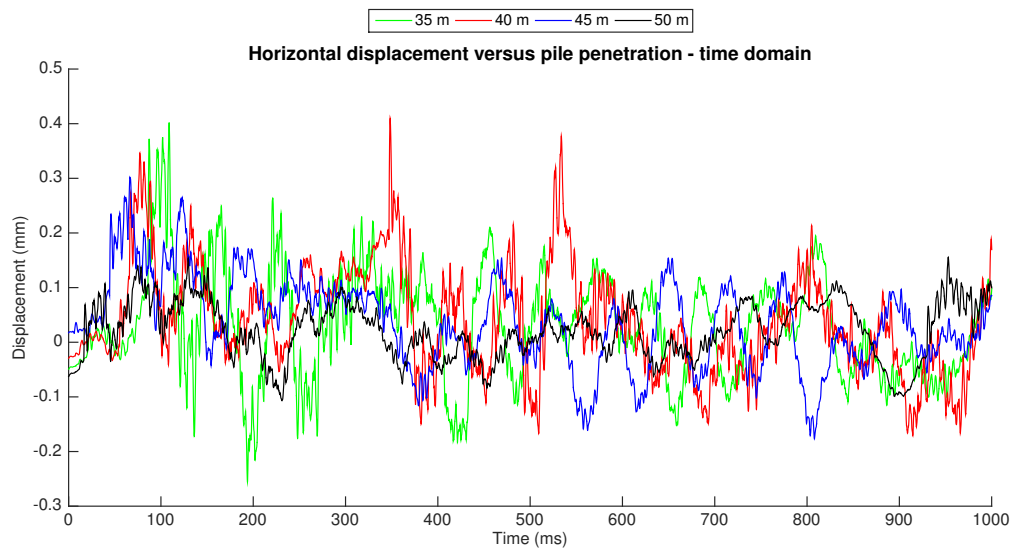


Figure 5.8: Global displacement of the horizontal motions of the pile sleeve (i.e. in the direction where the accelerometer measures and the sleeve is loaded) as a function of the pile penetration length for a constant value of the interaction stiffness.

This effect may be explained by a simple case of an impulsive, "end loaded" cantilever beam, that has no static deformation. Consider the deformability of two identical beams, one long and one short beam. It can be shown that the flexibility of the longer beam is higher, which means that its ability to deform is higher. Since the energy input to a system is dependent on the ability to deform (see (5.1)), the work performed on the longer beam is higher.

Chapter 6

Conclusions

The problem that was analysed in this thesis is one of complex nature. HMC engineers encountered high design loads from pile driving during the design stage of two conductor templates. In Chapter 2, the problem was formulated as “*Pile guiding support structures are likely to be over-designed as not much is known about the effect of the dynamic pile driving loads onto these guiding structures.*” The used method to derive the design loads was based on a vibration study that was conducted on a similar conductor template. In this vibration study, four accelerometers were placed on a template and measured accelerations during pile driving. These showed maximum peak accelerations up to 300 m/s^2 , as described in Chapter 1. It also showed that the measured accelerations increased rapidly as the pile reached his final penetration. The findings of the Britannia vibration study were applied into the latest design cases by applying Newton’s second law of motion over the mass of the pile sleeve. Design loads that were found are out of proportions and most likely lead to over-designs.

In this thesis, a model has been developed that describes the response of the situation (see Figure 3.1) to an impulsive load. The model consists of two sub-models that interact with each other; first a model that describes pile vibrations in longitudinal and transverse directions and second, a model that describes vibrations in the template. Each of these two sub-models are based on one-dimensional vibration theories, as described in Chapter 3. Non-linear springs, that only transmit compressive forces, describe the interaction between the two sub-models. The magnitude of these non-linear springs has been linearised and based on the radial deformability of the pile. A detailed, one-dimensional model of the hammer (i.e. the hammer model) has been formulated in order to accurately describe the impulsive force and to correctly include the mass distribution at the top of the hammer.

The steps taken to verify and validate the model(s) is described and briefly discussed in Chapter 4. Other output of the model is presented in Chapter 5 This Chapter contains the conclusions and propositions that are based on the output of the model.

HAMMER FORCE INPUT

In Section 4.3 is shown that the hammer model can be used to reasonably approximate the force input that occurs from pile driving. The modelled force-time diagram differs from measured values only in the duration of the pulse. Characteristic for an hydraulic hammer are the mass distribution of the ram, the mass and deformability of the anvil and the amount of energy of the blow. It is probable that the mass distribution that was used to describe the ram differs from the actual situation. The force-time diagram shows reflections from the soil-pile interface, this occurrence is owing to the methods used to model interaction between soil and pile. If the interaction between pile and soil took the stick-slip mechanism into account, then the wave reflections that originate from the soil are presumably smaller.

VALIDATION OF THE FORCE INTERACTION

Unfortunately it has not seemed possible to accurately validate the model with the methods available, there are two main reasons for this.

First, the amount and quality of the data that was available to validate is insufficient.

- The problem consists of the interaction of two structures that each have their own characteristics. Available data only considered local motions of one of the structures; the motions of the other structure, i.e. the pile, in the measured case are unknown. In this model, the force that induces the transverse motions of the pile is based on a method used by other authors (Hanna, 1989; Tsouvalas and Metrikine, 2013) and based on the rotational freedom of the hammer / follower connection. The resulting transverse vibrations are solely based on the shear excitation at the hammer / follower interface, excitations due to lateral expansion of the longitudinal motions are excluded.

Measurement data could have given more insight in the motions of the pile and therefore in the mechanism that influences the contact with the pile sleeve. Helpful would be if the difference between the transverse motions due to bending of the pile (or the first circumferential mode of a cylindrical shell, $n = 1$) and the radial expansion of the longitudinal motions (or the ring mode of a cylindrical shell, $n = 0$) is measured. This can possibly be done by installing accelerometers along the circumference of the pile. Data output of these (fictional) measurements may also be used to validate the response to the hammer force input more accurately.

- Accurate details on the measurement equipment of the accelerations was missing. It is therefore unclear if the bandwidth of the equipment was sufficient. Vibrations up to, presumably, 200 Hz were shown in the vibration monitoring report, at this stage it is unclear if higher frequency vibrations occur.
- Raw data of the measurements was not available and the report did not include frequency spectra of the accelerations. Only time-domain validation was possible.

Second, the assumptions made during modelling of the structures.

- In this case, the pile was modelled using one dimensional theories. Deformations of the pile can be described by these one-dimensional theories when considering the global displacement. Contact problems, such as this one, are characterised by some sort of deformation of the two structures that make contact. In this case, the radial deformation of the pile is possibly of importance in the load transfer. One dimensional theories clearly do not suffice to describe this contact problem, as in-plane deformations are not modelled. Approximations of this interaction stiffness have been made, but qualitative results cannot be given.
- The plate girders in the template have been modelled as beams, despite their relative thickness. In beams, waves propagate in one direction. Here, the plate girders are locally loaded over the cross-sectional height, because the pile and sleeve make contact at the upper sleeve. This local load introduction will in reality cause an arbitrary response over the height of the plate girder; waves will propagate in multiple directions. Local variations in the motions over the height of the beam are not captured with one dimensional theories. Since it is most likely these local variations that are measured with the accelerometers, it seems not possible to reproduce them with one dimensional theories.

It is not unlikely that a higher order template model, loaded by the same contact forces as this one dimensional model, shows accelerations of the measured order. Despite the fact that conclusions cannot be drawn with full confidence, speculations based on the results of the model will be given in the next section.

LOAD TRANSFER MECHANISM

The situation is described by the free vibration, i.e. unforced, motions of two structures. Initially the pile is loaded by an impulsive force, causing it to vibrate in its natural frequencies. The highly irregular force transfer (see Figure 5.3) causes the template to start vibrating in its own natural frequencies.

Energy is transferred between the pile and the template upon contact. This energy propagates through the adjacent plate girders as stress waves, of which the highest frequency waves propagate fastest.

Figure 5.4 seemed to show the presence of a cut-off frequency for lower values of the interaction stiffness. It is plausible that vibrations above this cut-off frequency in the pile are damped and will not propagate into the template. The exact value of this cut-off frequency can only be computed with a more detailed model, as it is dependent on the natural frequencies that correspond to the interaction.

In Chapter 5 has been shown that the stiffness of the interaction is of major influence to the magnitude of both the static force as well as the largest dynamic force amplitude. The exact value of the radial pile stiffness is dependent on the magnitude of the interaction; a larger interaction indicates a larger load area which influences the displacement. The exact interaction behaviour can only be found by considering the radial deformation in the model. Increasing measured accelerations are most likely caused by the increasing radial stiffness of the pile as the distance between pile sleeve and follower decreases. In Section 4.4.1 is shown that the influence of boundary conditions of a pile on the radial deformation is significant. As the pile is penetrated deeper, the distance between the pile sleeve and the follower / pile interface decreases. The presence of this follower possibly stiffens the interaction between pile and pile sleeve, causing higher measured accelerations.

On top of this, it has been shown in Section 5.4 that the horizontal response in the template is negatively correlated to the pile penetration length for a constant interaction stiffness. This is under the assumption that the transverse force input remains constant over the pile penetration length. Higher accelerations as the pile reaches its final penetration depth are probably not caused by the penetration itself.

The interaction stiffness seemed to scale linearly with the total impulse transferred during the first natural period of the pile, as shown in Section 5.2. Figure 5.3 shows that the magnitude of the force amplitudes of the considered cases are approached by the static force. Regarding the range of values for the radial pile stiffness, it seems unlikely that the force amplitudes exceed the values shown in this figure. However, the stiffness of the interaction is very much case specific. The presence of the follower has not been modelled and its influence is therefore unknown.

All in all, these results give more insight in the load transfer mechanism. Increasing accelerations and increasing loads for higher pile penetrations are probably caused by the increasing radial stiffness of the pile. More research is however required to draw conclusions with full confidence.

Chapter 7

Recommendations

It can not be highlighted enough that the results derived from this model are speculations. Conclusions cannot be drawn based on the results shown in this report, they can only be used as a guide for further research.

The magnitude of the dynamic forces during one pile natural period have been shown in Figure 5.2. This figure indicates that the magnitude of the dynamic force is roughly equal to the static force. Caution needs to be taken with this graph because of one, again, the lack of validation and two the dynamic nature of the forces. The force radiates outward from the pile sleeve into the connecting plate girders. At the point of application, this force might induce a high local stress that is not present in the static situation. This high local stress may cause local failure in a weld or it may decrease the fatigue lifetime of the material. It is also the local motions that have been captured by the accelerometer, a better means of assessing peak accelerations is by checking the integral over the peak (i.e. the change in velocity). By this means the value of the peak acceleration is put in perspective with respect to the motions of the template.

7.1. MODELLING

In a future approach, it is recommended that the pile is modelled as a thin cylindrical shell. By this means it is possible to capture the radial expansion of the longitudinal motions accurately, as well as the radial deformation that is governing in the interaction between pile and sleeve. The approach for the two dimensional model would be different than the approach for this model in terms of the description of the hammer and in terms of the modelling of the soil. The most straightforward method to model the response of the cylinder, is to describe the force input as a kinematic boundary. It is important to capture the inertia of the hammer, as it determines the flexibility in the bending motions of the pile. The vertical reaction in the soil is overestimated in the current model, it is required to describe the stick-slip effect in the soil to exclude non-existing wave reflections.

If the same template is used in further research; describe the connecting plate girders as plates. By this means it is possible to describe local deformations and local peak stress values. Validation of the model would be easier, as it is the local deformations and motions that are generally measured. It is also these local deformations that have the highest stress values; it is up to the designer if high peak stresses during pile driving is allowed.

A huge drawback of modelling the system by the means described above is the computational time and complexity of the model. The current model has fully been programmed in MathWorks® MATLAB R2015a for its educational value, a more complex model would require more knowledge on programming which makes commercial software a requirement. Other solving strategies than finite element modelling is not recommended, due to the non-linearities in the various contact problems and the complexity of the template structure.

7.2. MEASURING

An expansion of this project would require more measurement data. For instance measurements on the motions and strains of the pile. In this situation it is advised to use accelerometers to measure the motions of the pile. Strain gauges should be used to measure the vertical force input and possibly the variation in the vertical force along the circumference.

Measurements on the template should include strain gauges along several positions of the connecting elements. By this means it is possible to measure the strains locally and possibly interpolate the results to gain understanding in the variation of the strains along the element.

It is important to gain knowledge along every step of the model; from force input to pile motions and finally to template strains. This gives the researcher more confidence in making conclusions and deriving the actual force transfer mechanism that occurs during pile driving.

Measurement equipment that is capable of detecting high frequency vibrations is desired. The vibrations associated with pile driving may range up to a 4 kHz, depending on the characteristics of the hammer. It is important to capture the vibrations along the whole frequency spectrum of the force input.

Bibliography

- Baranov, VA. On the calculation of excited vibrations of an embedded foundation. *Voprosy Dynamiki Prochnosti*, 14:195–209, 1967.
- Bardell, N.S.; Langley, R.S., and Dunsdon, J.M. On the free in-plane vibration of isotropic rectangular plates. *Journal of Sound and Vibration*, 191(3):459 – 467, 1996.
- Beredugo, Y. O. and Novak, M. Coupled horizontal and rocking vibration of embedded footings. *Canadian Geotechnical Journal*, 9(4):477–497, 1972.
- De Silva, Clarence W. *Vibration and shock handbook*. CRC Press, 2005.
- Deeks, A. J. and Randolph, M. F. Analytical modelling of hammer impact for pile driving. *International Journal for Numerical and Analytical Methods in Geomechanics*, 17(5):279–302, 1993.
- Dobry, R. and Gazetas, G. Dynamic response of arbitrarily shaped foundations. *Journal of Geotechnical Engineering*, 112(2):109–135, 1986.
- Friedman, Z. and Kosmatka, J.B. An improved two-node timoshenko beam finite element. *Computers & Structures*, 47(3):473 – 481, 1993.
- Gazetas, G. and Dobry, R. Simple radiation damping model for piles and footings. *Journal of Engineering Mechanics*, 110:937–956, 1984.
- Graff, Karl F. *Wave motion in elastic solids*. Courier Corporation, 2012.
- Hanna, S.Y. Load transfer mechanism to offshore jackets during pile driving. In *Offshore Technology Conference*, pages 321–330, 1989.
- Heerema, Fabrication Group. Britannia satellites platform, 2006. URL <http://hfg.heerema.com/content/activities/projects/show/project/britannia-satellites-platform/>.
- IHC Hydrohammer - *Equipment sales manual*. IHC Merwede, 3 edition, February 2009.
- Journée, J.M.J. and Massie, W.W. *Offshore Hydromechanics*. Delft University of Technology, 2001.
- Leissa, Arthur W. *Vibration of shells*, volume 288. Scientific and Technical Information Office, National Aeronautics and Space Administration Washington, DC, USA, 1973.
- Lysmer, John and Richart, Frank Edwin. Dynamic response of footings to vertical loading. *Journal of the Soil Mechanics and Foundations Division*, 92(1):65–91, 1966.
- Morison, JR; Johnson, JW; Schaaf, SA, and others, . The force exerted by surface waves on piles. *Journal of Petroleum Technology*, 2(05):149–154, 1950.
- Naggar, M.H. El and Novak, M. Non-linear model for dynamic axial pile response. *Journal of Geotechnical Engineering*, 120:308–329, 1994.
- Novak, M. Dynamic stiffness and damping of piles. *Canadian Geotechnical Journal*, 11(4):574–598, 1974.
- Offshore-Technology.com, . Britannia, u.k. URL <http://www.offshore-technology.com/projects/britannia/>.

- Paskin, Mike. Britannia platform, new ltc module attached., 2013. URL <https://www.flickr.com/photos/thulobaba/9618773903>.
- Rao, S. S. *Vibration of Continuous Systems*. John Wiley & Sons, 2007.
- Roebben, Gert; Bollen, B; Brebels, A; Van Humbeeck, Jan, and Van der Biest, Omer. Impulse excitation apparatus to measure resonant frequencies, elastic moduli, and internal friction at room and high temperature. *Review of scientific instruments*, 68(12):4511–4515, 1997.
- Rossross, M. et al. Jacket tow and installation. Exercise report, Norwegian University for Science and Technology, 2000.
- Sargent, Robert G. Verification and validation of simulation models. In *Proceedings of the 37th conference on Winter simulation*, pages 130–143. winter simulation conference, 2005.
- Smith, E.A. Pile-driving analysis by the wave equation. *American Society of Civil Engineers*, 1960.
- Timoshenko, Stephen P. Theory of bending, torsion and buckling of thin-walled members of open cross section. *Journal of the Franklin Institute*, 239(4):249 – 268, 1945.
- Tsouvalas, A. and Metrikine, A.V. A semi-analytical model for the prediction of underwater noise from offshore pile driving. *Journal of Sound and Vibration*, 332:3232–3257, 2013.
- Tsouvalas, A. and Metrikine, A.V. A three-dimensional vibroacoustic model for the prediction of underwater noise from offshore pile driving. *Journal of Sound and Vibration*, 333(8):2283–2311, 2014.
- van Esch, P. Britannia project vibration monitoring. Technical report, HeereMac v.o.f., 1995.
- Verruijt, A. *Soil Dynamics*. Delft University of Technology, 2008.
- Vuik, Cornelis; van Beek, P; Vermolen, F, and van Kan, J. *Numerieke methoden voor differentiaalvergelijkingen*, volume 159. VSSD, 2006.

Appendix A

Theories of Continuous Vibration

A.1. INTRODUCTION

During this thesis, only one dimensional theories were used. In one dimensional theories, motions are considered only dependent on one space variable. In the derivation of these theories, the works of Graff (2012) and Rao (2007) were used.

Along this thesis, the Cartesian coordinate system $OXYZ$ is used where no other coordinate system is explicitly mentioned. The displacements in the x , y and z directions are respectively

$$u(x, y, z, t) \qquad v(x, y, z, t) \qquad w(x, y, z, t) \qquad (\text{A.1})$$

and rotations around these axes are respectively

$$\psi(x, y, z, t) \qquad \phi(x, y, z, t) \qquad \theta(x, y, z, t) \qquad (\text{A.2})$$

A.1.1. STRAINS AND STRESSES.

Stress - strain relations can generally be described using Hooke's law

$$\begin{aligned} \varepsilon_{xx} &= \frac{1}{E} \{ \sigma_{xx} - \nu(\sigma_{yy} + \sigma_{zz}) \} & \varepsilon_{xy} &= \frac{1}{G} \tau_{xy} \\ \varepsilon_{yy} &= \frac{1}{E} \{ \sigma_{yy} - \nu(\sigma_{xx} + \sigma_{zz}) \} & \varepsilon_{yz} &= \frac{1}{G} \tau_{yz} \\ \varepsilon_{zz} &= \frac{1}{E} \{ \sigma_{zz} - \nu(\sigma_{xx} + \sigma_{yy}) \} & \varepsilon_{xz} &= \frac{1}{G} \tau_{xz} \end{aligned} \qquad (\text{A.3})$$

in which σ denote principal stresses, τ denote shear stresses, ν is Poisson's ratio and E and G are Young's modulus and the shear modulus respectively.

A.2. APPROACH

There are several methods available to derive the governing equations of motion of a beam. They can be subdivided into three different approaches: the equilibrium approach, the variational approach and the integral equation approach.

The equilibrium approach is based on the force and moment equilibrium and *Newton's second law of motion* on an element. The constitutive engineering relations can be used to describe the force equilibrium in terms of displacement, from which the governing equations can be derived.

The variational approach considers the extremes of a functional to derive the equations of motion. This functional may be the energy balance of a system. Suppose the energy in this system is stored in terms of kinetic or potential energy only. If no work is performed on the system and the system is undamped,

no energy enters or leaves the system over time. This can mathematically be expressed using *Hamilton's principle* (A.4), which considers the variation of the functional with respect to time.

$$\delta\Pi = \int_{t_1}^{t_2} (\delta U - \delta T) dt = 0 \quad (\text{A.4})$$

in which the strain energy U and the kinetic energy T are

$$U = \frac{1}{2} \int_V \{\sigma\}^T \{\varepsilon\} dV \quad T = \frac{1}{2} \int_V \rho \left(\left(\frac{\partial u}{\partial t} \right)^2 + \left(\frac{\partial v}{\partial t} \right)^2 + \left(\frac{\partial w}{\partial t} \right)^2 \right) dV \quad (\text{A.5})$$

The integral equations approach considers the effect of impulse response functions, known as *Green's function*, on a system. A distributed load can be viewed as a set of impulses. To incorporate the effect of this distributed load on the system, the effect of impulses over the dimensions of the system can be incorporated by means of integration.

Due to the relatively easy implementation of the variational method, this method is used to derive the governing equations of the theories considered.

A.3. RAYLEIGH-LOVE THEORY FOR AXIAL VIBRATION

This theory only considers principal stresses to be present in the $y - z$ plane along the length of the beam, all other principal stresses and shear stresses are zero. Hooke's law can be rewritten into

$$\begin{aligned} \varepsilon_{xx} &= \frac{1}{E} \sigma_{xx} & \varepsilon_{yy} &= -\nu \frac{1}{E} \sigma_{xx} & \varepsilon_{zz} &= -\nu \frac{1}{E} \sigma_{xx} \\ \varepsilon_{xy} &= 0 & \varepsilon_{yz} &= 0 & \varepsilon_{xz} &= 0 \end{aligned} \quad (\text{A.6})$$

As strains are basically the displacement in a direction over the length in that direction, the strains can be described in terms of the displacements as

$$\varepsilon_{xx} = \frac{\partial u}{\partial x} \quad \varepsilon_{yy} = -\nu \cdot \frac{\partial u}{\partial x} \quad \varepsilon_{zz} = -\nu \cdot \frac{\partial u}{\partial x} \quad (\text{A.7})$$

The displacement field for the longitudinal deformation of a bar can be expressed as

$$u(x, y, z, t) = u(x, t) \quad v(x, y, z, t) = -\nu \cdot y \frac{\partial u}{\partial x} \quad w(x, y, z, t) = -\nu \cdot z \frac{\partial u}{\partial x} \quad (\text{A.8})$$

The lateral displacement (v, w) of an element along the cross section depends on the position of that element along this cross-section (y, z).

For the strain energy the following relation can be found, the integral over the cross sectional plane can easily be computed as it must be equal to the cross sectional area.

$$U = \frac{E}{2} \int_V \left(\frac{\partial u}{\partial x} \right)^2 dV = \frac{EA}{2} \int_0^L \left(\frac{\partial u}{\partial x} \right)^2 dx \quad (\text{A.9})$$

The kinetic energy can be computed by differentiating (A.8) with respect to t and applying these terms in (A.5).

$$T = \frac{1}{2} \int_V \rho \left(\left(\frac{\partial u}{\partial t} \right)^2 + \nu^2 (y^2 + z^2) \left(\frac{\partial^2 u}{\partial x \partial t} \right)^2 \right) dV \quad (\text{A.10})$$

$$= \frac{1}{2} \int_0^L \int_A \rho \left(\left(\frac{\partial u}{\partial t} \right)^2 + \nu^2 (y^2 + z^2) \left(\frac{\partial^2 u}{\partial x \partial t} \right)^2 \right) dA dx \quad (\text{A.11})$$

The cross sectional area is a function in the y and z plane, therefore (A.10) can be rewritten into (A.12).

$$T = \frac{1}{2} \int_0^L \left\{ \rho \left(\frac{\partial u}{\partial t} \right)^2 \int_A dA + \rho \nu^2 \left(\frac{\partial^2 u}{\partial x \partial t} \right)^2 \int_A (y^2 + z^2) dA \right\} dx \quad (\text{A.12})$$

Both area integrals can be computed as

$$\int_A dA = A \quad \int_A (y^2 + z^2) dA = I_p = I_z + I_y \quad (\text{A.13})$$

which makes T in (A.12)

$$T = \frac{1}{2} \int_0^L \left\{ \rho A \left(\frac{\partial u}{\partial t} \right)^2 + \rho I_p \nu^2 \left(\frac{\partial^2 u}{\partial x \partial t} \right)^2 \right\} dx \quad (\text{A.14})$$

Hamilton's equation can subsequently be solved by applying (A.9) and (A.14) into (A.4).

$$\delta \Pi = \int_{t_1}^{t_2} \int_0^L \left\{ \frac{dF}{du_x} \delta u_x + \frac{dF}{d\dot{u}} \delta \dot{u} + \frac{dF}{d\dot{u}_x} \delta \dot{u}_x \right\} dx dt \quad (\text{A.15})$$

in which u_x is the derivative of u with respect to x , \dot{u} is the derivative of u with respect to t and

$$F(u_x, \dot{u}, \dot{u}_x) = \frac{EA}{2} \left(\frac{\partial u}{\partial x} \right)^2 - \frac{\rho A}{2} \left(\frac{\partial u}{\partial t} \right)^2 - \frac{\rho I_p \nu^2}{2} \left(\frac{\partial^2 u}{\partial x \partial t} \right)^2 \quad (\text{A.16})$$

The double integral in (A.15) can be evaluated as the superposition of three separate integrals:

$$\int_{t_1}^{t_2} \int_0^L \left\{ \frac{dF}{du_x} \delta u_x \right\} dx dt = \int_{t_1}^{t_2} dt \left\{ \frac{dF}{du_x} \delta u \Big|_0^L - \int_0^L \frac{\partial}{\partial x} \left(\frac{dF}{du_x} \right) \delta u dx \right\} \quad (\text{A.17})$$

$$\int_{t_1}^{t_2} \int_0^L \left\{ \frac{dF}{d\dot{u}} \delta \dot{u} \right\} dx dt = \int_0^L dx \left\{ \frac{dF}{d\dot{u}} \delta \dot{u} \Big|_{t_1}^{t_2} - \int_{t_1}^{t_2} \frac{\partial}{\partial t} \left(\frac{dF}{d\dot{u}} \right) \delta \dot{u} dt \right\} \quad (\text{A.18})$$

$$\begin{aligned} \int_{t_1}^{t_2} \int_0^L \left\{ \frac{dF}{d\dot{u}_x} \delta \dot{u}_x \right\} dx dt &= \int_{t_1}^{t_2} dt \frac{dF}{d\dot{u}_x} \delta \dot{u} \Big|_0^L - \int_{t_1}^{t_2} \int_0^L \frac{\partial}{\partial t} \left(\frac{dF}{d\dot{u}_x} \right) \delta \dot{u}_x dx dt \\ &= \int_{t_1}^{t_2} dt \frac{dF}{d\dot{u}_x} \delta \dot{u} \Big|_0^L - \int_0^L dx \left\{ \frac{dF}{d\dot{u}_x} \delta \dot{u} \Big|_{t_1}^{t_2} - \int_{t_1}^{t_2} \frac{\partial}{\partial x \partial t} \left(\frac{dF}{d\dot{u}_x} \right) \delta \dot{u}_x dt \right\} \end{aligned} \quad (\text{A.19})$$

Filling the found integrals in (A.17)-(A.19) into (A.15) gives

$$\int_{t_1}^{t_2} dt \left[\frac{dF}{du_x} + \frac{\partial}{\partial t} \left(\frac{dF}{d\dot{u}_x} \right) \right]_0^L \delta u + \int_0^L dx \left[\frac{dF}{d\dot{u}} - \frac{dF}{d\dot{u}_x} \right]_{t_1}^{t_2} \delta \dot{u} \quad (\text{A.20})$$

$$+ \int_{t_1}^{t_2} \int_0^L \left\{ \frac{\partial}{\partial x} \left(\frac{dF}{du_x} \right) + \frac{\partial}{\partial t} \left(\frac{dF}{d\dot{u}} \right) + \frac{\partial}{\partial x \partial t} \left(\frac{dF}{d\dot{u}_x} \right) \right\} \delta u dx dt = 0 \quad (\text{A.21})$$

The first term in above expression is satisfied by the boundary conditions and the second term is satisfied by the initial conditions which leaves the third term that is satisfied when

$$\frac{\partial}{\partial x} \left(\frac{dF}{du_x} \right) + \frac{\partial}{\partial t} \left(\frac{dF}{d\dot{u}} \right) + \frac{\partial}{\partial x \partial t} \left(\frac{dF}{d\dot{u}_x} \right) = 0 \quad (\text{A.22})$$

This equation can be rewritten with (A.16) into the governing differential equation for Rayleigh-Love theory of longitudinal vibration

$$\boxed{\rho A \frac{\partial^2 u}{\partial t^2} - \rho \nu^2 I_p \frac{\partial^4 u}{\partial x^2 \partial t^2} - EA \frac{\partial^2 u}{\partial x^2} = 0} \quad (\text{A.23})$$

The boundary conditions at $x = 0$ and $x = L$ are satisfied when

$$\left[EA \frac{\partial u}{\partial x} + \rho I_p \nu^2 \frac{\partial^3 u}{\partial x \partial t^2} \right]_0^L \delta u = 0 \quad (\text{A.24})$$

This expression is satisfied for a free end and fixed end:

$$\boxed{EA \frac{\partial u}{\partial x} + \rho I_p \nu^2 \frac{\partial^3 u}{\partial x \partial t^2} = 0} \quad \text{or} \quad \boxed{u(x, t) = 0} \quad (\text{A.25})$$

A.4. RAYLEIGH THEORY FOR LATERAL VIBRATION

Rayleigh's theory for lateral vibration assumes that all vertical deformations are caused by the difference in axial displacement over the height of the beam. The displacement field that founds this theory can be expressed as

$$u(x, y, z, t) = -z \frac{\partial w(x, t)}{\partial x} \quad v(x, y, z, t) = 0 \quad w(x, y, z, t) = w(x, t) \quad (\text{A.26})$$

As only strains in the cross-sectional plane are considered, they can be expressed as

$$\varepsilon_{xx} = -z \frac{\partial^2 w}{\partial x^2} \quad \varepsilon_{yy} = 0 \quad \varepsilon_{zz} = 0 \quad (\text{A.27})$$

The effect of the *Poisson* expansion in transverse direction is neglected, therefore the stresses can be expressed as

$$\begin{aligned} \sigma_{xx} &= E\varepsilon_{xx} & \sigma_{yy} &= 0 & \sigma_{zz} &= 0 \\ \sigma_{xy} &= 0 & \sigma_{yz} &= 0 & \sigma_{xz} &= 0 \end{aligned} \quad (\text{A.28})$$

As the variational approach only requires the displacement field, the formulation of stresses and strains, an expression for the kinetic and strain energy can be formed.

$$U = \frac{E}{2} \int_V z^2 \left(\frac{\partial^2 w}{\partial x^2} \right)^2 dV = \frac{EI_y}{2} \int_0^L \left(\frac{\partial^2 w}{\partial x^2} \right)^2 dx \quad (\text{A.29})$$

The kinetic energy can be computed by differentiating (A.26) with respect to t and applying these terms in (A.5).

$$\begin{aligned} T &= \frac{1}{2} \int_V \rho \left(\left(\frac{\partial w}{\partial t} \right)^2 + z^2 \left(\frac{\partial w}{\partial x} \right)^2 \right) dV \\ &= \frac{1}{2} \int_0^L \left(\rho A \left(\frac{\partial w}{\partial t} \right)^2 + \rho I_y \left(\frac{\partial^2 w}{\partial x \partial t} \right)^2 \right) dx \end{aligned} \quad (\text{A.30})$$

The functional that is used in the expression of Hamilton's principle (A.15) is:

$$F(w_x, \dot{w}, \dot{w}_x) = \frac{EI_y}{2} \left(\frac{\partial^2 w}{\partial x^2} \right)^2 - \frac{\rho A}{2} \left(\frac{\partial w}{\partial t} \right)^2 - \frac{\rho I_y}{2} \left(\frac{\partial^2 w}{\partial x \partial t} \right)^2 \quad (\text{A.31})$$

The Euler-Lagrange equation of the problem can be found by applying steps (A.17) - (A.19), and is

$$\frac{\partial^2}{\partial x^2} \left(\frac{dF}{dw_{xx}} \right) + \frac{\partial}{\partial t} \left(\frac{dF}{d\dot{w}} \right) + \frac{\partial}{\partial x \partial t} \left(\frac{dF}{d\dot{w}_x} \right) = 0 \quad (\text{A.32})$$

Applying the functional (A.31) in the Euler-Lagrange equation (A.32), the governing equation for Rayleigh's beam theory for transverse vibration can be found.

$$\boxed{\rho A \frac{\partial^2 w}{\partial t^2} - \rho I_y \frac{\partial^4 w}{\partial x^2 \partial t^2} + EI_y \frac{\partial^4 w}{\partial x^4} = 0} \quad (\text{A.33})$$

The boundary conditions at $x = 0$ and $x = L$ are satisfied when

$$\left(EI_y \frac{\partial^2 w}{\partial x^2} \right) \delta \left(\frac{\partial w}{\partial x} \right) \Big|_0^L = 0 \quad (\text{A.34})$$

$$\left(EI_y \frac{\partial^3 w}{\partial x^3} - \rho I_y \frac{\partial^3 w}{\partial x \partial t^2} \right) \delta w \Big|_0^L = 0 \quad (\text{A.35})$$

are defined.

A.5. TIMOSHENKO THEORY FOR LATERAL VIBRATION

Timoshenko assumed that both shear and bending deformation influenced the vertical displacement of a beam. As the in-plane displacement is only influenced by the rotational component, the displacement field can be expressed as

$$u(x, y, z, t) = -z\phi(x, t) \quad v(x, y, z, t) = 0 \quad w(x, y, z, t) = w(x, t) \quad (\text{A.36})$$

The contribution of shear displacement to the total slope of the centreline of an element can be found by subtracting the rotational contribution from the total slope. The strains that are considered in this theory are:

$$\begin{aligned} \varepsilon_{xx} &= -z \frac{\partial \phi}{\partial x} & \varepsilon_{yy} &= 0 & \varepsilon_{zz} &= 0 \\ \varepsilon_{xy} &= 0 & \varepsilon_{yz} &= 0 & \varepsilon_{xz} &= \frac{\partial w}{\partial x} - \phi \end{aligned} \quad (\text{A.37})$$

The shear contribution is multiplied by a shear coefficient κ , as the shear force at a cross section is not simply the maximum shear stress times the cross-sectional area. This coefficient can be derived by considering the ratio between the ultimate shear force and the ultimate shear stress times the area of a cross section. The shear coefficient is influenced by the geometry of the cross section.

$$\begin{aligned} \sigma_{xx} &= E\varepsilon_{xx} & \sigma_{yy} &= 0 & \sigma_{zz} &= 0 \\ \sigma_{xy} &= 0 & \sigma_{yz} &= 0 & \sigma_{xz} &= \kappa G \cdot \varepsilon_{xz} \end{aligned} \quad (\text{A.38})$$

As the variational approach only requires the displacement field, the formulation of stresses and strains, an expression for the kinetic and strain energy can be formed.

$$U = \frac{1}{2} \int_V E z^2 \left(\frac{\partial \phi}{\partial x} \right)^2 + \kappa G \left(\frac{\partial w}{\partial x} - \phi \right)^2 dV = \frac{1}{2} \int_L EI_y \left(\frac{\partial \phi}{\partial x} \right)^2 + \kappa AG \left(\frac{\partial w}{\partial x} - \phi \right)^2 dx \quad (\text{A.39})$$

The kinetic energy can be computed by differentiating (A.36) with respect to t and applying these terms

in (A.5).

$$\begin{aligned} T &= \frac{1}{2} \int_V \rho \left(\left(\frac{\partial w}{\partial t} \right)^2 + z^2 \left(\frac{\partial \phi}{\partial t} \right)^2 \right) dV \\ &= \frac{1}{2} \int_0^L \left(\rho A \left(\frac{\partial u}{\partial t} \right)^2 + \rho I_y \left(\frac{\partial \phi}{\partial t} \right)^2 \right) dx \end{aligned} \quad (\text{A.40})$$

The functional that is used in the expression of Hamilton's principle (A.15) is:

$$F(\phi_x, \dot{\phi}, \phi, w_x, \dot{w}) = \frac{EI_y}{2} \left(\frac{\partial \phi}{\partial x} \right)^2 + \frac{\kappa AG}{2} \left(\frac{\partial w}{\partial x} - \phi \right)^2 - \frac{\rho A}{2} \left(\frac{\partial w}{\partial t} \right)^2 - \frac{\rho I_y}{2} \left(\frac{\partial \phi}{\partial t} \right)^2 \quad (\text{A.41})$$

The Euler-Lagrange equation of the problem can be found by applying steps (A.17) - (A.19), and is

$$\frac{\partial}{\partial x} \left(\frac{dF}{d\phi_x} \right) + \frac{\partial}{\partial t} \left(\frac{dF}{d\dot{\phi}} \right) + \left(\frac{\partial F}{\partial \phi} \right) + \frac{\partial}{\partial x} \left(\frac{dF}{dw_x} \right) + \frac{\partial}{\partial t} \left(\frac{dF}{d\dot{w}} \right) = 0 \quad (\text{A.42})$$

Applying the functional (A.41) in the Euler-Lagrange equation (A.42), the governing equations for Timoshenko's beam theory for transverse vibration of constant cross sections can be found.

$$\boxed{\rho A \frac{\partial^2 w}{\partial t^2} - \kappa AG \left(\frac{\partial^2 w}{\partial x^2} - \frac{\partial \phi}{\partial x} \right) = 0} \quad \boxed{\rho I_y \frac{\partial^2 \phi}{\partial t^2} - \kappa AG \left(\frac{\partial w}{\partial x} - \phi \right) - EI_y \frac{\partial^2 \phi}{\partial x^2} = 0} \quad (\text{A.43})$$

The boundary conditions at $x = 0$ and $x = L$ are satisfied when

$$\kappa AG \left(\frac{\partial w}{\partial x} - \phi \right) \delta w \Big|_0^L = 0 \quad (\text{A.44})$$

$$\left(EI \frac{\partial \phi}{\partial x} \right) \delta \phi \Big|_0^L = 0 \quad (\text{A.45})$$

are defined.

A.6. TORSIONAL VIBRATION

The general theory on torsional vibration considers mainly the influence of shear resistance along a cross-section. In open cross-sections such as the ones considered, significant bending stresses might contribute to the torsional stiffness of the cross-section. It has therefore been decided to include the bending stresses that occur in the flanges. The variation of the horizontal (v) displacement of a flange in the longitudinal direction causes displacements in longitudinal direction. Its relation, along with the displacements in horizontal and vertical directions, can be expressed as (A.46).

$$u(x, y, z, t) = y \cdot z \cdot \frac{\partial \psi}{\partial x} \quad v(x, y, z, t) = -z \cdot \psi(x, t) \quad w(x, y, z, t) = y \cdot \psi(x, t) \quad (\text{A.46})$$

The strains in the cross-section can be derived by taking the derivative in the displacement direction, with respect to the longitudinal direction.

$$\begin{aligned} \varepsilon_{xx} &= y \cdot z \cdot \frac{\partial^2 \psi(x, t)}{\partial x^2} & \varepsilon_{yy} &= 0 & \varepsilon_{zz} &= 0 \\ \varepsilon_{xy} &= \frac{\partial v}{\partial x} = -z \frac{\partial \psi}{\partial x} & \varepsilon_{xz} &= \frac{\partial w}{\partial x} = y \frac{\partial \psi}{\partial x} & \varepsilon_{yz} &= 0 \end{aligned} \quad (\text{A.47})$$

If the effect of the Poisson's expansion is excluded, the stresses can be found by multiplying the shear stresses by the shear modulus and the normal stresses by the Young's modulus.

$$\sigma_{xx} = y \cdot z \cdot E \frac{\partial^2 \psi}{\partial x^2} \quad \tau_{xy} = -zG \frac{\partial \psi}{\partial x} \quad \tau_{xz} = yG \frac{\partial \psi}{\partial x} \quad (\text{A.48})$$

The moments of inertia in (A.49) can be used to simplify the expressions for the strain energy into (A.50).

$$\int_A y^2 + z^2 dA = I_z + I_y = I_p \quad \int_A y^2 z^2 dA \approx I_{fl} \frac{h^2}{2} \quad (\text{A.49})$$

in which I_p is the polar moment of inertia, I_{fl} is the moment of inertia of the flange and h is the height of the element.

$$U = \frac{1}{2} \int_L \left\{ EI_{fl} \frac{h^2}{2} \left(\frac{\partial^2 \psi}{\partial x^2} \right)^2 + GI_p \cdot \left(\frac{\partial \psi}{\partial x} \right)^2 \right\} dx \quad (\text{A.50})$$

The expression for the kinetic energy is found in the conventional way, as has been presented in the previous sections. The effect of axial inertia is excluded here.

$$T = \frac{1}{2} \int_L \left\{ \rho I_p \left(\frac{\partial \psi}{\partial t} \right)^2 \right\} dx \quad (\text{A.51})$$

The functional that is used in the expression of Hamilton's principle (A.53) is:

$$F(\psi_x, \dot{\psi}, \psi_{xx}) = \frac{EI_{fl} h^2}{2} \left(\frac{\partial^2 \psi}{\partial x^2} \right)^2 + \frac{GI_p}{2} \left(\frac{\partial \psi}{\partial x} \right)^2 - \frac{\rho I_p}{2} \left(\frac{\partial \psi}{\partial t} \right)^2 \quad (\text{A.52})$$

The Euler-Lagrange equation of the problem can be found by applying steps (A.17) - (A.19), and is

$$\frac{\partial}{\partial x} \left(\frac{dF}{d\psi_x} \right) + \frac{\partial}{\partial t} \left(\frac{dF}{d\dot{\psi}} \right) + \frac{\partial^2}{\partial x^2} \left(\frac{dF}{d\psi_{xx}} \right) = 0 \quad (\text{A.53})$$

Applying the functional (A.52) in the Euler-Lagrange equation (A.53), the governing equations for the used Torsional vibration theory of constant cross sections can be found.

$$\boxed{\rho I_p \frac{\partial^2 \psi}{\partial t^2} - GI_p \frac{\partial^2 \psi}{\partial x^2} + EI_{fl} \frac{h^2}{2} \frac{\partial^4 \psi}{\partial x^4} = 0} \quad (\text{A.54})$$

The boundary conditions at $x = 0$ and $x = L$ are satisfied when

$$\left(GI_p \frac{\partial \psi}{\partial x} - EI_{fl} \frac{h^2}{2} \frac{\partial^3 \psi}{\partial x^3} \right) \delta \psi \Big|_0^L = 0 \quad (\text{A.55})$$

$$\left(EI_{fl} \frac{h^2}{2} \frac{\partial^2 \psi}{\partial x^2} \right) \delta \left(\frac{\partial \psi}{\partial x} \right) \Big|_0^L = 0 \quad (\text{A.56})$$

are defined.

Appendix B

Finite Difference Formulations

One dimensional vibration theories were used in this thesis to describe the longitudinal and transverse vibrations of the pile. In this Appendix, only the methods used to derive the longitudinal equations are presented. The methods used to derive the transverse equations are found using the same procedures.

The numerical methods that are considered in this thesis both discretise the space domain into a finite amount of elements. Suppose space domain consists of N elements of finite length Δx . Each element is bound to two nodes, of which the system contains $N + 1$. The position of node n is

$$x_n = n \cdot \Delta x \quad (\text{B.1})$$

The principle of the finite difference method originates from Taylor expansion. Suppose we search for the first discrete derivative. The displacement f of nodes $n + 1$ and $n - 1$ can be expressed in terms of the Taylor expansion around node f_n . (Vuik et al., 2006)

$$f_{n+1} = f_n + \Delta x \frac{\partial f_n}{\partial x} + \mathcal{O}(\Delta x^2) \quad f_{n-1} = f_n - \Delta x \frac{\partial f_n}{\partial x} + \mathcal{O}(\Delta x^2) \quad (\text{B.2})$$

Subtraction of both formulae and subsequently division by $2\Delta x$ gives a function for the first derivative of node n in space. The order of the numerical error of this derivative is $\mathcal{O}(\Delta x^2)$.

$$\frac{\partial f_n}{\partial x} = \frac{f_{n+1} - f_{n-1}}{2\Delta x} \quad (\text{B.3})$$

In a similar way, higher order derivatives can be derived:

$$\frac{d^2 f_n}{dx^2} = \frac{f_{n-1} - 2 \cdot f_n + f_{n+1}}{\Delta x^2} \quad (\text{B.4})$$

$$\frac{d^3 f_n}{dx^3} = \frac{-f_{n-2} + 2f_{n-1} - 2 \cdot f_{n+1} + f_{n+2}}{\Delta x^3} \quad (\text{B.5})$$

$$\frac{d^4 f_n}{dx^4} = \frac{f_{n-2} - 4f_{n-1} + 6f_n - 4 \cdot f_{n+1} + f_{n+2}}{\Delta x^4} \quad (\text{B.6})$$

The next step would be to discretise the differential equations that are presented in Section 3.1.

B.1. DISCRETISATION OF AXIAL EQUATIONS

The axial equations consist of the equations that describe the pile and follower (3.1), the hammer casing and ram(3.17) and anvil (3.18). In order to keep overview of all equations, the space domain is subdivided into the sections that were defined in Figure 3.4 and Table 3.2.

B.1.1. DISCRETISATION OF THE GOVERNING EQUATIONS

The governing equations (3.1) and (3.17) that were defined in sections 3.1.1 and 3.2.2, can be rewritten as

$$\begin{aligned} \frac{d^2}{dt^2} \left[\rho A_P w_n + \rho \nu^2 I_P \frac{-w_{n-1} + 2 \cdot w_n - w_{n+1}}{\Delta z^2} \right] + \frac{d}{dt} [c_A^s \cdot w_n] \\ + \left[E A_P \frac{-w_{n-1} + 2 \cdot w_n - w_{n+1}}{\Delta z^2} + k_A^s \cdot w_n \right] = \rho A_P \cdot g \end{aligned} \quad (\text{B.7})$$

for the section of the pile that is below the seabed ($z > z_P^{(mid)}$) and

$$\frac{d^2}{dt^2} \left[\rho A_i w_n + \rho \nu^2 I_i \frac{-w_{n-1} + 2 \cdot w_n - w_{n+1}}{\Delta z^2} \right] + \left[E A_i \frac{-w_{n-1} + 2 \cdot w_n - w_{n+1}}{\Delta z^2} \right] = \rho A_i \cdot g \quad (\text{B.8})$$

for the sections that are above the seabed ($z < z_P^{(mid)}$). In these equations, i stands for the section in Table 3.2 considered.

Equation (B.8) can also be written as:

$$\begin{bmatrix} \ddots & \ddots & \ddots & 0 & \dots & 0 \\ 0 & C_1 & C_2 & C_1 & 0 & \vdots \\ \vdots & 0 & C_1 & C_2 & C_1 & 0 \\ 0 & \dots & 0 & \ddots & \ddots & \ddots \end{bmatrix} \times \begin{bmatrix} \vdots \\ w_{n-1} \\ w_n \\ w_{n+1} \\ w_{n+2} \\ \vdots \end{bmatrix} = \begin{bmatrix} \vdots \\ \rho A_i \cdot g \\ \rho A_i \cdot g \\ \vdots \end{bmatrix} \quad (\text{B.9})$$

In which:

$$\begin{aligned} C_1 &= \frac{d^2}{dt^2} \left(-\rho \nu^2 I_i \frac{1}{\Delta z^2} \right) - E A_i \frac{1}{\Delta z^2} \\ C_2 &= \frac{d^2}{dt^2} \left(\rho A_i + \rho \nu^2 I_i \frac{2}{\Delta z^2} \right) + E A_i \frac{2}{\Delta z^2} \end{aligned}$$

At for instance the left end boundary of the space domain, node (n), the equations above require input from node ($n - 1$) which lies outside the space domain. This so called dummy node can be solved for using the predefined boundary conditions.

B.1.2. DISCRETISATION OF THE BOUNDARY AND INTERFACE CONDITIONS

The boundary and interface conditions can be subdivided into categories as follows

1. Free end, such as the top of the ram or both ends of the hammer.
2. Forced end, e.g. the piletip or the interface between ram and anvil.
3. Interface between two continuous sections
4. Interface between two continuous sections with a force input

DISCRETISATION OF FREE ENDS

A free end is characterised as an end where no force input is present, for Rayleigh-Love theory of axial vibration it is defined as (B.10).

$$\rho \nu^2 I_i \frac{\partial^3 w_i}{\partial z \partial t^2} + E A_i \frac{\partial w_i}{\partial z} = 0 \quad (\text{B.10})$$

Discretisation with the aid of (B.3) gives the following scheme for a free end on section i :

$$\frac{d^2}{dt^2} \rho \nu^2 I_i \left[\frac{-w_{n-1,i} + w_{n+1,i}}{2\Delta z} \right] + E A_i \left[\frac{-w_{n-1,i} + w_{n+1,i}}{2\Delta z} \right] = 0 \quad (\text{B.11})$$

DISCRETISATION OF FORCED ENDS

A forced end is characterised as an end where force input like a spring and/or damper is present, for Rayleigh-Love theory of axial vibration it is defined as (B.10).

$$\rho\nu^2 I_i \frac{\partial^3 w_i}{\partial z \partial t^2} + EA_i \frac{\partial w_i}{\partial z} = P \quad (\text{B.12})$$

Discretisation with the aid of (B.3) gives the following scheme for a free end on section i :

$$\frac{d^2}{dt^2} \rho\nu^2 I_i \left[\frac{-w_{n-1,i} + w_{n+1,i}}{2\Delta z} \right] + EA_i \left[\frac{-w_{n-1,i} + w_{n+1,i}}{2\Delta z} \right] = P \quad (\text{B.13})$$

In this equation, P for the pile tip for example becomes

$$P = -k_A^t \cdot w_{n,P} \quad (\text{B.14})$$

For the ram end, P becomes

$$P = -k_A \cdot (w_{n,R3} - w_{m,A})$$

in which n is the node index of the ram end and m is the node index of the anvil.

DISCRETISATION OF INTERFACES

Interfaces between sections are considered as two separate end nodes. Solving for continuity in displacement gives the node scheme in Figure B.1. A dummy node is present on either side of the end nodes of the two sections. The interface conditions that were defined in (3.4) and (3.22) are all computed in similarly using (B.3).

$$\begin{aligned} & \frac{d^2}{dt^2} \rho\nu^2 I_i \left[\frac{-w_{n-1,i} + w_{n+1,i}^*}{2\Delta z} \right] + EA_i \left[\frac{-w_{n-1,i} + w_{n+1,i}^*}{2\Delta z} \right] \quad (\text{B.15}) \\ & = \frac{d^2}{dt^2} \rho\nu^2 I_{i+1} \left[\frac{-w_{n-1,i+1}^* + w_{n+1,i+1}}{2\Delta z} \right] \\ & + EA_{i+1} \left[\frac{-w_{n-1,i+1}^* + w_{n+1,i+1}}{2\Delta z} \right] \end{aligned}$$

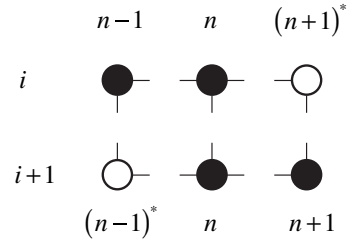


Figure B.1: Nodes $(n-1)$, n and $n+1$ and dummy nodes $(n-1)^*$ and $(n+1)^*$ around the interface of sections i and $i+1$.

DISCRETISATION OF INTERFACES WITH FORCE INPUT

The interface between the subsequent hammer sections $H1$ and $H2$ are influenced by the presence of the anvil, as can be seen in Figure 3.4 and was defined in (3.24).

$$\begin{aligned} & \frac{d^2}{dt^2} \rho\nu^2 \left[I_{H1} \frac{-w_{n-1,H1} + w_{n+1,H1}^*}{2\Delta z} - I_{H2} \frac{-w_{n-1,H2}^* + w_{n+1,H2}}{2\Delta z} \right] \quad (\text{B.16}) \\ & + E \left[A_{H1} \frac{-w_{n-1,H1} + w_{n+1,H1}^*}{2\Delta z} - A_{H2} \frac{-w_{n-1,H2}^* + w_{n+1,H2}}{2\Delta z} \right] = k_H (w_{m,A} - w_{n,H1}) \end{aligned}$$

In (B.16) m indicates the node index of the anvil.

B.1.3. EMBEDDING THE DISCRETISED BOUNDARY AND INTERFACE CONDITIONS

The goal of embedding the boundary and interface conditions is to remove all dummy nodes, as used in paragraph B.1.2 from the discretised equations yielding $N+1$ times $N+1$ matrices in the form of (B.9). Creating indices of the positions of all nodes along the space domain helps keeping an overview of the set of equations, see Table B.1.

Section	Boundary indices	Interface indices	Other
Ram	N_{R0}	N_{R1}	
	N_{R3}	N_{R2}	
Hammer	N_{H0}	N_{H1}	
	N_{H2}		
Anvil			N_A
Follower	N_{F0}	N_{P0}	
Pile		N_{P0}	
	N_{P2}	N_{P1}	

Table B.1: Boundary and interface indices in the space domain.

The set of equations below determine the dynamic behaviour of the left boundary of the ram, with index N_{R0} , is

$$\left(M_{N_{R0}} \frac{d^2}{dt^2} + K_{N_{R0}} \right) \begin{bmatrix} w_{N_{R0}-1} \\ w_{N_{R0}} \\ w_{N_{R0}+1} \end{bmatrix} = \begin{bmatrix} \rho A_{R1} \cdot g \\ 0 \end{bmatrix} \quad (\text{B.17})$$

In which

$$M_{N_{R0}} = \rho \times \begin{bmatrix} -\nu^2 I_{R1} \frac{1}{\Delta z^2} & A_{R1} + \nu^2 I_{R1} \frac{2}{\Delta z^2} & -\nu^2 I_{R1} \frac{1}{\Delta z^2} \\ -\nu^2 I_{R1} \frac{1}{2\Delta z} & 0 & \nu^2 I_{R1} \frac{1}{2\Delta z} \end{bmatrix}$$

and

$$K_{N_{R0}} = EA_{R1} \times \begin{bmatrix} -\frac{1}{\Delta z^2} & \frac{2}{\Delta z^2} & -\frac{1}{\Delta z^2} \\ -\frac{1}{2\Delta z} & 0 & \frac{1}{2\Delta z} \end{bmatrix}$$

Gauss elimination of the second row with

$$L_1 + \frac{2}{\Delta z} L_2 \quad (\text{B.18})$$

in which L_i is the i -th row of the scheme in (B.17), yields the equation of motion for node N_{R0} :

$$\rho \times \begin{bmatrix} A_{R1} + \nu^2 I_{R1} \frac{2}{\Delta z^2} \\ -\nu^2 I_{R1} \frac{2}{\Delta z^2} \end{bmatrix}^T \times \frac{d^2}{dt^2} \begin{bmatrix} w_{N_{R0}} \\ w_{N_{R0}+1} \end{bmatrix} + EA_{R1} \times \begin{bmatrix} \frac{2}{\Delta z^2} \\ -\frac{2}{\Delta z^2} \end{bmatrix}^T \times \begin{bmatrix} w_{N_{R0}} \\ w_{N_{R0}+1} \end{bmatrix} = \rho A_{R1} \cdot g \quad (\text{B.19})$$

All other boundary conditions, for the indices included in Table B.1 can be found in a similar manner.

For the right boundary of the ram N_{R3} , equation of motion is dependent on the adjacent node of the ram $N_{R3} - 1$ and the node of the anvil N_A . Its equation of motion can be written in discrete terms as:

$$\rho \times \begin{bmatrix} -\nu^2 I_{R3} \frac{2}{\Delta z^2} \\ A_{R3} + \nu^2 I_{R3} \frac{2}{\Delta z^2} \\ 0 \end{bmatrix}^T \times \frac{d^2}{dt^2} \begin{bmatrix} w_{N_{R3}-1} \\ w_{N_{R3}} \\ w_{N_A} \end{bmatrix} + EA_{R1} \times \begin{bmatrix} -\frac{2}{\Delta z^2} \\ \frac{2}{\Delta z^2} + \frac{2}{\Delta z} k_A \\ -\frac{2}{\Delta z} k_A \end{bmatrix}^T \times \begin{bmatrix} w_{N_{R3}-1} \\ w_{N_{R3}} \\ w_{N_A} \end{bmatrix} = \rho A_{R3} \cdot g \quad (\text{B.20})$$

The boundaries of the hammer are N_{H0} :

$$\rho \times \begin{bmatrix} A_{H1} + \nu^2 I_{H1} \frac{2}{\Delta z^2} \\ -\nu^2 I_{H1} \frac{2}{\Delta z^2} \end{bmatrix}^T \times \frac{d^2}{dt^2} \begin{bmatrix} w_{N_{H0}} \\ w_{N_{H0+1}} \end{bmatrix} + EA_{H1} \times \begin{bmatrix} \frac{2}{\Delta z^2} \\ -\frac{2}{\Delta z^2} \end{bmatrix}^T \times \begin{bmatrix} w_{N_{H0}} \\ w_{N_{H0+1}} \end{bmatrix} = \rho A_{H1} \cdot g \quad (\text{B.21})$$

and N_{H3} :

$$\rho \times \begin{bmatrix} -\nu^2 I_{H3} \frac{2}{\Delta z^2} \\ A_{H3} + \nu^2 I_{H3} \frac{2}{\Delta z^2} \end{bmatrix}^T \times \frac{d^2}{dt^2} \begin{bmatrix} w_{N_{H3-1}} \\ w_{N_{H3}} \end{bmatrix} + EA_{H3} \times \begin{bmatrix} -\frac{2}{\Delta z^2} \\ \frac{2}{\Delta z^2} \end{bmatrix}^T \times \begin{bmatrix} w_{N_{H3-1}} \\ w_{N_{H3}} \end{bmatrix} = \rho A_{H3} \cdot g \quad (\text{B.22})$$

The pile/follower section has two boundaries, one at the top where it is bound to the anvil and one at the bottom, where it is bound to the soil. The equation of motion for the top of the follower becomes:

$$\rho \times \begin{bmatrix} 0 \\ A_F + \nu^2 I_F \frac{2}{\Delta z^2} \\ -\nu^2 I_F \frac{2}{\Delta z^2} \end{bmatrix}^T \times \frac{d^2}{dt^2} \begin{bmatrix} w_{N_A} \\ w_{N_{F0}} \\ w_{N_{F0+1}} \end{bmatrix} + EA_F \times \begin{bmatrix} -\frac{2}{\Delta z} k_A \\ \frac{2}{\Delta z^2} + \frac{2}{\Delta z} k_A \\ -\frac{2}{\Delta z^2} \end{bmatrix}^T \times \begin{bmatrix} w_{N_A} \\ w_{N_{F0}} \\ w_{N_{F0+1}} \end{bmatrix} = \rho A_F \cdot g \quad (\text{B.23})$$

Up to now, all boundaries have been above the seabed where (B.8) was the governing equation. The final boundary condition is placed below the seabed at a certain penetration where (B.7) is the governing equation. The equation of motion for node N_{P2} is:

$$\rho \times \begin{bmatrix} -\nu^2 I_P \frac{2}{\Delta z^2} \\ A_P + \nu^2 I_P \frac{2}{\Delta z^2} \end{bmatrix}^T \times \frac{d^2}{dt^2} \begin{bmatrix} w_{N_{P2-1}} \\ w_{N_{P2}} \end{bmatrix} + \begin{bmatrix} 0 \\ c_A^s + \frac{2}{\Delta z} c_A^t \end{bmatrix}^T \times \frac{d}{dt} \begin{bmatrix} w_{N_{P2-1}} \\ w_{N_{P2}} \end{bmatrix} \quad (\text{B.24})$$

$$+ EA_P \times \begin{bmatrix} -\frac{2}{\Delta z^2} \\ \frac{2}{\Delta z^2} + k_A^s + \frac{2}{\Delta z} k_A^t \end{bmatrix}^T \times \begin{bmatrix} w_{N_{P2-1}} \\ w_{N_{P2}} \end{bmatrix} = \rho A_P \cdot g$$

in which k_A^s is the shaft stiffness and k_A^t is the tip stiffness of the soil.

The interface conditions are embedded in a similar way, suppose the interface between the first and second ram section, node index N_{R1} , can be described with

$$\left(M_{N_{R1}} \frac{d^2}{dt^2} + K_{N_{R1}} \right) \begin{bmatrix} w_{N_{R1-1}}^* \\ w_{N_{R1-1}} \\ w_{N_{R1}} \\ w_{N_{R1+1}} \\ w_{N_{R1+1}}^* \end{bmatrix} = \begin{bmatrix} \rho A_i \cdot g \\ 0 \\ 0 \end{bmatrix} \quad (\text{B.25})$$

in which

$$M_{N_{R1}} = \begin{bmatrix} 0 & -\nu^2 I_{R1} \frac{1}{\Delta z^2} & A_{R1} + \nu^2 I_{R1} \frac{2}{\Delta z^2} & 0 & -\nu^2 I_{R1} \frac{1}{\Delta z^2} \\ -\nu^2 I_{R2} \frac{1}{\Delta z^2} & 0 & A_{R2} + \nu^2 I_{R2} \frac{2}{\Delta z^2} & -\nu^2 I_{R2} \frac{1}{\Delta z^2} & 0 \\ \nu^2 I_{R2} \frac{1}{2\Delta z} & -A_{R1} \frac{1}{2\Delta z} & 0 & -A_{R2} \frac{1}{2\Delta z} & \nu^2 I_{R1} \frac{1}{2\Delta z} \end{bmatrix}$$

$$K_{N_{R1}} = \begin{bmatrix} 0 & -A_{R1} \frac{1}{\Delta z^2} & A_{R1} \frac{2}{\Delta z^2} & 0 & -A_{R1} \frac{1}{\Delta z^2} \\ -A_{R2} \frac{1}{\Delta z^2} & 0 & A_{R2} \frac{2}{\Delta z^2} & -A_{R2} \frac{1}{\Delta z^2} & 0 \\ A_{R2} \frac{1}{2\Delta z} & -\nu^2 I_{R1} \frac{1}{2\Delta z} & 0 & -\nu^2 I_{R2} \frac{1}{2\Delta z} & A_{R1} \frac{1}{2\Delta z} \end{bmatrix}$$

The equation of motion for node N_{R1} can be found with the following scheme:

$$\frac{1}{2}L_1 + \frac{1}{2}L_2 + \frac{1}{\Delta z}L_3 \quad (\text{B.26})$$

in which L_i is the i -th row of the scheme in (B.25). The result is

$$\rho \begin{bmatrix} -\nu^2 I_{R1} \frac{1}{\Delta z^2} \\ \frac{1}{2}(A_{R1} + A_{R2}) + \nu^2 (I_{R1} + I_{R2}) \frac{1}{\Delta z^2} \\ -\nu^2 I_{R2} \frac{1}{\Delta z^2} \end{bmatrix}^T \times \frac{d^2}{dt^2} \begin{bmatrix} w_{N_{R1}-1} \\ w_{N_{R1}} \\ w_{N_{R1}+1} \end{bmatrix} \quad (\text{B.27})$$

$$+ E \begin{bmatrix} -A_{R1} \frac{1}{\Delta z^2} \\ (A_{R1} + A_{R2}) \frac{1}{\Delta z^2} \\ -A_{R2} \frac{1}{\Delta z^2} \end{bmatrix}^T \times \begin{bmatrix} w_{N_{R1}-1} \\ w_{N_{R1}} \\ w_{N_{R1}+1} \end{bmatrix} = \frac{1}{2}\rho (A_{R1} + A_{R2}) \cdot g$$

The scheme for the interface at N_{R2} is exactly the same as (B.27), only A_{R2} and I_{R2} in (B.27) are replaced with A_{R3} and I_{R3} and A_{R1} and I_{R1} in (B.27) are replaced with A_{R2} and I_{R2} . Similarly for interface N_{P0} where $R1$ is replaced with F and $R2$ is replaced with P .

B.1.4. NATURAL FREQUENCIES

Now that the inertia, stiffness and damping matrices are composed, characteristics of the system such as the natural frequencies, modes of vibration and resonance frequencies can be determined.

Natural frequencies of a system can be found by assuming a motion in the form

$$\vec{x} = \vec{C} \cdot e^{st}$$

The system in (B.9) becomes the linear eigenvalue problem in (B.28).

$$(s^2 M + K) \vec{x} = 0 \quad (\text{B.28})$$

or

$$(M^{-1} \times K) \vec{x} = s^2 \vec{x} \quad (\text{B.29})$$

The modes of vibration (or: eigenvectors) of the eigenvalue problem in (B.28) or (B.29) correspond to the natural frequencies (or: eigenvalues).

Resonance frequencies can be found by solving the following quadratic eigenvalue problem:

$$(s^2 M + s \cdot C + K) \vec{x} = 0 \quad (\text{B.30})$$

Appendix C

Finite Element Formulations

This appendix can be used as a reference if you're interested in the basics of (beam) finite element modelling. A finite element formulation of a differential equation, like finite difference formulations, discretise the space domain in a finite amount of elements. Where the FDM originates from solving a discretised version of the differential equations, the FEM uses another approach. The response of a single element can be described in terms of the deformations of the two nodes that form its boundaries. Shape functions in the form of Lagrange or Hermite polynomials are used to describe the deformation field of an element or a set of elements. The higher the amount elements included, the higher the order of the polynomial. In this thesis, only the deformation along a single element is considered.

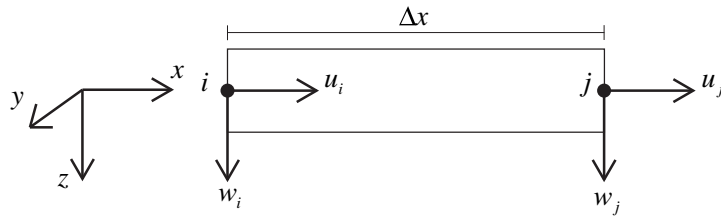


Figure C.1: Two dimensional representation of an element of length Δx that is bound to nodes i and j .

Consider an element with length Δx , the nodes that form the boundaries of the element are named i and j . Each node may displace in three directions and may rotate around these three directions. The notations for these deformations are introduced in Appendix A.

The deformation of each element is described by three second order and one fourth order partial differential equations, as introduced in Section 3.5. Each of these equations determine the order of the shape functions.

The construction can be described by a mass and stiffness matrix, which take into account the resistance of each element to deformations of all degrees of freedom. Each element has its own contribution to these matrices. The matrices of the total construction will be the superposition of the effects of all individual elements. Section C.2 first describes the equations for a beam element with its longitudinal axis coinciding with the global x -direction. If the longitudinal axis of an element does not coincide with the global x -direction, the equations can be modified as is described in Section C.3

C.1. SHAPE FUNCTIONS

LONGITUDINAL DEFORMATION

The longitudinal deformation is described by Rayleigh-Love theory. This is a second order partial differential equation that requires two defined boundary conditions. The static differential equation is

found when all time derivatives in (3.64) are discarded

$$EA \frac{d^2 u}{dx^2} = 0 \quad (\text{C.1})$$

The solution to the static differential equation, the axial displacement along the element length, is a simple linear relation as shown in (C.2).

$$u(x) = C_1 x + C_2 \quad (\text{C.2})$$

The integration coefficients C_1 and C_2 are found by satisfying the boundary conditions. Suppose two combinations of boundary conditions, the first is a unity displacement of node i while node j remains undeformed. The second is a unity displacement of node j while node i remains undeformed. Mathematically this is

$$u_i = u(0) = 1 \quad u_j = u(\Delta x) = 0 \quad \text{and} \quad u_i = 0 \quad u_j = 1 \quad (\text{C.3})$$

The equations that satisfy the boundary conditions for unitary displacements are

$$u(x) = 1 - \frac{x}{\Delta x} \quad u(x) = \frac{x}{\Delta x} \quad (\text{C.4})$$

The deformation as a function of position along the elements longitudinal axis can be expressed as a function of the displacements of the boundary nodes as (C.5). This displacement function (3.64) will be used to find the finite element formulation of the problem.

$$u(x) = N_u \times \vec{u} = \begin{bmatrix} 1 - \frac{x}{\Delta x} \\ \frac{x}{\Delta x} \end{bmatrix}^T \times \begin{bmatrix} u_i \\ u_j \end{bmatrix} \quad (\text{C.5})$$

LATERAL DEFORMATION

The method that is used to derive the finite element formulation for a Timoshenko beam element has been described by Friedman and Kosmatka (1993), this explanation follows their approach. The static differential equations that are used to derive the shape functions are (C.6) and (C.7).

$$-\kappa_z AG \left(\frac{\partial^2 w}{\partial x^2} - \frac{\partial \phi}{\partial x} \right) = 0 \quad (\text{C.6})$$

$$\kappa_z AG \left(\frac{\partial w}{\partial x} - \phi \right) + EI_y \frac{\partial^2 \phi}{\partial x^2} = 0 \quad (\text{C.7})$$

The deflection of the beam is approximated with a cubic polynomial for the displacement w and a quadratic polynomial for the rotation.

$$w(x) = C_1 \left(\frac{x}{\Delta x} \right)^3 + C_2 \left(\frac{x}{\Delta x} \right)^2 + C_3 \left(\frac{x}{\Delta x} \right) + C_4 \quad \phi(x) = C_5 \left(\frac{x}{\Delta x} \right)^2 + C_6 \left(\frac{x}{\Delta x} \right) + C_7 \quad (\text{C.8})$$

Two second order partial differential equations require the definition of four boundary conditions: the vertical displacements and rotations at each node. The influence of each boundary condition is included with one shape function. Suppose the deformations of both nodes are described with

$$w(0) = w_i \quad w(\Delta x) = w_j \quad \phi(0) = \phi_i \quad w(\Delta x) = \phi_j \quad (\text{C.9})$$

Then the four shape functions can be found by applying the boundary conditions (C.10), (C.11), (C.12) and (C.13) respectively on the polynomials of (C.8).

$$w_i = 1 \quad \phi_i = 0 \quad w_j = 0 \quad \phi_j = 0 \quad (\text{C.10})$$

$$w_i = 0 \quad \phi_i = 1 \quad w_j = 0 \quad \phi_j = 0 \quad (\text{C.11})$$

$$w_i = 0 \quad \phi_i = 0 \quad w_j = 1 \quad \phi_j = 0 \quad (\text{C.12})$$

$$w_i = 0 \quad \phi_i = 0 \quad w_j = 0 \quad \phi_j = 1 \quad (\text{C.13})$$

The found shape functions for the displacement in vertical direction $w(x)$ are (C.14)

$$w(x) = N_w \cdot \vec{w} = \begin{bmatrix} \frac{1}{1+\beta_z} \left(2 \left(\frac{x}{\Delta x} \right)^3 - 3 \left(\frac{x}{\Delta x} \right)^2 - \beta_z \left(\frac{x}{\Delta x} \right) + (1+\beta_z) \right) \\ \frac{\Delta x}{1+\beta_z} \left(\left(\frac{x}{\Delta x} \right)^3 - \left(2 + \frac{\beta_z}{2} \right) \left(\frac{x}{\Delta x} \right)^2 + \left(1 + \frac{\beta_z}{2} \right) \left(\frac{x}{\Delta x} \right) \right) \\ - \frac{1}{1+\beta_z} \left(2 \left(\frac{x}{\Delta x} \right)^3 - 3 \left(\frac{x}{\Delta x} \right)^2 - \beta_z \left(\frac{x}{\Delta x} \right) \right) \\ \frac{\Delta x}{1+\beta_z} \left(\left(\frac{x}{\Delta x} \right)^3 - \left(1 - \frac{\beta_z}{2} \right) \left(\frac{x}{\Delta x} \right)^2 - \frac{\beta_z}{2} \left(\frac{x}{\Delta x} \right) \right) \end{bmatrix}^T \times \begin{bmatrix} w_i \\ \phi_i \\ w_j \\ \phi_j \end{bmatrix} \quad (\text{C.14})$$

and the found shape functions for the rotation $\phi(x)$ are (C.15).

$$\phi(x) = N_\phi \cdot \vec{w} = \begin{bmatrix} \frac{6}{(1+\beta_z)\Delta x} \left(\left(\frac{x}{\Delta x} \right)^2 - \left(\frac{x}{\Delta x} \right) \right) \\ \frac{1}{1+\beta_z} \left(3 \left(\frac{x}{\Delta x} \right)^2 - (1-\beta_z) \left(\frac{x}{\Delta x} \right) + (1+\beta_z) \right) \\ - \frac{6}{(1+\beta_z)\Delta x} \left(\left(\frac{x}{\Delta x} \right)^2 - \left(\frac{x}{\Delta x} \right) \right) \\ \frac{1}{1+\beta_z} \left(3 \left(\frac{x}{\Delta x} \right)^2 - (2-\beta_z) \left(\frac{x}{\Delta x} \right) \right) \end{bmatrix}^T \times \begin{bmatrix} w_i \\ \phi_i \\ w_j \\ \phi_j \end{bmatrix} \quad (\text{C.15})$$

In both equations, β_z is the ratio between the bending stiffness and shear stiffness of the cross section.

$$\beta_z = \frac{12}{\Delta x^2} \left(\frac{EI_y}{\kappa_z AG} \right) \quad (\text{C.16})$$

The horizontal transverse shape functions can be found by interchanging β_z with β_y , the definition of β_y is (C.17).

$$\beta_y = \frac{12}{\Delta x^2} \left(\frac{EI_z}{\kappa_y AG} \right) \quad (\text{C.17})$$

TORSIONAL DEFORMATION

Torsional deformation consist of the influence of St. Venant's theorem and the influence of flange bending (or: warping). The shape functions are sought by assuming that the effects of St. Venant's theorem and flange bending can be superimposed.

$$-GI_P \frac{\partial^2 \psi}{\partial x^2} + EI_x \frac{\partial^4 \psi}{\partial x^4} = 0 \quad (\text{C.18})$$

in which

$$I_x = I_{fl,z} \frac{h^2}{2}$$

The solutions of (C.19) and (C.20) are both solutions to the static differential equation (C.18).

$$GI_P \frac{\partial^2 \psi_1}{\partial x^2} = 0 \quad (\text{C.19})$$

$$EI_x \frac{\partial^4 \psi_2}{\partial x^4} = 0 \quad (\text{C.20})$$

Now, the shape function for ψ_1 is a simple first order polynome, such as the shape function defined for the longitudinal deformation (C.21):

$$\psi_1(x) = N_{\psi_1} \times \vec{\psi} = \begin{bmatrix} 1 - \frac{x}{\Delta x} \\ \frac{x}{\Delta x} \end{bmatrix}^T \times \begin{bmatrix} \psi_i \\ \psi_j \end{bmatrix} \quad (\text{C.21})$$

The flanges at the top and bottom of the beams are welded to stiffener plates along the circumference of the conductors. It restricts the rotation of the upper and lower flanges independent of each other. Suppose the torsional rotation of the beam can be described in terms of the lateral displacement of the upper and lower flange as

$$\psi(x) = \frac{h^2}{2} \cdot v_{fl}(x)$$

The goal is to describe $\psi(x)$ in terms of the boundary conditions ψ_1 and ψ_2 , which are respectively (C.24) and (C.25).

$$v_{fl}(0) = \frac{2}{h^2} \quad \frac{dv_{fl}}{dx}(0) = 0 \quad v_{fl}(\Delta x) = 0 \quad \frac{dv_{fl}}{dx}(\Delta x) = 0 \quad (\text{C.22})$$

$$v_{fl}(0) = 0 \quad \frac{dv_{fl}}{dx}(0) = 0 \quad v_{fl}(\Delta x) = \frac{2}{h^2} \quad \frac{dv_{fl}}{dx}(\Delta x) = 0 \quad (\text{C.23})$$

Or in terms of ψ :

$$\psi(0) = 1 \quad \frac{d\psi}{dx}(0) = 0 \quad \psi(\Delta x) = 0 \quad \frac{d\psi}{dx}(\Delta x) = 0 \quad (\text{C.24})$$

$$\psi(0) = 0 \quad \frac{d\psi}{dx}(0) = 0 \quad \psi(\Delta x) = 1 \quad \frac{d\psi}{dx}(\Delta x) = 0 \quad (\text{C.25})$$

What rests are the first and third Hermite cubic shape functions:

$$\psi_2(x) = N_{\psi_2} \times \vec{\psi} = \begin{bmatrix} 2\left(\frac{x}{\Delta x}\right)^3 - 3\left(\frac{x}{\Delta x}\right)^2 + 1 \\ -2\left(\frac{x}{\Delta x}\right)^3 + 3\left(\frac{x}{\Delta x}\right)^2 \end{bmatrix}^T \times \begin{bmatrix} \psi_i \\ \psi_j \end{bmatrix} \quad (\text{C.26})$$

C.2. FINITE ELEMENT FORMULATION

The next step in deriving the mass and stiffness matrices is to apply the found shape functions of section C.1 into the kinetic and strain energy formulations of the various theories introduced in Appendix A. By this means it is possible to describe the interaction between the two end-nodes in terms of the inertia and stiffness of the connecting element.

The aim of this section is to create a set of equations in the form of (C.27),

$$M\ddot{\Delta} + K\Delta = \Phi \quad (\text{C.27})$$

in which the motion vector is

$$\Delta = \begin{bmatrix} \Delta_i^T & \Delta_j^T \end{bmatrix}^T \quad \Delta_i = \begin{bmatrix} u_i & v_i & w_i & \psi_i & \phi_i & \theta_i \end{bmatrix}^T \quad (\text{C.28})$$

and the force vector is

$$\Phi = \begin{bmatrix} \Phi_i^T & \Phi_j^T \end{bmatrix}^T \quad \Phi_i = \begin{bmatrix} F_x^i & F_y^i & F_z^i & M_x^i & M_y^i & M_z^i \end{bmatrix}^T \quad (\text{C.29})$$

The M and K matrices are both of size 12×12 . The entry of matrices M and K of row n and column m are named m_{nm} and k_{nm} for convenience. For instance, an entry in row 7 and column 1 indicates the influence of the horizontal displacement of node i on the horizontal force at node j .

LONGITUDINAL DEFORMATION

The derivation of the contribution of the longitudinal vibrations to the mass and stiffness matrices will be presented as a guide for the method. The strain energy of this method (A.9) can be written in terms of the shape functions of the longitudinal displacements (C.5) to yield the longitudinal contribution to the stiffness matrix K_u (C.30).

$$K_u = \frac{EA}{2} \int_0^{\Delta x} \left[\frac{d}{dx} N_u(x) \right]^T \times \left[\frac{d}{dx} N_u(x) \right] dx \quad (\text{C.30})$$

The contribution of this theory to the mass and stiffness matrices only has influence on the axial displacements of the nodes. In order to keep the formulae organised, only the relevant entries of the matrices will be presented. After integrating over the length of the element, the entries to the stiffness matrix yield (C.31).

$$\begin{bmatrix} k_{11} & k_{17} \\ k_{71} & k_{77} \end{bmatrix} = \frac{EA}{\Delta x} \begin{bmatrix} 1 & -1 \\ -1 & 1 \end{bmatrix} \quad (\text{C.31})$$

Similarly for the mass matrices, the solution shows (C.32).

$$\begin{bmatrix} m_{11} & m_{17} \\ m_{71} & m_{77} \end{bmatrix} = \frac{\rho A \Delta x}{6} \begin{bmatrix} 2 & 1 \\ 1 & 2 \end{bmatrix} + \frac{\rho I_p \nu^2}{\Delta x} \begin{bmatrix} 1 & -1 \\ -1 & 1 \end{bmatrix} \quad (\text{C.32})$$

LATERAL DEFORMATION

The procedure used to find the mass and stiffness contributions of the lateral motions is similar as the procedure described above, and has been published by Friedman and Kosmatka (1993). The shape functions will be placed in (A.39) and (A.40) and integrated over the length of the element. What rests are the symmetric matrices (C.33) and (C.34) for the stiffness and mass contributions for lateral displacement in y direction and the symmetric matrices (C.35) and (C.36) for the contributions for lateral displacement in z direction.

$$\begin{bmatrix} k_{22} & k_{26} & k_{28} & k_{212} \\ & k_{66} & k_{68} & k_{612} \\ & & k_{88} & k_{812} \\ & & & k_{1212} \end{bmatrix} = \frac{EI_z}{(1 + \beta_y) \Delta x^3} K(\beta_y) \quad (\text{C.33})$$

$$\begin{bmatrix} m_{22} & m_{26} & m_{28} & m_{212} \\ & m_{66} & m_{68} & m_{612} \\ & & m_{88} & m_{812} \\ & & & m_{1212} \end{bmatrix} = \frac{\rho A \Delta x}{210(1 + \beta_y)^2} M_{\rho A}(\beta_y) + \frac{\rho I}{30(1 + \beta_y)^2 \Delta x} M_{\rho I_z}(\beta_y) \quad (\text{C.34})$$

$$\begin{bmatrix} k_{33} & k_{35} & k_{39} & k_{311} \\ & k_{55} & k_{59} & k_{511} \\ & & k_{99} & k_{911} \\ & & & k_{1111} \end{bmatrix} = \frac{EI_y}{(1 + \beta_y) \Delta x^3} K(\beta_z) \quad (\text{C.35})$$

$$\begin{bmatrix} m_{33} & m_{35} & m_{39} & m_{311} \\ & m_{55} & m_{59} & m_{511} \\ & & m_{99} & m_{911} \\ & & & m_{1111} \end{bmatrix} = \frac{\rho A \Delta x}{210(1 + \beta_z)^2} M_{\rho A}(\beta_z) + \frac{\rho I}{30(1 + \beta_z)^2 \Delta x} M_{\rho I_y}(\beta_z) \quad (\text{C.36})$$

Each matrix is a function of the bending stiffness over shear stiffness ratio β . This ratio can be found with (C.37).

$$\beta_y = \frac{12}{\Delta x^2} \left(\frac{EI_z}{\kappa_y AG} \right) \quad \beta_z = \frac{12}{\Delta x^2} \left(\frac{EI_y}{\kappa_z AG} \right) \quad (\text{C.37})$$

The matrices $K(\beta)$, $M_{\rho I}(\beta)$ and $M_{\rho A}(\beta)$ are shown in (C.38), (C.39) and (C.40) respectively.

$$K(\beta) = \begin{bmatrix} 12 & 6\Delta x & -12 & 6\Delta x \\ (4 + \beta)\Delta x^2 & -6\Delta x & (2 - \beta)L^2 & \\ & 12 & -6\Delta x & \\ & & (4 + \beta)\Delta x^2 & \end{bmatrix} \quad (\text{C.38})$$

$$M_{\rho I}(\beta) = \begin{bmatrix} 36 & -(15\beta - 3)\Delta x & -36 & -(15\beta - 3)\Delta x \\ (10\beta^2 + 5\beta + 4)\Delta x^2 & (15\beta - 3)\Delta x & (5\beta^2 - 5\beta - 1)\Delta x^2 & \\ & 36 & (15\beta - 3)\Delta x & \\ & & (10\beta^2 + 5\beta + 4)\Delta x^2 & \end{bmatrix} \quad (\text{C.39})$$

$$M_{\rho A}(\beta) = \begin{bmatrix} (70\beta^2 + 147\beta + 78) & (35\beta^2 + 77\beta + 44)\frac{\Delta x}{4} & (35\beta^2 + 63\beta + 27) & -(35\beta^2 + 63\beta + 26)\frac{\Delta x}{4} \\ & (7\beta^2 + 14\beta + 8)\frac{\Delta x^2}{4} & (35\beta^2 + 63\beta + 26)\frac{\Delta x}{4} & -(7\beta^2 + 14\beta + 6)\frac{\Delta x^2}{4} \\ & & (70\beta^2 + 147\beta + 78) & -(35\beta^2 + 77\beta + 44)\frac{\Delta x}{4} \\ & & & (7\beta^2 + 14\beta + 8)\frac{\Delta x^2}{4} \end{bmatrix} \quad (\text{C.40})$$

TORSIONAL DEFORMATION

The shape functions (C.21) and (C.26), placed in the formulations for the strain and kinetic energy formulation for torsional vibration (A.50) and (A.51) yield the torsional stiffness contribution (C.41) and (C.42).

$$\begin{bmatrix} k_{44} & k_{410} \\ k_{104} & k_{1010} \end{bmatrix} = \left(\frac{G \cdot I_p}{\Delta x} + \frac{6EI_{fl}h^2}{\Delta x^3} \right) \begin{bmatrix} 1 & -1 \\ -1 & 1 \end{bmatrix} \quad (\text{C.41})$$

$$\begin{bmatrix} m_{44} & m_{410} \\ m_{104} & m_{1010} \end{bmatrix} = \frac{\rho I_p L}{6} \begin{bmatrix} 2 & 1 \\ 1 & 2 \end{bmatrix} \quad (\text{C.42})$$

C.3. ELEMENTS IN ARBITRARY DIRECTIONS

Up until now we have assumed an element with the x direction coinciding the longitudinal axis. The template structure (see Figure 3.7) that is to be modelled with the above introduced equations, consists of elements that have their longitudinal axes in the $x - y$ plane. This section will introduce the methods used to derive the equations of interest for an element that has its longitudinal axis under an angle α with the x -axis, such as schematically shown below.

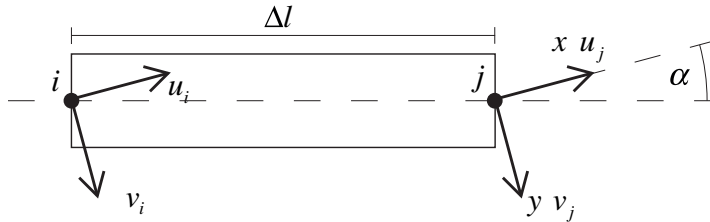


Figure C.2: Top view of an element of length Δl that is bound to nodes i and j

Consider (C.43),

$$l_x = \cos \alpha \qquad l_y = \sin \alpha \qquad (\text{C.43})$$

then the displacement in longitudinal and transverse direction of the beam, u and v , can be described in terms of the displacements of the nodes \bar{u} and \bar{v} (C.44).

$$u = l_x \cdot \bar{u} + l_y \cdot \bar{v} \qquad v = -l_y \cdot \bar{u} + l_x \cdot \bar{v} \qquad (\text{C.44})$$

The same relations can be found for the rotations around the x and y axes.

$$\psi = l_x \cdot \bar{\psi} + l_y \cdot \bar{\phi} \qquad \phi = -l_y \cdot \bar{\psi} + l_x \cdot \bar{\phi} \qquad (\text{C.45})$$

The relations between the element deformations and the node deformations can be expressed in matrix-vector notation as (C.46). In this equation Δ is the deformation vector with respect to the longitudinal direction of the element and $\bar{\Delta}$ is the deformation vector of the nodes (C.28).

$$\Delta = T_\alpha \times \bar{\Delta} \qquad (\text{C.46})$$

and in which the transfer matrix can be found with

$$T_\alpha = \begin{bmatrix} T_1 & & & \\ & T_1 & & \\ & & T_1 & \\ & & & T_1 \end{bmatrix} \qquad T_1 = \begin{bmatrix} l_x & l_y & & \\ -l_y & l_x & & \\ & & & 1 \end{bmatrix} \qquad (\text{C.47})$$

Here is shown that the displacement vector with respect to the longitudinal axis of the element can be found from the geometry of the element and the displacement vector of the nodes. The same is valid for the force vector Φ .

A similar method can be used to determine the transfer matrix for an element that has its longitudinal direction in a $x - y - z$ plane.

Suppose the force balance for this element, with respect to the longitudinal axis of the element is expressed as

$$M\ddot{\Delta} + K\Delta = \Phi \qquad (\text{C.48})$$

then

$$[M \times T_\alpha] \frac{d^2}{dt^2} \bar{\Delta} + [K \times T_\alpha] \bar{\Delta} = [T_\alpha \times \Phi] \qquad (\text{C.49})$$

or

$$\bar{M} \frac{d^2}{dt^2} \bar{\Delta} + \bar{K} \bar{\Delta} = \bar{\Phi} \qquad (\text{C.50})$$

in which

$$\begin{aligned} \bar{M} &= T_\alpha^T \times M \times T_\alpha \\ \bar{K} &= T_\alpha^T \times K \times T_\alpha \end{aligned}$$

C.4. ELEMENT OFFSET AT NODES

The connection of elements to the conductors occur at the surface of the tubular structure. The position of the end-nodes does therefore not coincide with the position of the end of the beam, as shown schematically in Figure C.4. Each conductor here is assumed to be infinitely rigid, which means that the deformation of node j can be expressed in terms of the deformation of node j^* . When the section $j^* - j$ is considered a rigid body, the deformation relations in (C.51) can easily be found.

$$\begin{aligned} u_j &= u_j^* - l_x \cdot \Delta O \cdot \theta_j^* & \psi_j &= \psi_j^* \\ v_j &= v_j^* + l_y \cdot \Delta O \cdot \theta_j^* & \phi_j &= \phi_j^* \\ w_j &= w_j^* + l_x \cdot \Delta O \cdot \psi_j^* - l_y \cdot \Delta O \cdot \phi_j^* & \theta_j &= \theta_j^* \end{aligned} \qquad (\text{C.51})$$

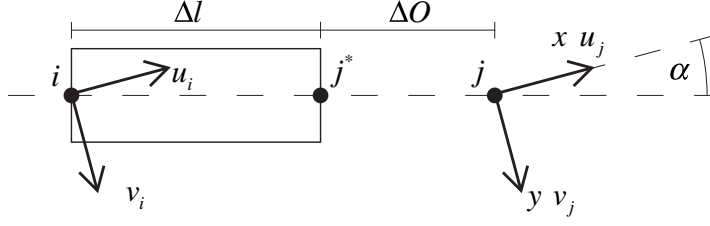


Figure C.3: Top view of an element of length Δl that is bound to nodes i and j^* . Node j^* is situated at a distance ΔO from node j .

Expressed in the matrix vector notation of (C.27) this is

$$\Delta_j = T_{\Delta O} \times \Delta_j^*$$

in which

$$T_{\Delta O} = \begin{bmatrix} 1 & & & & -l_x \cdot \Delta O \\ & 1 & & & l_y \cdot \Delta O \\ & & 1 & l_x \cdot \Delta O & -l_y \cdot \Delta O \\ & & & 1 & \\ & & & & 1 \\ & & & & & 1 \end{bmatrix} \quad (\text{C.52})$$

The same method can be used to find the relation between the interface forces and moments at j^* and j . It can be proven that the force relation is found with

$$\Phi_j = T_{\Delta O}^T \times \Phi_j^* \quad (\text{C.53})$$

The force balance around node j^* can be rewritten in terms of the force balance around node j . The balance around j^* being

$$M \frac{d^2}{dt^2} \Delta_j^* + K \Delta_j^* = \Phi_j^*$$

then

$$[T_{\Delta O}^T \times M \times T_{\Delta O}] \frac{d^2}{dt^2} \Delta_j + [T_{\Delta O}^T \times K \times T_{\Delta O}] \Delta_j = \Phi_j \quad (\text{C.54})$$

C.5. APPLICATION INTO TEMPLATE MODEL

The template model is built by following the steps that are listed below.

1. First of all, the details of the template are programmed. Important here are the positions of the conductors (or further named nodes) in the $x - y$ plane. The $x - y$ plane is specifically mentioned as the construction considered has no members, boundary conditions excluded, that extend into the z -direction. Further requirements are the geometry and position of each member and the offset at each node.
2. It is important to number the nodes and number the degrees of freedom that each node has. A node might be connected to multiple elements. In order to include the effect of each element, the placement of the mass and stiffness details of each element within the mass and stiffness matrix of the template needs to be defined.
3. The next step would be to determine the length of each member by taking the offset into account. The length and projected length in x and y direction can be used to determine the direction of the member with respect to the global x direction (i.e. angle α).
4. Each member can then be subdivided into an arbitrary amount of elements, with a minimum of one. A single element is only able to describe the first mode of vibration. It may be required to include higher order modes of vibration for some elements, especially the elements that are located close to the driven pile.
5. Mass and stiffness matrices (Section C.2), transfer matrices for elements in arbitrary directions (Section C.3) and transfer matrices for node offsets (Section C.4) can be defined. After applying the appropriate transfer matrices to the matrices of the element, they can be placed within the matrices of the template. As soon as the effects of each element is included, the template model is nearly fully defined.
6. The final step would be to define the boundary conditions. The boundary conditions of the construction considered were introduced in Section 3.5. They were modelled as three beam elements that extend in the positive z -direction from nodes $J1$ - $J3$ to nodes $J1^*$ - $J3^*$. The latter nodes form the connection with the mud-mat. The horizontal displacement of each node is restricted. It means that the rows and columns corresponding to the horizontal displacements can be removed from the element matrix.

C.6. DEFINITION OF THE PILE/TEMPLATE INTERFACE.

This section of the Appendix follows the numerical interpretation of the interface definitions as described in Section 3.6. As was discussed before, the pile is modelled as a continuous Rayleigh-beam. The lateral displacement may vary over the height of the pile sleeve. The modelled element length is 0.5 meter, which means that four nodes might interact with the 1.5 m tall pile sleeve. For convenience, these nodes are named top down $i = 1, 2, 3, 4$.

The displacement field is approximated with a fourth order Lagrange polynomial as in (C.55). Here, u_i is the horizontal displacement and z_i is the vertical coordinate of node i .

$$P_4(z) = \sum_{i=1}^4 u_i \cdot \left(\prod_{\substack{j=1 \\ j \neq i}}^4 \frac{z - z_j}{z_i - z_j} \right) \quad (\text{C.55})$$

The relative displacement between the pile and the sleeve, as a function of the vertical coordinate, is (C.56)

$$q_{h,template}(z, t) = -K \cdot (P_4(z, t) - u_S(t) + z \cdot \phi_S(t)) \quad (\text{C.56})$$

in which u_S and ϕ_S are the horizontal displacement and rotation of the sleeve respectively. A pre-condition for the force transfer is that the relative displacement at a certain coordinate is positive. It

is possible that only part of the sleeve section is in contact, which means that a part of the modelled springs are activated.

In order to check which parts of the pile are in contact, the section of the pile is subdivided into four separate sections. In other words, the interface is modelled by four non-tension springs. The total force transferred, i.e. the integral over the relative displacement, in each section is estimated. A precondition for contact is that the force transferred over the height of the section is larger than zero. Mathematically it can be described as (C.57).

$$\begin{aligned}
 F_1 &= K \int_{z_1}^{\frac{z_1+z_2}{2}} (P_4(z) - u_S + z \cdot \phi_S) dz & F_2 &= K \int_{\frac{z_1+z_2}{2}}^{\frac{z_2+z_3}{2}} (P_4(z) - u_S + z \cdot \phi_S) dz \\
 F_3 &= K \int_{\frac{z_2+z_3}{2}}^{\frac{z_3+z_4}{2}} (P_4(z) - u_S + z \cdot \phi_S) dz & F_4 &= K \int_{\frac{z_3+z_4}{2}}^{z_4} (P_4(z) - u_S + z \cdot \phi_S) dz
 \end{aligned} \tag{C.57}$$

in which K is the spring stiffness of the interaction. Each of the four 'springs' is switched on upon contact and switched off when the interaction forces become tensile. Each contact force can be written in terms of the displacements of the four pile nodes and the motions of the conductor. In matrix-vector notation that is (C.58).

$$\begin{bmatrix} q_1 \\ q_2 \\ q_3 \\ q_4 \\ F_x^S \\ M_y^S \end{bmatrix} = \tilde{K} \times \begin{bmatrix} u_1 \\ u_2 \\ u_3 \\ u_4 \\ u_S \\ \phi_S \end{bmatrix} \tag{C.58}$$

When force F_i becomes positive, the added stiffness matrix \tilde{K}_i is added to the existing stiffness matrix. This matrix is subtracted again when F_i becomes negative.

